Predicting the Electrophysiological Responses of Murine Alpha Retinal Ganglion Cells to Artificial and Natural Visual Stimuli

Predicting the Electrophysiological Responses of Murine Alpha Retinal Ganglion Cells to Artificial and Natural Visual Stimuli

A dissertation presented

by

Brenna Marie Krieger

to

The Committee on Higher Degrees in Biophysics

in partial fulfillment of the requirements

for the degree of

Doctor of Philosophy

in the subject of

Biophysics

Harvard University

Cambridge, Massachusetts

October 2014

Dissertation Advisor: Dr. Markus Meister Brenna Marie Krieger

Predicting the Electrophysiological Responses of Murine Alpha Retinal Ganglion Cells to Artificial and Natural Visual Stimuli

Abstract

The retina sends many parallel channels of visual information to the brain through the axons of >20 retinal ganglion cell (RGC) populations. The purpose of these distinct circuits for vision remains an open question. Recent results suggest that each cell type responds selectively to a specific feature of the visual scene. These conclusions are derived primarily from experiments with artificial visual stimuli. It is unknown whether the insights gathered under such conditions extend to the natural environment in which the retina evolved. One can address this question by building a mathematical model of RGC responses to artificial stimuli and then testing how well that same model performs with natural visual input. For several RGC types this exercise has failed dramatically, indicating an imperfect understanding of their neural code.

Here we focus on the mouse alpha RGCs, which possess large cell bodies, stout axons, and wide receptive fields. Three subtypes had been previously defined based on their responses to light steps: On-Sustained, Off-Sustained, and Off-Transient. We targeted these RGCs for recording using a transgenic mouse line in which GFP is expressed in all alpha subtypes. Quantitative analysis of the recorded light responses revealed four distinct physiological cell types: an On-Transient alpha RGC in addition to the other three type previously identified. Using both artificial stimuli and natural movies,

we measured the visual responses of the mouse alpha cells. We then constructed a simple cascade-style model to link the stimulus to the firing rate.

Based on electrophysiological recording and modeling, we found the visual messages the four alpha RGCs send to the brain to be similar in that they are minimally processed versions of the visual scene. Spatial averaging minimally influenced the responses of the alpha RGCs to the natural movies. Additionally, a simple linear-nonlinear model accounted very well for the visual responses of all four alpha RGC subtypes, correctly predicting at least 70% of the variance in firing. The same model worked for both artificial stimuli (e.g. random flicker) and natural stimuli (mouse-cam and simulated-mouse movies). This successful account of alpha cell function will be valuable as a retina model for understanding cortical vision in the behaving mouse.

TABLE OF CONTENTS

Dedication

I would like to dedicate this thesis to my wonderful family and friends. They have enriched my life and brought me more joy than I can ever express. Their continual support made this work possible. Specifically, I would like to thank my parents: Dr. George W. Krieger and Aimee S. Krieger. To my dad, for teaching me the value of hard work, and to my mom, for always believing in me. I would like to thank my sister, Hilary Krieger, for sending comic relief and continued encouragement from across the continent. A special thanks goes to Dr. Jeffrey Teigler for convincing me to see these past years to their conclusion and providing guidance during the thesis writing process. I owe gratitude to the Harvard Program in Biophysics for the endless assistance from Michele Eva with all aspects of the Ph.D. process and Jim Hogle for his academic support. Lastly, I would like to thank Prof. Markus Meister for the weekly meetings that helped keep me on track, and the current and previous members of the Meister lab for their help and support.

Thank you!

Chapter 1: Introduction

An intuitive place to begin to learn about the brain is with the sensory systems. The only knowledge we possess of the natural world is derived from the interpretation of neural signals carrying sensory information. This information stems from the transformation of external sensory input, such as light, by sensory neural structures, such as the retina, into electrical signals. This process ultimately drives our daily lives. As humans, vision is our primary sense and almost half of our cerebral cortex is dedicated to processing visual information from the retina. Partly for this reason and partly because of experimental considerations, the retina has been a very popular model system to study neural circuitry. The retina is an ideal system to study neuroscience because it is the only part of the central nervous system that is easily accessed, it has a stereotyped layered structure across vertebrates, the output is readily recorded, and the light input is both easily controlled and quantified.

From the time of Ramon y Cajal in the 1800's, we have had a reasonable idea of the neural layers that comprise the retina[1]. Over time, many details have been added to the schematic, but the general structure remains true. Photoreceptors, in the form of rods and cones at the back of the retina, absorb incoming photons to begin the process of phototransduction. The visual information is synaptically passed to the bipolar cells and from there to the retinal ganglion cells (RGCs). Lateral inhibition from horizontal and amacrine cells modify this primary vertical information flow. Overall approximately 50 cell types comprise the retina[2]. The axons of the RGCs form the optic nerve, which is the sole source of visual input to the mammalian brain. We can easily monitor the activity of the RGCs with electrode arrays or, as in this study, patch pipettes. This allows us to display visual stimuli to the retina and readout the information meant for the brain. Since

visual input can be easily parameterized and deconstructed, the correlation between various aspects of the stimulus and the RGC responses can be found. This also means that the retina serves as an excellent system to model neural processing. Neural signals arise on the level of molecules and ion channels, yet the eventual readout is on the scale of animal behavior. Thus the study of any part of the central nervous system can focus on a number of different length scales. Characterizing the transformation of light into electrical signals that are sent to the brain provides a starting point for decoding the visual processing that leads to behavior. Therefore, it is important to extract the transfer function that the retina uses to process visual input.

References

1. Cajal, S.R. (1893). La retine des vertebres. Cellule *9*, 17–257.

2. Masland, R.H. (2001b). The fundamental plan of the retina. Nat. Neurosci. *4*, 877–886.

Chapter 2: Materials and Methods

2.1 General procedures and materials

Mice. The detailed methods for generating the KCNG4^{Cre} transgenic mouse line has been previously reported[1,2]. In short, the KCNG4^{Cre} line was created by inserting cre recombinase into the translation start codon of the potassium channel modulator *kcng4* gene by homologous recombination. The cre-positive cells were visualized by crossing with either the cre-dependent *Thy1-STOP-YFP* or *Ai3* (JAX stock number: 007903) fluorescent reporter lines expressing EYFP [3,4]. All experiments were conducted in accordance with protocols approved by the Institutional Animal Care and Use Committees at Harvard University and the California Institute of Technology.

Electrophysiology. Mice were dark adapted for at least 1 hour prior to euthanization by cervical dislocation. The retina was isolated under infrared illumination into Ames oxygenated with 95% O2, 5% CO2 at room temperature. A ~2-3 mm aperture was cut into nitrocelluose filter paper and the retina was mounted ganglion cells (RGCs) facing up. The experiment was conducted with the retina in a superfusion chamber heated to 34-36 degrees C. A two-photon microscope was used to identify fluorescent RGCs for loose cell-attached recording. Data acquisition and the two-photon microscope were controlled using custom LabView software. Patch electrodes (2-5 MOhm) filled with Ames medium were used to record action potentials that were subsequently amplified with a Multiclamp 700B amplifier (Molecular Devices). Custom programs in IGOR (Wavemetrics Inc.) were used for spike thresholding and analysis.

Stimulation. Light stimuli were created using the Psychophysics Toolbox extensions in Matlab[5–7]. A modified Texas Instruments Lightcrafter with a custom lens system focused the stimuli onto the retinal photoreceptors (frame rate 60 Hz, magnification 9.1 um/pixel, intensity 10 mW/m^2). Cones mediate vision at high light levels and, in the mouse retina, they typically coexpress two opsins: short (S) – and middle (M) wavelength sensitive with peak sensitivities of 360 and 508 nm, respectively[8]. The average stimulus intensity expressed in photoisomerizations per second for each of the three mouse photoreceptors corresponds to 5.7×10^3 R*/s for rod, 2.1×10^3 R*/s for M cone, and 4.8×10^3 R*/s for S cone. The relative intensities of the LEDs were chosen such that the rods and M cones are each equally excited by the UV and green LEDs (Figure 2.1). Movies were acquired at 150 fps, or 20 fps for the mouse cam movie, and scaled to approximate the input to the retina. Eye movements were assumed to be negligible and not accounted for in the stimulus[9]. Movie manipulations were performed in Matlab. Blurring of the simulated mouse movie was performed using the modulation transfer function from Geng et al. (2011).

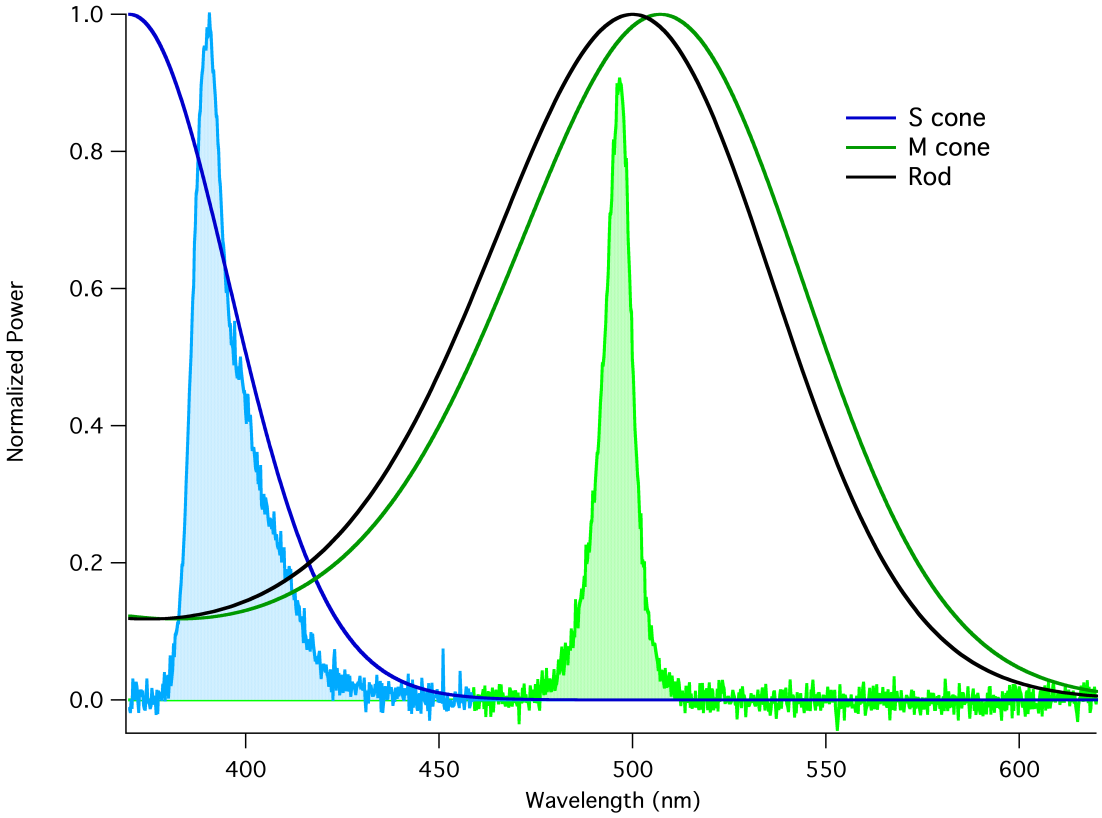

Figure 2.1: Emission spectra of the stimulator LEDs (filled) and absorption spectra of the murine photoreceptors.

Specific stimuli. To measure many of the receptive field properties of the A-RGCs we utilized a so-called growing spot stimulus. In this stimulus, spots centered over the receptive field are flashed "on" for 1 second and "off" to background grey for 1 second. Figure 2.2 shows the example stimulus for an Off-RGC. When the stimulus was "on", it was of the preferred polarity to drive the current RGC. The purpose of this stimulus was to measure the size of the receptive field, the strength of the surround, the latency of response, and many other parameters. Additionally, the peak firing rate to each spot as a function of the spot size was used to estimate the spatial receptive field in the absence of a receptive field from reverse correlation with a binary checkerboard stimulus.

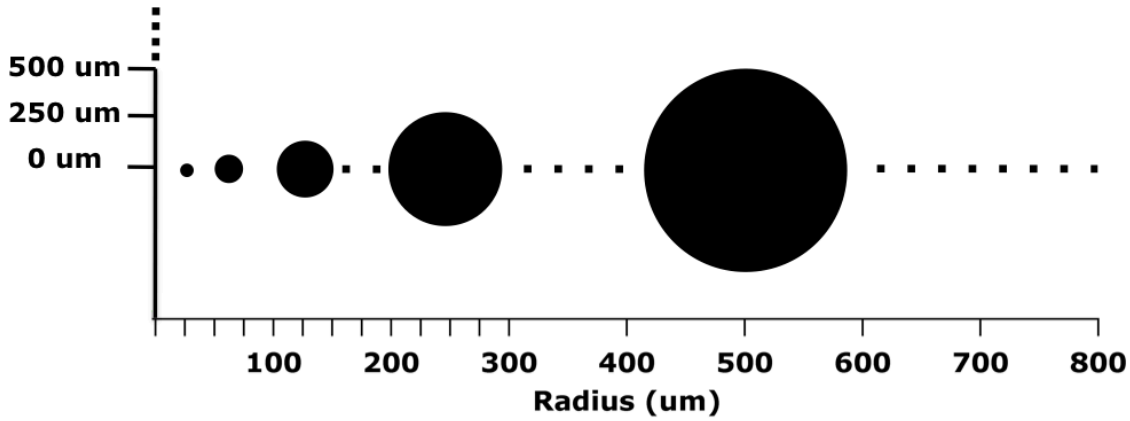

Figure 2.2 Schematic of the growing spot stimulus utilized in Chapters 3 and 5. Each tick mark indicates a size of spot that was displayed. The center of the receptive field was more finely probed.

Calculation of physiological parameters. Many parameters were calculated from the growing spot stimulus so for each cell, the stimulus was repeated 3-8 times over the course of the experiment (Figure 2.2). For the baseline firing rate measurement and each subsequent spot size, the peristimulus time histogram (PSTH) was calculated by binning at 25 ms. The baseline firing rate was the average firing rate over the first 2 seconds. The optimal size was the spot that elicited the peak firing rate. The PSTH of the optimal size was used to determine the latency of response, i.e. the time to peak of PSTH. The surround strength was calculated as 1 minus the ratio of the peak firing rate at R = 800 μm to the absolute peak firing rate from the optimal spot size.

Histology. After electrophysiological experiments, some retinas were fixed in fresh 4% paraformaldehyde in PBS at 4 degrees C for two hours for further characterization of the On-transient alpha retinal ganglion cells. After fixation, the retinas were washed and incubated at 4 degrees C with primary antibodies for 4-5 days. Secondary antibody incubation at room temperature for 2 hours preceded mounting on a glass slide with spacers, ganglion cell side up, with Prolong Gold. Whole mount images were obtained on a LSM 710 inverted NLO microscope at 20X (Zeiss). The primary antibodies used were: anti-green fluorescent protein (~rabbit, IgG, Life Technologies) and anti-nonphosphoneurofilament H (~mouse [1:1000], SMI-32, Sternberger Monoclonals Incorporated).

Response similarity to manipulated movies. The extracellular spiking responses of retinal ganglion cells (RGCs) were recorded under stimulation by sequential natural

movies. Each movie was repeated 4-8 times and the spike trains to individual repeats were binned at 33 ms, i.e. 2 times the frame rate of the stimulus. To assess the similarity of retinal ganglion cell responses under different natural movies, Pearson's correlation coefficient was calculated for each combination of the binned spike trains (twice the stimulus frame rate; ~33 ms). The coefficients from the individual repeats were averaged. This analysis was performed both across the manipulated movies and within the original movie. The correlation between repeats of the original movie was used as an estimate of neural noise. Subsequent correlation values were normalized by the average neural noise for each cell type.

Spatiotemporal receptive fields. Receptive fields were mapped using a checkerboard pattern, with $(45.5\ \text{um})^2$ checkers, flickering randomly either black or white at 60 Hz[10,11]. The spike-triggered average was calculated from 600 seconds of white noise stimulation by standard reverse correlation methods, i.e. adding together all the chunks of stimuli preceding a spike and dividing by the number of spikes[12]. In cases where only the temporal receptive fields were mapped by using a flickering spot plus surround annulus centered over the cell, the spatial receptive field was estimated by fitting a difference of Gaussians to the peak firing rate verses radius curve (see **Specific Stimuli**). To reduce noise, the temporal filter calculated from the data was fit with T(t) parameterized by the following equation[11].

$$T(t) = (t/\tau_1)^{n_1} e^{-n_1(t/\tau_1 - 1)} - a(t/\tau_2)^{n_2} e^{-n_2(t/\tau_2 - 1)} \qquad \text{(Eqn. 2.1)}$$

These five parameters also served as the initial parameters when the model fit the temporal kernel.

Modeling. We predicted the visual responses of the alpha retinal ganglion cells using cascade models composed of linear filters and static nonlinearities. For each instance of model fitting, we used separate training and testing datasets to prevent fitting of the noise, i.e. overfitting. In general, the input to the model for each frame was calculated by convolving the movie with the approximate spatial receptive field and the pixels restricted to the center averaged. Each spatially uniform stimulus channel was linearly convolved with the parameterized temporal filter before rectification with a log-sigmoid nonlinearity. The parameters for the nonlinearity and, in some cases the temporal kernel, were fit in IGOR using the Levenberg-Marquardt algorithm for least squares fitting (Wavemetrics, Inc). Initial guesses for the temporal filters were computed by fitting the spike-triggered average with Equation 2.1 as described above. The output of the model was interpreted to be the firing rate of the neuron. Model performance was assessed by calculating the average correlation between the predicted firing rate and the individual spike train to repetitions of the stimulus (see "Response similarity to manipulated movies.")

Fitting a model to white-noise stimuli. To fit the responses to white-noise stimuli, we generated a stimulus ~700 seconds long that consisted of random sequences interspersed every 100 second with 10 seconds of the same stimulus. The model was fit to the long, 600 seconds, sequence responses binned at the frame rate, 17 ms, to increase the number of stimulus combinations encountered by the model. The parameters fit to the long sequence were tested by calculating the predicted firing rate to the repeated sequence. The goodness-of-fit was assessed as described in "Modeling."

Fitting a model to natural movie stimuli. The natural movies described in the "Stimulation" section were of very limited length compared to the white-noise stimuli. Thus to fit models to 30 seconds – 1 minute of repetitions of the data we broke the data into ~7 second chunks and iteratively fit the model by leaving out one chunk of the data. The model was iteratively tested by predicting the firing rate to each excluded chunk and the average constituted the model performance. The goodness-of-fit measure was the average correlation as for the white-noise stimuli.

4-by-4 subunit model. In Matlab, the two natural movies were multiplied by a mask of R = 250 um and the remaining pixels split into an even 4-by-4 grid. The pixel intensities within each of the 16 squares were summed for each frame in time producing a 16-by-"# of frames" matrix that served as the input to the model. The model consisted of 16 identical subunits. Each subunit filtered the 1-dimensional stimulus input with a temporal kernel and passed that filtered stimulus through a log-sigmoid static nonlinearity. The parameters for the temporal kernel and static nonlinearity were shared across all subunits. All the rectified subunit outputs were individually scaled and added together before being passed through a final log-sigmoid nonlinearity. Initial guesses for the temporal filters were computed by fitting the spike-triggered average with Equation 2.1 as described above. The rest of the parameters were set to unity except for the maximum firing rate for the last nonlinearity stage, which was set to a reasonable value (~100). Least-squares fitting was used to find the optimal parameters by allowing the Levenberg-Marquardt algorithm in IGOR (Wavemetrics Inc) to minimize chi-square. From the initial guess the

model looped through fitting subspaces of parameters. Each set of parameters was fit 5 times and the model was allowed to loop through all parameter subspaces until convergence. In practice, less than 5 loops were required. The model output was interpreted as the predicted firing rate. The goodness-of-fit was calculated by the average correlation as described in "Modeling."

2.2 References

1. Duan, X., Krishnaswamy, A., De la Huerta, I. & Sanes, J. R. Type II Cadherins Guide Assembly of a Direction-Selective Retinal Circuit. *Cell* **158,** 793–807 (2014).

2. Kim, I.-J., Zhang, Y., Meister, M. & Sanes, J. R. Laminar restriction of retinal ganglion cell dendrites and axons: subtype-specific developmental patterns revealed with transgenic markers. *J. Neurosci.* **30,** 1452–1462 (2010).

3. Buffelli, M. *et al.* Genetic evidence that relative synaptic efficacy biases the outcome of synaptic competition. *Nature* **424,** 430–434 (2003).

4. Madisen, L. *et al.* A robust and high-throughput Cre reporting and characterization system for the whole mouse brain. *Nat. Neurosci.* **13,** 133–40 (2010).

5. Kleiner, M., Brainard, D. & Pelli, D. What's new in Psychtoolbox-3? in *Percept. 36 ECVP Abstrast Suppl.* (2007).

6. Brainard, D. H. The Psychophysics Toolbox. *Spat. Vis.* **10,** 433–436 (1997).

7. Pelli, D. G. The VideoToolbox software for visual psychophysics: transforming numbers into movies. *Spat. Vis.* **10,** 437–442 (1997).

8. Wang, Y., Weick, M. & Demb, J. Spectral and temporal sensitivity of cone-mediated responses in mouse retinal ganglion cells. *J. Neurosci.* **31,** 7670–7681 (2011).

9. Andermann, M. L., Kerlin, A. M. & Reid, R. C. Chronic cellular imaging of mouse visual cortex during operant behavior and passive viewing. *Front Cell Neurosci* **4,** 3 (2010).

10. Chichilnisky, E. J. A simple white noise analysis of neuronal light responses. *Network* **12,** 199–213 (2001).

11. Pitkow, X. & Meister, M. Decorrelation and efficient coding by retinal ganglion cells. *Nat. Neurosci.* **15,** 628–635 (2012).

12. Pillow, J. W. & Simoncelli, E. P. Dimensionality reduction in neural models : An information-theoretic generalization of spike-triggered average and covariance analysis. 414–428 (2006).

Chapter 3: Discovering the Physiological Receptive Field Properties of the Mouse Alpha Retinal Ganglion Cells

3.1 Introduction: The Mouse Alpha Retinal Ganglion Cells

Though complexity in the retina has been documented since Ramon y Cajal's (1893) report cataloguing the diversity of RGCs of the vertebrate retina, types of RGCs were not recognized until the 1970s when receptive field size differences due to eccentricity were taken into account[1,2]. Of the approximately 20 types of retinal ganglion cells (RGCs) that have subsequently been morphologically identified in the mammalian retina, one class of cells called the alpha RGCs (A-RGCs) has arguably been studied the most extensively [3–5]. The A-RGCs were among the first to be classified based on possessing the largest soma and dendritic arbor of all the neurons in the ganglion cell layer[6,7]. The same neurons were found to be labeled by the reduced-silver method that stains for neurofilaments[8]. Over the past few decades, RGCs with large somas and dendritic fields have been found in over 20 mammalian species by the reduced-silver method and, more recently, neurofilament staining with antibodies has revealed A-RGC analogs in the human retina[5,6,9–11]. Therefore, due to their conservation across species and easily identifiable morphology, the A-RGCs have often served as "model ganglion cells" to study computations in the retina[12–20]. From these efforts, many specific synaptic mechanisms have been elucidated, but the fundamental properties of the A-RGC message that is conveyed to the brain are not known. We aimed to map the physiological receptive field properties of the mouse A-RGCs to better understand their visual message.

It is important to emphasize that the A-RGC classification is morphological. The defining elements are staining positive for markers of neurofilament while possessing large cell bodies and dendritic fields. A number of secondary characteristics have also been attributed to the A-RGCs. The cells typically possess roughly circular dendritic

arbors that are unistratified within the inner plexiform layer (IPL). In general, 2-6 primary dendrites stem from the soma of the A-RGCs with radial branches that rarely overlap. They also possess the thickest axons and make up less than 10% of the overall ganglion cell population[5,6]. The physiology of the A-RGCs across species is less clearly defined. The A-RGCs in the cat retina were found to correspond to the previously identified Y-cell population[21]. The Y-cells were classified based on their brisk-transient, i.e. rapid and short, responses to light stimuli and their spatially nonlinear receptive fields as assessed by responses to inverting gratings. Two types of Y-cells were defined based on having either On- or Off-center receptive fields. On cells across the retina respond to an increase in light intensity and are inhibited by a decrease in intensity whereas Off cells respond in the opposite manner. The physiology of cells with A-RGC morphology has been reported in a few mammals other than the cat including the rabbit, mouse, guinea pig, primate, and gerbil[22–28]. Some of these A-RGCs have been found to differ substantially in their physiology from their cat analogs.

Recently, the mouse has become a common model system for studying mammalian vision. Besides the many advantages of working with a mammal smaller than a primate or cat, the crucial factor has been the widespread availability of transgenic mice[29]. Before now, studies on the mouse A-RGCs have not taken advantage of transgenic technology and instead relied upon rough morphological criteria for cell selection. By recording from mouse RGCs with the largest somas (~20 μm) at random and filling the cells with fluorescent dye for morphological reconstruction, three types were defined: Off-Transient, Off-Sustained, and On-Sustained[3,20,25,30–32]. The Off-Transient cells were the most similar to the feline brisk-transient analogs and responded

to a decrease in light intensity with a brief increase in firing rate. The Off- and On-Sustained cells displayed maintained responses to their preferred light stimuli. Cells in these original reports were not stained with a marker for neurofilament and thus were not verified to be A-RGCs. Recently, the KCNG4-cre transgenic mouse line was shown to selectively label the A-RGCs in the ganglion cell layer when crossed with the *Thy1-STOP-YFP* fluorescent reporter[33]. With this tool, we can specifically examine A-RGC physiology in the mouse retina to complement previous reports[25,30,31].

For the first time, the entire mouse A-RGC population can be reliably targeted. We probed their receptive field properties by recording extracellular action potentials to visual input to ask, what physiological properties are shared across the mouse A-RGC population? Specifically, we wondered whether the Off A-RGCs could be quantitatively separated into two classes based on their physiology alone. We also assessed the diversity in the On A-RGCs with the same criterion. In addition, we looked for other criteria by which to recognize the cells when randomly patching or during extracellular array recording. Ultimately, we aimed to delineate the receptive field properties of the mouse A-RGCs to better understand their visual message conveyed to the brain.

3.2 Physiological Classification of the Off and On Alpha RGCs

Pang, Gao, and Wu (2003) were the first to perform voltage-clamp recordings and subsequent morphological reconstruction on alpha retinal ganglion cells (RGCs) in the mouse. Similar to studies in other mammals, they chose to target the RGCs with the largest somas (20-25 μm diameter) for consistency. Based on that morphological criterion, they identified three types of mouse alpha-RGCs (A-RGCs): Off-Transient, Off-Sustained, and On-Sustained[25]. Other labs have conducted similar experiments by randomly patching large, RGCs in the mouse and all have agreed with this original classification[20,30,31,34].

3.2.1 Separating the Off Alpha Retina Ganglion Cells into Sustained and Transient Types

We have confirmed the existence of two populations of mouse Off A-RGCs, corresponding to the transient and sustained types, and we developed a quantitative criterion by which the types can be classified based on their spiking responses. Using the $KCNG4^{Cre}$ transgenic mouse line from the lab of Dr. Joshua R. Sanes that selectively expresses a fluorescent protein in the A-RGCs when crossed with the cre-dependent *Thy1-STOP-YFP* reporter mouse line, we recorded the extracellular spiking responses of the Off A-RGCs to a sequence of dark spots of increasing radius flashed at 1 Hz[35]. The purpose of this stimulus was to probe the properties of the circular center-surround receptive fields. We defined the spot size that elicited the peak firing rate to be the size of the receptive field center and we quantified the surround strength as the decrease in firing rate from the peak due to the addition of the inhibitory surround. As in previous reports, some cells responded with a brief burst of action potentials before returning to the

baseline firing rate and others maintained a steady, elevated discharge for most or all of the stimulus[20,31]. Surprisingly, it was difficult to classify all cells as either transient or sustained while recording because many of the cells were transiently excited to some degree and possessed high baseline firing rates. To quantify the time course of the responses, we fit the average response to the optimal spot size, i.e. the radius that elicited the peak firing rate, with an exponential function. The exponential fit gave the decay time constant, tau, and the steady state firing rate, Y0, of the neural response. Intuitively, one would expect a transient cell to have a short time constant and a low steady state response while a sustained cell should have a longer time constant and higher steady state response. In a plot of the steady state response (Y0) normalized by the peak firing rate versus the exponential decay time constant, we saw the two clusters predicted by intuition (Figure 3.1, n = 56). The transient cells clearly formed a discrete cluster in the bottom left corner with exponential time constants <150 ms and normalized steady state response < 0.1.

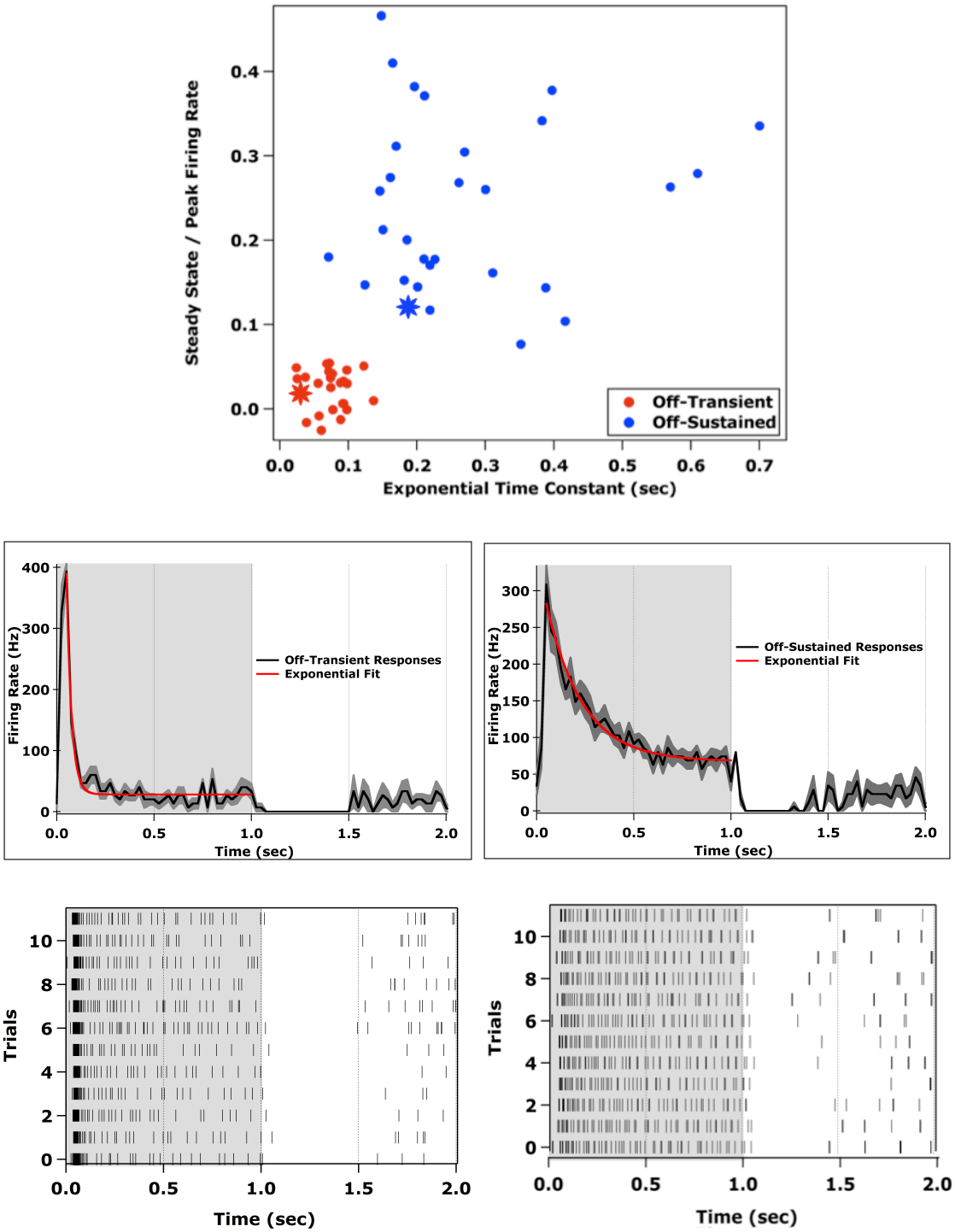

Figure 3.1: Steady state firing rate / Peak firing rate as a function of exponential decay time constant for all recorded Off A-RGCs (top, n = 56). Example exponential fits and light responses from an Off-Transient (left) and Off-Sustained (right) cell marked in the top graph with stars.

3.2.2. On Alpha Retinal Ganglion Cells Separate into Sustained and Transient Types

I also recorded from On A-RGCs in the KCNG4-cre mouse line and analyzed their spiking responses to a sequence bright spots of increasing radius flashed at 1 Hz. When the On cells were run through the same analysis as the Off cells, we were surprised to find a cluster of On-Transient cells (Figure 3.2, green). All reports mentioning mouse A-RGCs cite the existence of only On-Sustained cells, yet based on the same quantitative criterion developed for the Off RGCs, the On population also separated into two clusters. The less numerous transient cells possessed normalized steady state responses < 0.1 with exponential time constants <100 ms, 50 ms faster than the Off-Transient population. Unexpectedly, the On-Sustained population also had fast decay time constants (< 200 ms), but their normalized steady state responses fell into the same range as the Off-Sustained RGCs (~ 0.1 – 0.4). Fitting the On population with a double exponential did not reveal a different separation of the two types (data not shown).

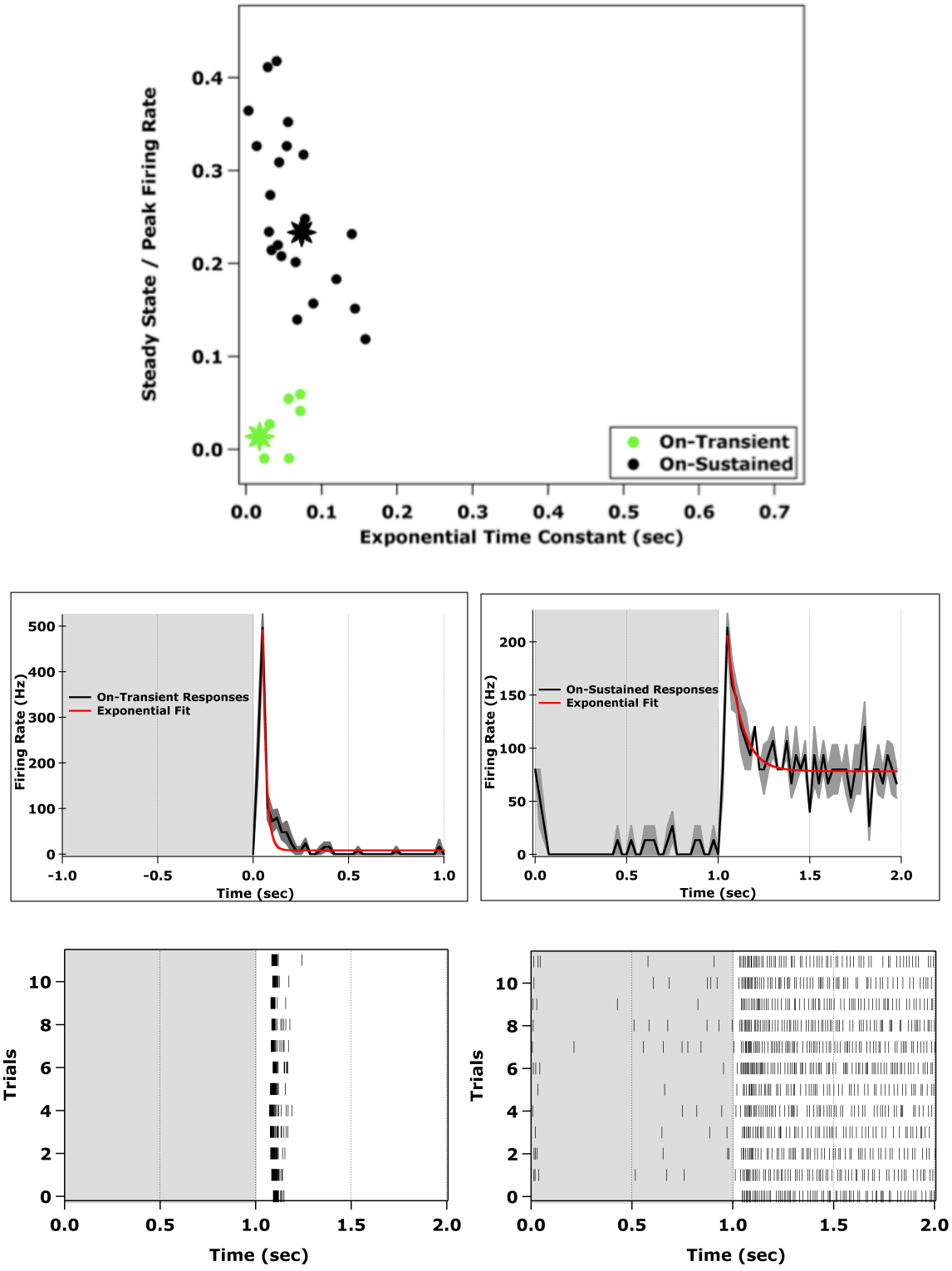

Figure 3.2: Steady state firing rate / Peak firing rate as a function of exponential decay time constant for all recorded On A-RGCs (top, n = 29). Example exponential fits and light responses from an On-Transient (left) and On-Sustained (right) cell marked in the top graph with stars.

To confirm the On-Transient cells to be alpha RGCs, two KCNG4^{Cre} retinas were stained with a neurofilament heavy-chain marker, the SMI32 antibody, after recording. This antibody has been shown to label A-RGCs in the mouse[4,34]. The same On-Transient cells that were targeted on the electrophysiology rig were located post-fixation. All tested cells were both YFP and neurofilament positive and thus meet the classic definition of A-RGCs (Figure 3.3, n=2). Therefore, the mouse On A-RGCs are not only sustained as claimed in previous reports, but display a diversity of light responses.

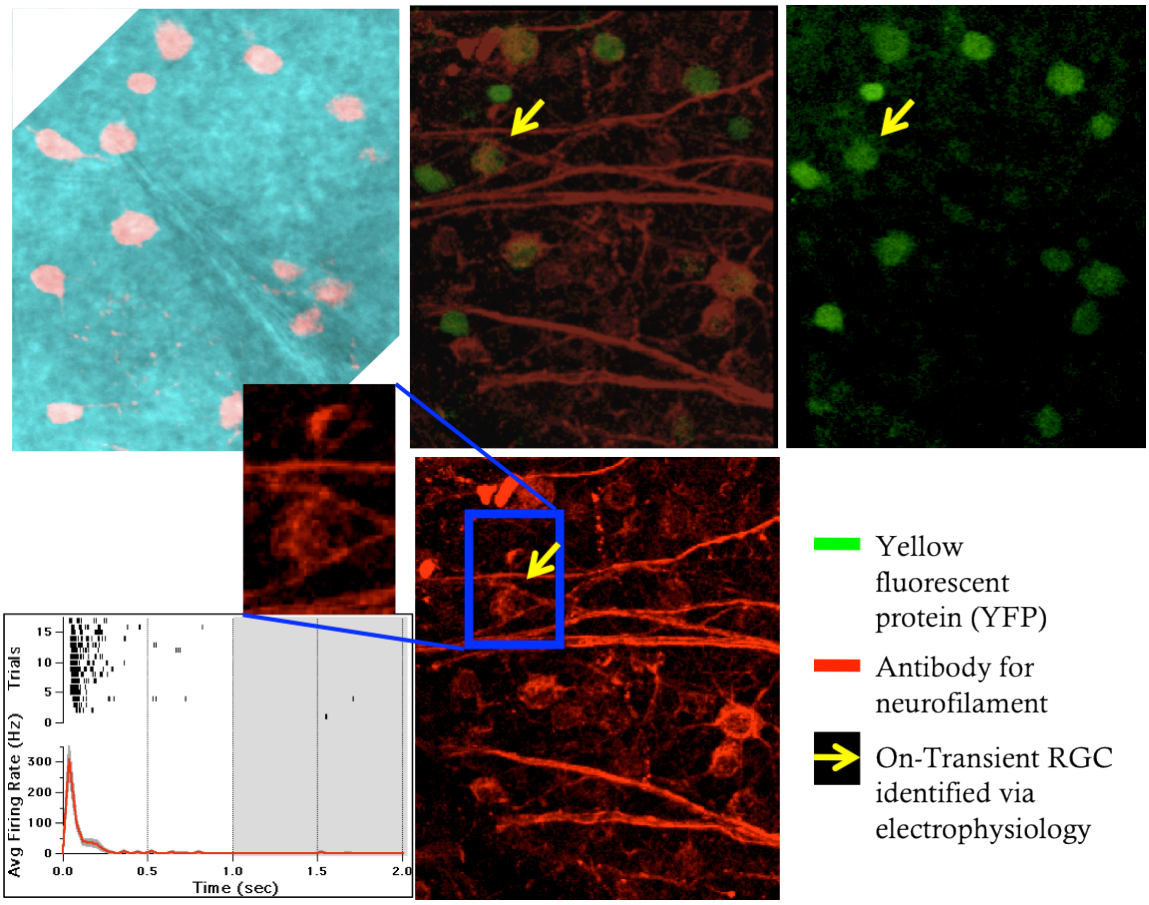

Figure 3.3: On-Transient RGCs fluorescently labeled in the KCNG4^{Cre} line are neurofilament positive (n=2). A screenshot from the 2-photon rig of the fluorescent RGCs with a single RGC targeted (top left) with On-Transient responses (bottom left). Post-experiment histology (center and right) shows the recorded cell to be positive for neurofilament marker SMI32 (red).

We compared the exponential fit parameters used to classify the Off and On populations across the entire A-RGC population. The sustained and transient cells were statistically different ($p < 10^{-10}$) in their steady state normalized by peak firing rates. The exponential decay time constants were statistically indistinguishable for the Off-Transient, On-Transient, and On-Sustained populations. The response decay time for the Off-Sustained RGCs was significantly longer ($p < 10^{-7}$) from the rest of the A-RGCs (Figure 3.4).

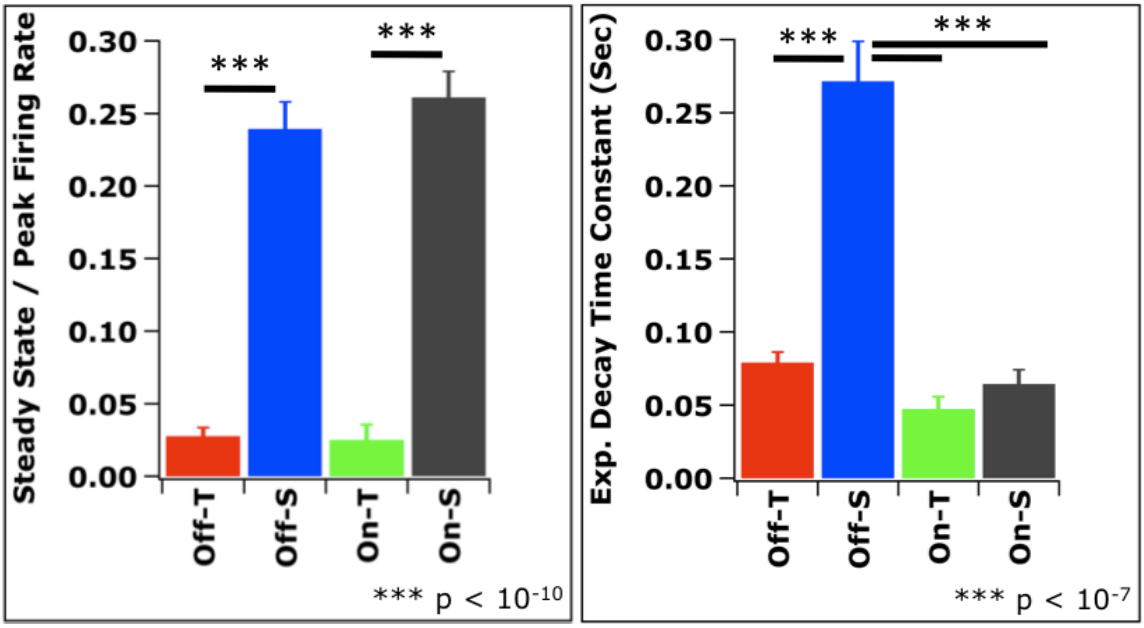

Figure 3.4: Steady state firing rate normalized by peak firing rate (left) and exponential decay time constant (right) for all A-RGCs.

Crucially, the light responses to the optimal spot for each of the four clusters found from the quantitative exponential decay analysis also qualitatively match (Figure 3.5). When comparing the time course of the Off (red) and On (green)-Transient cells by eye, they look almost identical. The majority of the On-Sustained (black) cells appear to briskly respond to the bright spot and then quickly decay to roughly one quarter of the peak firing rate. We next compared the receptive field parameters of these physiologically defined cell types.

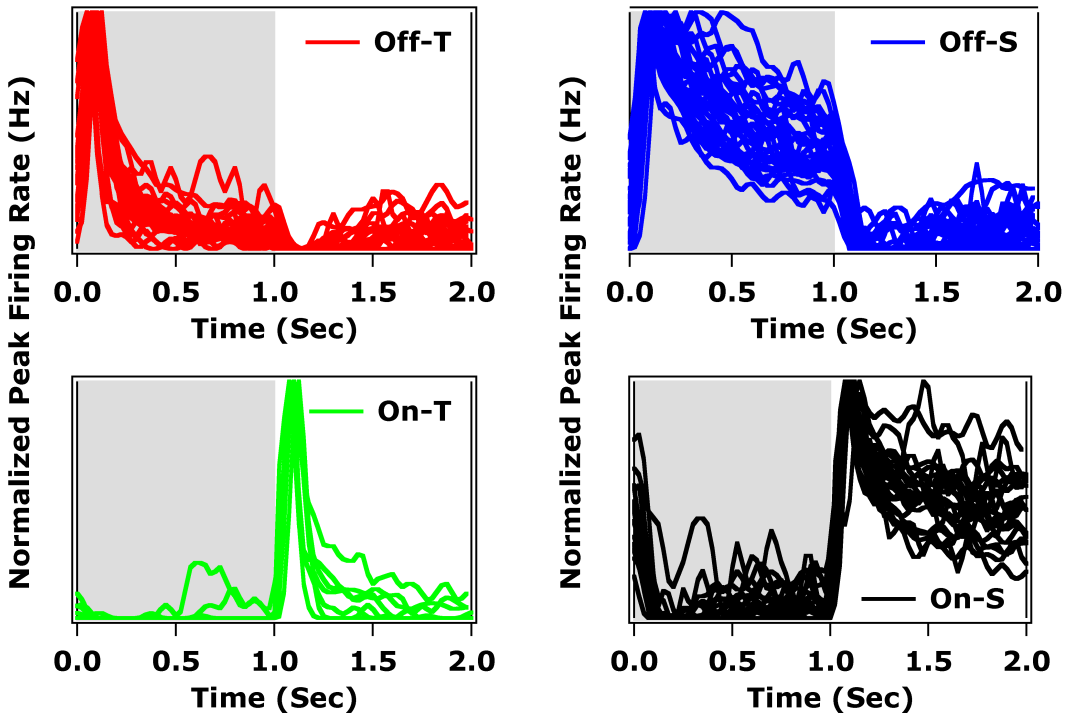

Figure 3.5: Peristimulus time histograms (PSTH) of the Off (top) and On (bottom) A-RGCs to the flashed optimal spot size of the preferred contrast. The polarity of the stimulus is shown in the background. The populations have been split based on the exponential fit analysis.

3.3 The Receptive Field Properties of the Mouse Alpha Retinal Ganglion Cells

Based on the physiological cell types defined by the exponential fit, we looked at a number of properties of the alpha RGCs to investigate the similarity of the entire alpha population.

To measure the spatial acuity of the A-RGCs, we showed a contrast-reversing stimulus that is commonly used to assess the degree of linear intensity summation across the receptive field[36]. A linear cell will not respond to such a stimulus with a maintained mean light intensity where light is simultaneously added and subtracted from the receptive field, but a cell that nonlinearly sums light will respond to each change (Figure 3.6). This kind of frequency-doubled response came to define the Y-cells of the cat retina[37–39]. Given that Y-cells were later identified to be the cat alpha cells based on morphological similarity, we expected all of the mouse alpha cells to have nonlinear spatial receptive fields[21,40]. By inverting high contrast gratings of increasing spatial frequency over the receptive field of an A-RGC, we asked whether we saw the frequency-doubled response indicative of nonlinear summation. If so, we assessed the spatial frequency limit of the frequency-doubled response as defined by the grid of highest spatial frequency that elicited a response 2 standard deviations above baseline. From the Off alpha population, we found a wide range of responses to this stimulus that ranged from a response to every grating to no response at all. The degree of nonlinear summation spanned from highly nonlinear, with a spatial acuity of 10 μm, to linear, with the cell summing across the entire 400 μm receptive field (Figure 3.6). The transient and sustained cells also tended to respond to fine gratings or thick gratings, respectively, supporting their classification by the exponential fit. By comparison, the On A-RGCs all

had nonlinear spatial receptive fields. With the exception of two On cells they were all sensitive to gratings with bars of 20 or 50 μm. In fact the Off-Transient, On-Transient, and On-Sustained cells had statistically indistinguishable acuities. Thus, the majority of the mouse A-RGCs possessed nonlinear receptive fields, with the exception of the Off-Sustained population.

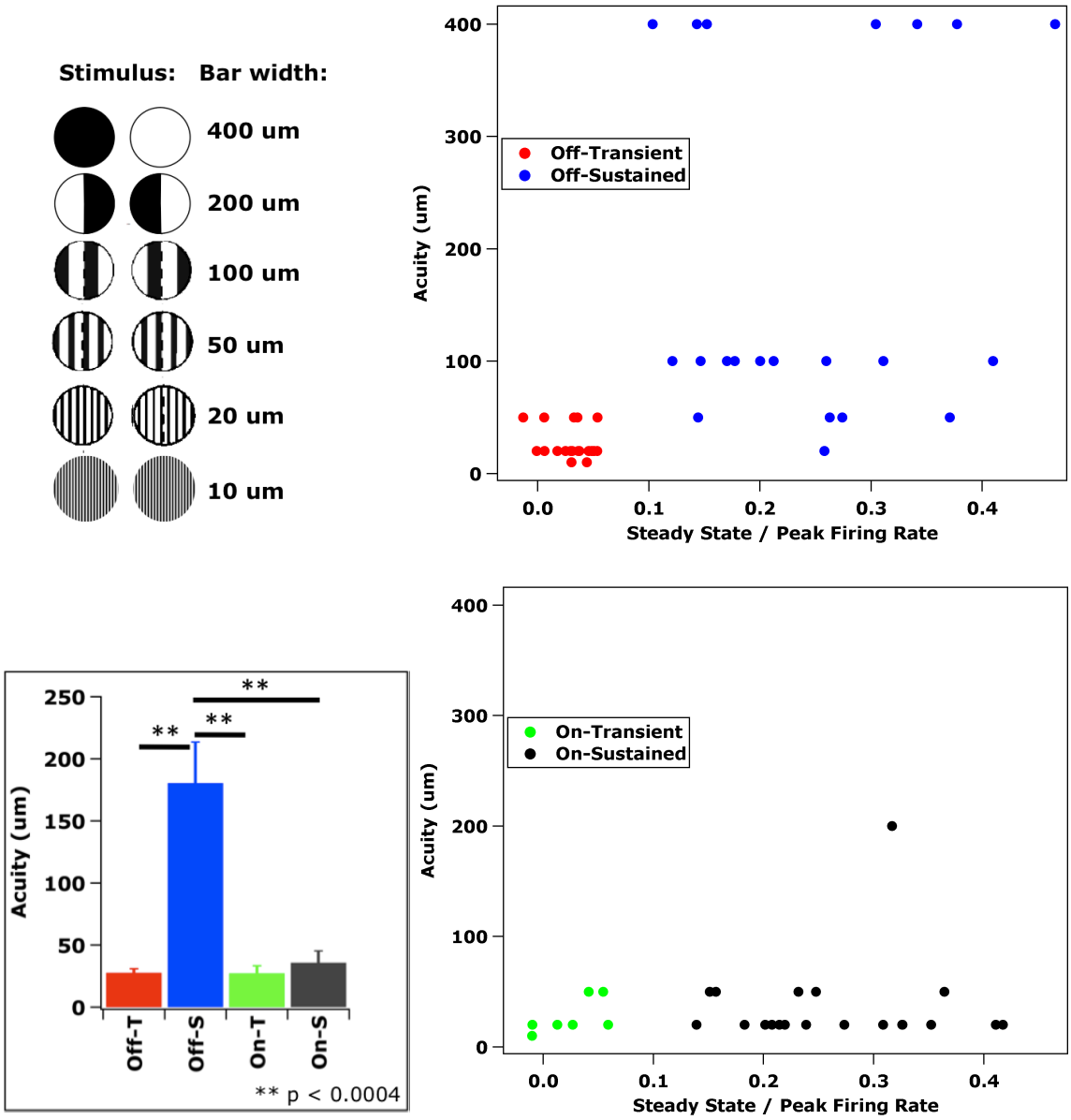

Figure 3.6: The majority of the A-RGCs in the mouse retina, with the exception of the Off-Sustained RGCs, have nonlinear receptive field centers with responses to each inversion of gratings down to ~ 30 um bars (~ 1 cycle per degree).

From the same growing-spot sequence stimulus described earlier, we quantified the baseline firing rate, strength of the surround, peak firing rate, latency to peak, and receptive field size. The baseline firing rate was calculated as the average firing rate before the growing spot stimulus began. Unsurprisingly the transient RGC types tended to have lower baseline firing rates than their sustained counterparts. The On-Transient firing rate was significantly lower than the rest of the A-RGCs (Figure 3.7, see Figures 3.1 & 3.2).

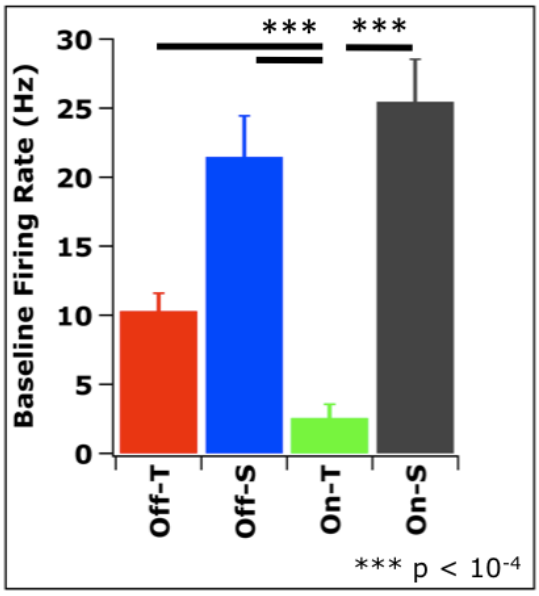

Figure 3.7: Average baseline firing rate measured before the beginning of each growing spot sequence repetition for the four A-RGC types. * indicates at least $p < 10^{-4}$. The Off-Transient (red) baseline firing rate is also significantly less ($p < 10^{-3}$) than the On-Sustained (black) baseline.**

To visualize the responses to the growing spot stimulus, we plotted the average peak firing rate to each spot size versus the radius of the stimulus for each of the A-RGC types (Figure 3.8, top). From this representation of the data, it is easy to gain a qualitative sense of the A-RGC responses. Most of the curves intersect the y-axis above zero indicating a non-zero baseline firing rate. The responses grow quickly with increasing spot size and all curves peak at approximately the same radius. At the largest spot sizes, the Off-Transient RGCs still respond with ~75% of their peak firing rate while the response from the On-Transient RGCs is reduced to about half the peak.

The decrease in firing rate to larger spot sizes was quantified by calculating a surround index. The surround index was computed as one minus the ratio of the response from the largest spot size (R=800 μm) to the response from the optimal spot (R~125 μm). Largely, we found the surround strength of the mouse A-RGCs to be weak, < 0.6, compared to non-alpha RGCs whose response often decreases to zero[36,41]. The Off-Transient and On-Transient had weaker and stronger surrounds, respectively, compared to the Off-Sustained RGCs ($p < 0.01$). The On population had slightly distinguishable surround strengths ($p < 0.05$) giving the On-Transient cells the strongest surrounds. We estimated the receptive field size to be the diameter of the spot that produced the peak firing rate of those tested. The receptive field sizes of the four alpha RGC types were statistically indistinguishable, except for the Off-Transient cells ($p < 0.01$). The Off-Transient cells had consistently smaller receptive fields by ~50 μm.

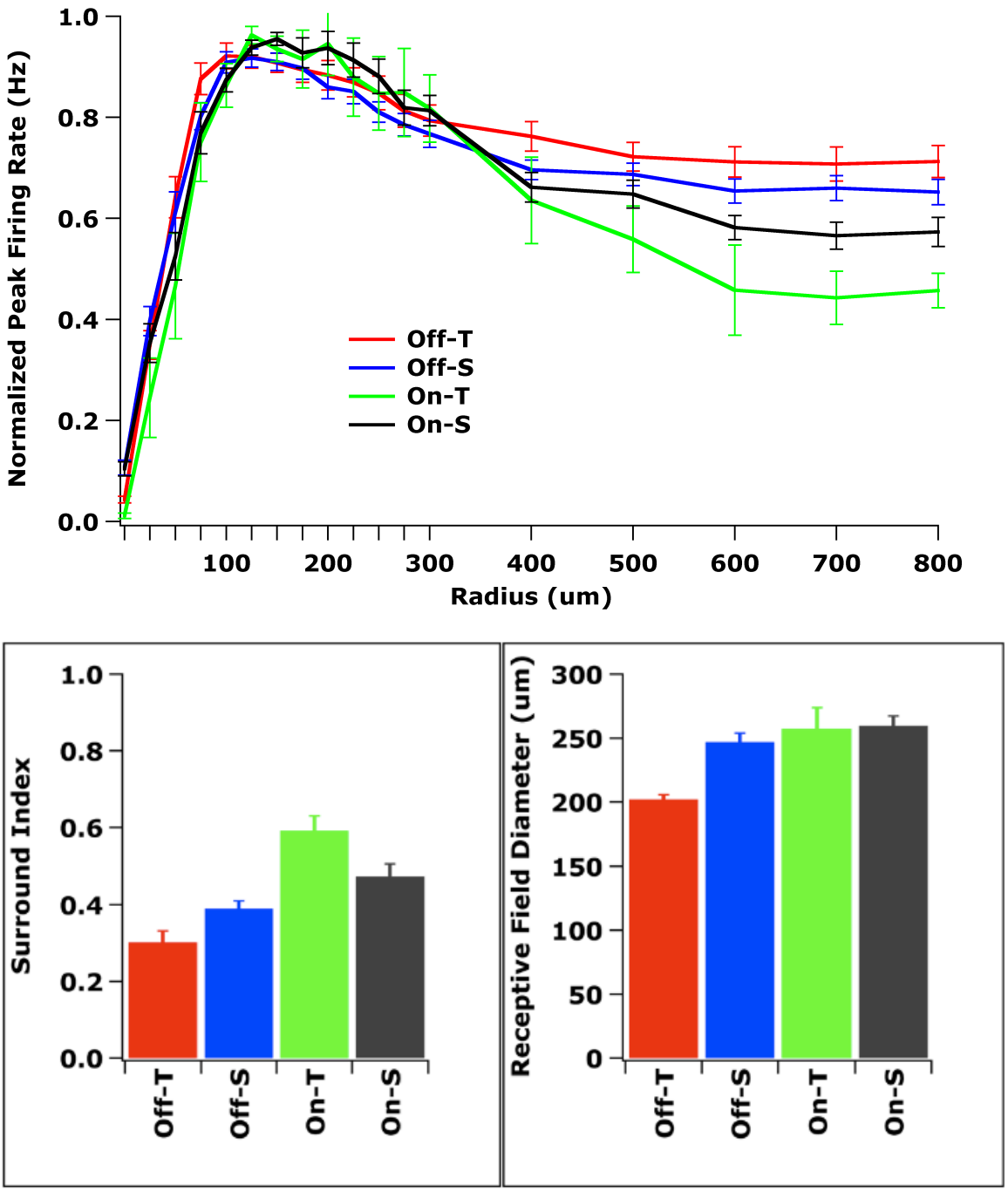

Figure 3.8: Average normalized peak response versus spot radius to the growing spot stimulus for the A-RGCs (top). Surround strengths and receptive field diameters calculated from the data in the top graph. Surround: 1-FR(R=800)/FR(R=peak R). Receptive field diameter: Radius of spot that corresponds to peak firing rate. All p-values (Student's 2 tailed t-test) were greater than 0.001.

The latency for each cell was calculated as the time to peak for the maximum response (Figure 3.9, left). The Off-Sustained cells were statistically slower than the Off-Transient cells ($p<0.01$) and the rest had equivalent latencies. Similarly, the average peak firing rates did not differ across the alpha population (Figure 3.8, right).

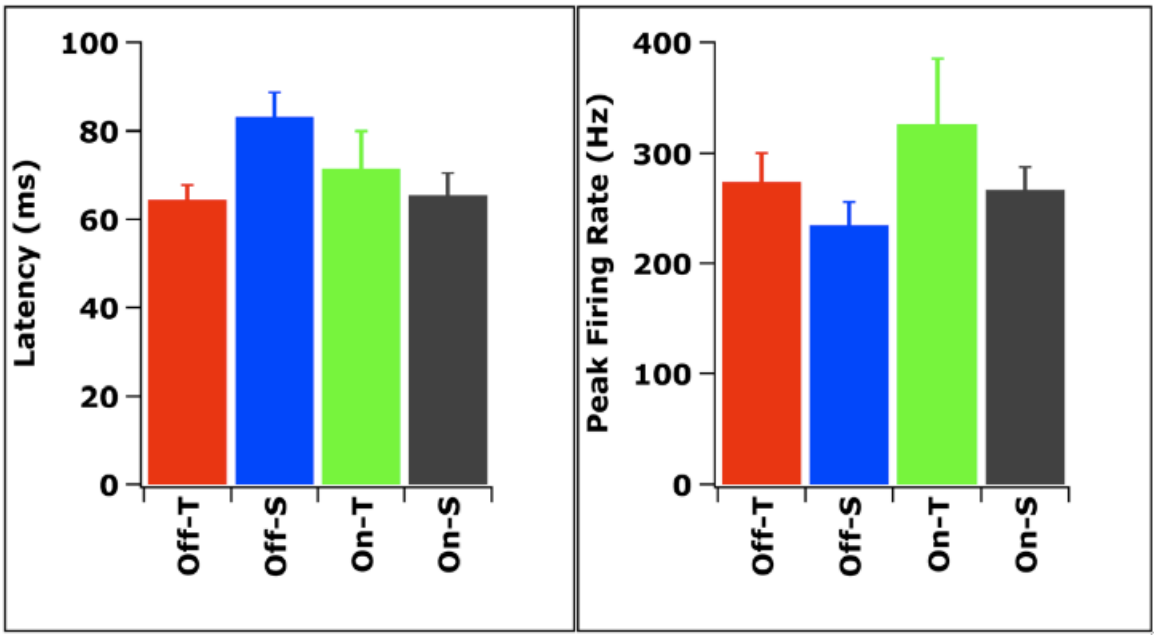

Figure 3.9: The time to peak (left) of the response to the optimal spot size that elicited the peak firing rate (right, 25 ms bins) during from the growing spot series.

We also checked for direction selectivity in the responses of the alpha RGCs. We found the cells to respond to spots of the preferred intensity moving over their receptive field (700 μm/s) any direction. This confirms previous reports that state alpha cells to be responsive to motion, but not direction selective[5] (Figure 3.10).

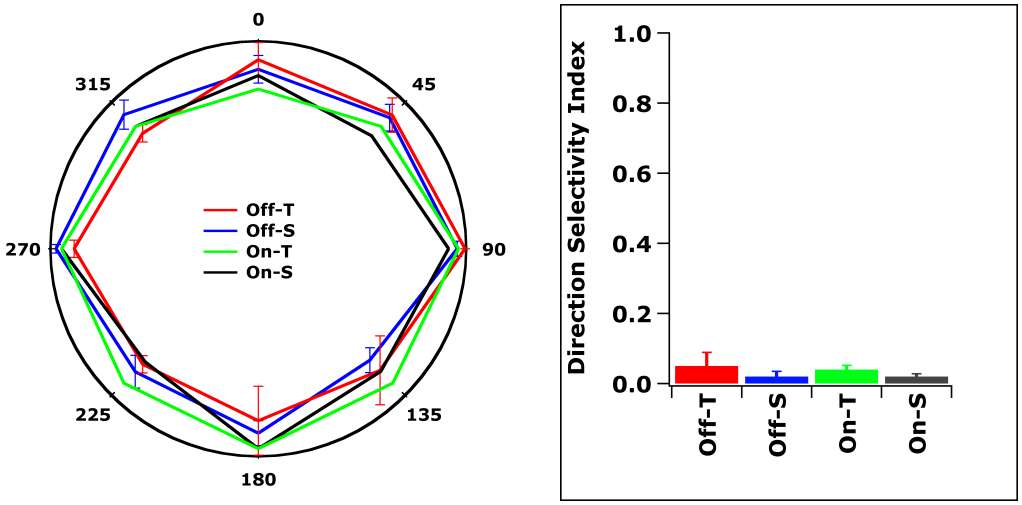

Figure 3.10: The A-RGCs respond to moving spots over their receptive fields, but they are not selective to motion in a particular direction.

Overall a number of receptive field parameters were shared by the alpha RGCs under our particular stimulus conditions (see Chapter 1: Methods). The Off-Sustained cells differ the most dramatically from the rest of the A-RGCs with a slower response decay and lower acuity. The On-Transient cells distinguish themselves with a very low baseline firing rate and the strongest surrounds. The Off-Transient cells have a slightly smaller receptive field diameter and the On-Sustained cells share all parameters with the other types.

3.4 The Unique Alpha Retinal Ganglion Cell Spike Shape with Prepotential

For the majority of extracellular recordings from A-RGCs, we saw a unique spike shape. In addition to sharp spikes, particularly at physiological temperatures, a fast prepotential was found to precede every spike (Figure 3.11). This spikelet was found in recordings from all four of the A-RGC types and thus did not correlate with the polarity or temporal dynamics of the RGC. In practice, this spike shape came to confirm the correct RGC had been patched with the electrode and, an experimenter randomly patching should be able to use this spike shape as an additional criterion for targeting mouse A-RGCs. It should be noted that we did not systematically rule out the possibility of other RGCs having the same shape, but we did not see the spikelet in any of the cells we randomly patched. The spikelet persisted during visual stimulation and thus appears to be part of the normal function of the A-RGCs.

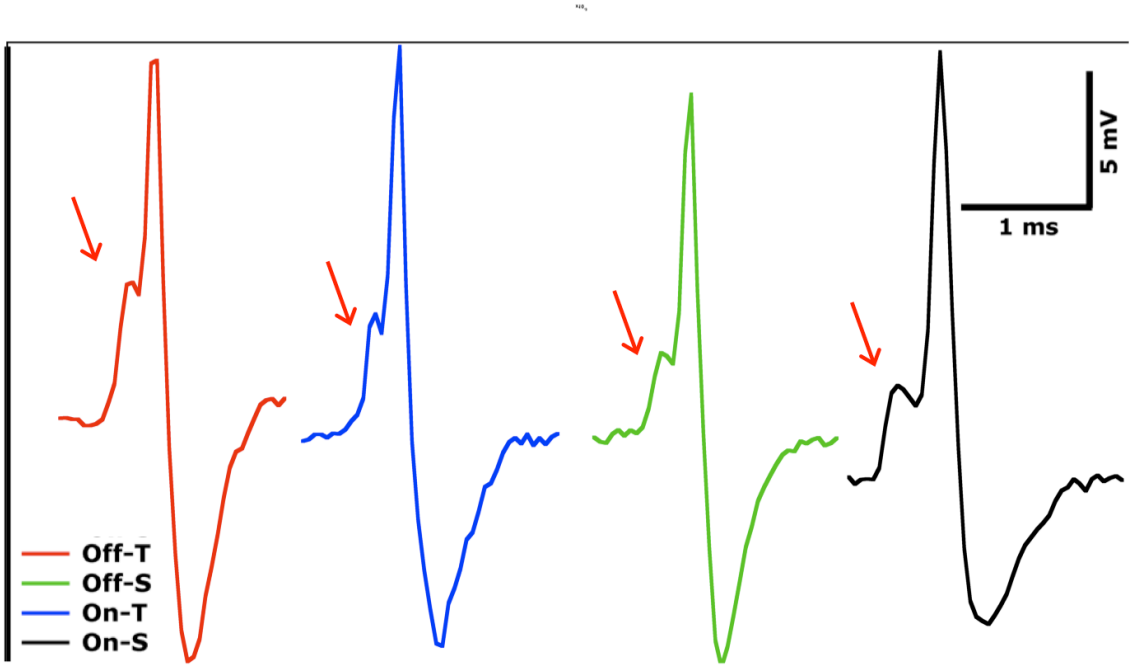

Figure 3.11: The spike shape with a prepotential (red arrow) is common to the class of A-RGCs.

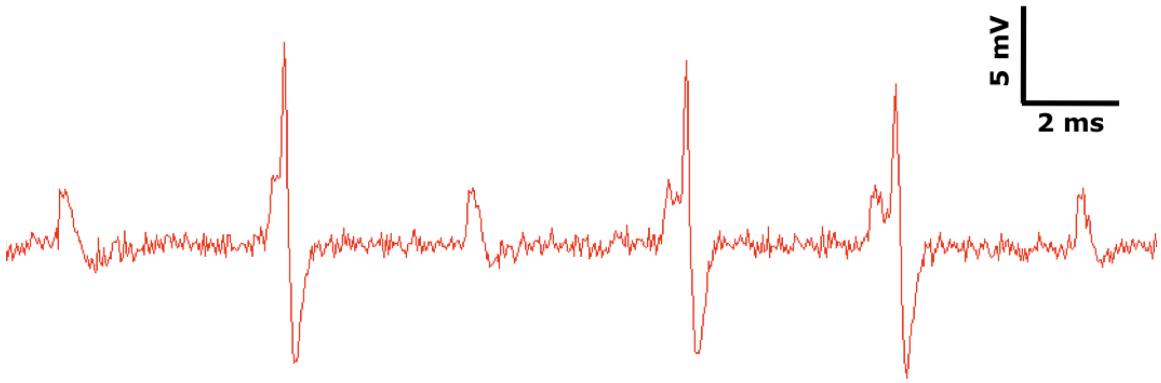

Figure 3.12: Spikelet before somatic spike fires with regularity, even in the absense of a full action potential.

For some recordings, the prepotential was seen to occur at regular intervals even in the absence of a somatic spike (Figure 3.12). This indicates that the spikelet may be the origin of the high baseline firing rate and regularity of the A-RGC action potentials[25,31]. From personal experience and previous work in the Meister lab (Y. Zhang, unpublished data), the distance between the prepotential and the somatic spike was seen to change according to temperature. While recording from an A-RGC and systematically varying the temperature, the time between the prepotential and the large spike increased on the order of 1 ms (Figure 3.13). The same behavior was not seen for a non-alpha RGC indicating this phenomenon is not common to all RGCs. The same expected changes in spike amplitude and duration were seen for the alpha and the non-alpha RGC suggesting the lack of prepotential in the non-alpha cell was not due to experimental error in temperature adjustment.

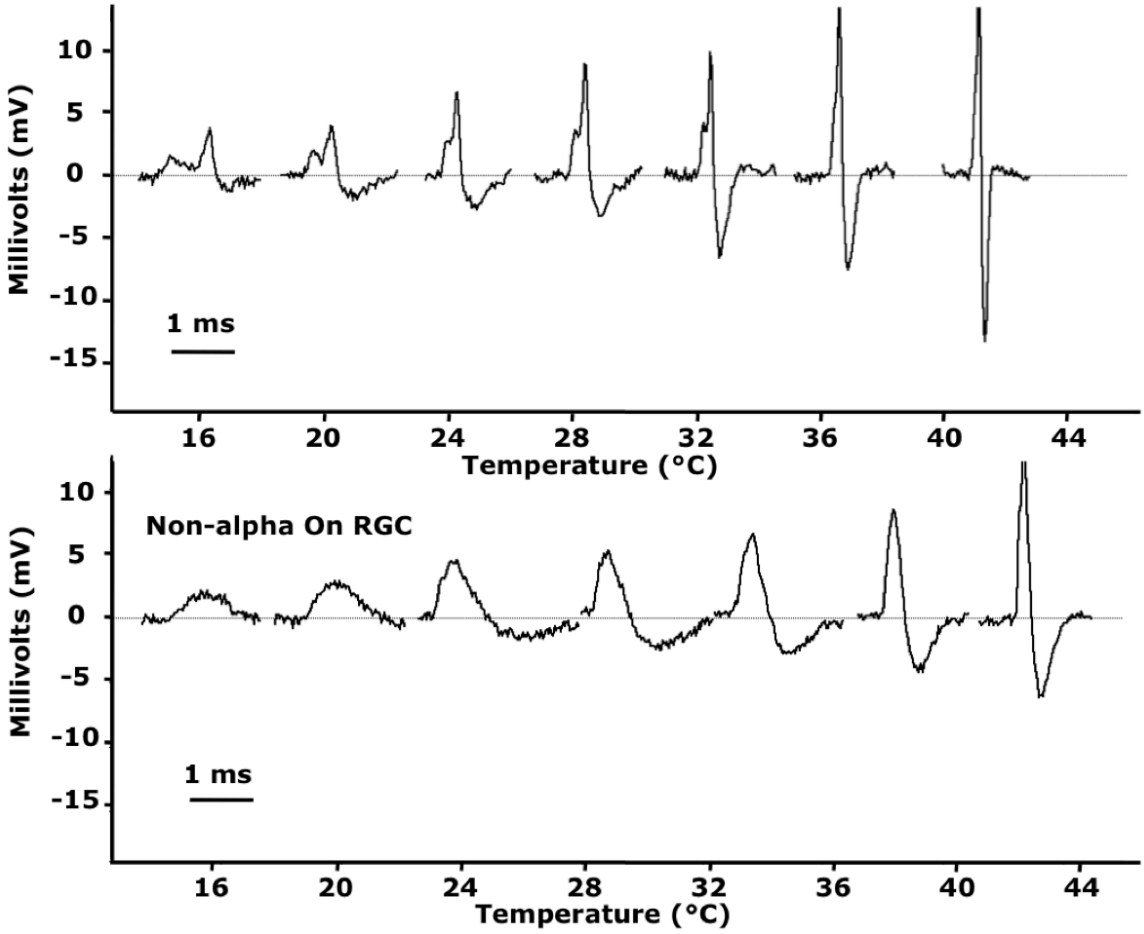

Figure 3.13: The time between the prepotential and the somatic spike on A-RGC action potential depends on bath temperature (top). The same trend in spike shape versus temperature is seen for a non-alpha RGC, but no prepotential becomes obvious at low bath temperatures (bottom).

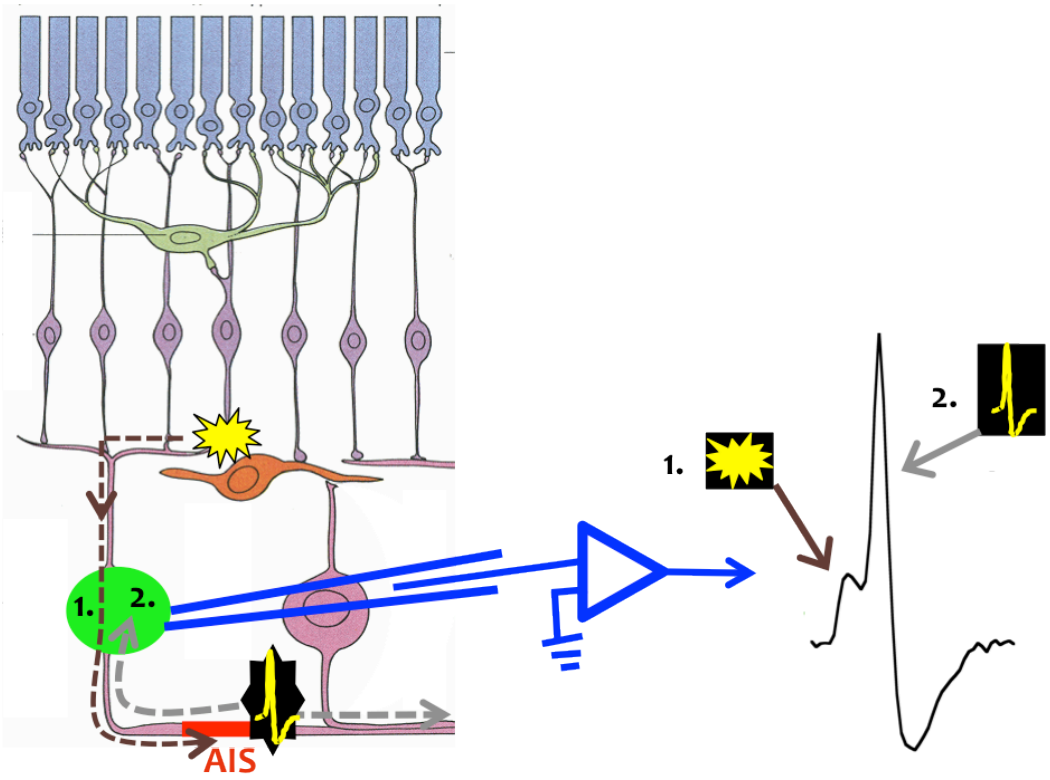

Figure 3.14: Schematic of A-RGC action potential. We propose the action potential originated in the dendrites.

The regularity of the prepotential and the indication it always precedes a full somatic spike led us to believe multiple spike generating mechanisms were at work in the A-RGCs. It is known that for some neurons, including RGCs, the actual site of somatic spike initiation lies away from the cell body at the axon initial segment (AIS)[42,43]. This region has the highest density of sodium channels and often possesses special channels not present in the soma[44–47]. However, the timing of the spikelet and the somatic spike suggests involvement of the dendrites. In the brain, fast prepotentials have been linked to spike initiation by dendritic spikes[48,49]. Additionally, some mammalian RGCs such as the On-Off direction selective and likely the A-RGCs, have been shown to be capable of dendritic spikes[50,51]. Considering the above properties of the A-RGC spike shape, we hypothesized that an active spike triggered in dendrites is passively conducted through the soma to the AIS to initiate a somatic spike. To test the hypothesis that both the dendrites and AIS play an active role in A-RGC spike initiation, we performed a rough calculation. The patch electrode should record current from the dendritic spike as it passes to the AIS and the somatic spike. Therefore the time between recording the small dendritic spike and the large action potential should match the time it takes for current to travel from the soma to the AIS and back. In mammals, including mice, the AIS has been shown to be 20-35 um down the axon from the cell bodies of RGCs[45,47,52]. This same work has also shown the size of the AIS to vary depending on the soma size with the largest somas possessing the longest AIS. Considering the A-RGCs should have the longest AIS and the point of lowest threshold may lie anywhere along that region, an estimate of 20 um for the distance from the soma to the point of action potential initiation is conservative. Estimating 3.5 m/s for the conduction velocity at 24 degrees C it should

take ~0.1 ms for the current to travel from the soma to the AIS and back[53]. This time scale is consistent with timing between the prepotential and full action potential from extracellular recordings from the mouse A-RGCs (Figure 3.13).

3.5 Discussion

3.5.1 Finding On-Transient Alpha Retinal Ganglion Cells in the Mouse

All earlier reports on mouse A-RGCs had agreed with the original finding of three physiological types corresponding to an Off-Transient, Off-Sustained, and On-Sustained[20,25,30,31,34]. We also agree with these earlier studies, but with the help of the KCNG4^{Cre} transgenic mouse line, we confirmed the existence of an On-Transient A-RGC type. Considering we found the On-Transient cells to be a slight minority of the On population (7/29 of On A-RGCs), they would be easier to miss in general. Therefore is it likely that during random patching experiments from other labs, occasional On-Transient responses from cells with large somas were discarded as anomalous. As opposed to some prominent differences in acuity and exponential decay time of the Off A-RGC, the entire On A-RGC population shares the majority of the receptive field parameters examined here. Their receptive field size, peak firing rate, acuity, latency, surround strength, and exponential decay time constant are all statistically indistinguishable. This hints that the computations performed by the On-Transient and -Sustained types are similar. The only striking difference is in comparing their baseline and the ratio of their steady to peak firing rates. These firing rate properties allow On-Transient cells to be clearly distinguished during the experiment (Figure 3.2, bottom). Further work is required to define the similarity in the visual messaged conveyed to the brain by the two On types.

It is still an open question whether the On-Transient RGCs are morphologically distinct from the On-Sustained RGCs via their lamination in the inner plexiform layer (IPL) or dendritic branching pattern. Evidence in the literature exists for both morphological and physiological diversity. All morphological studies of the mouse RGCs find multiple cells in the On sublamina with large somas and A-RGC-like morphology[3,4,54,55]. For example, Sun et al. (2002) claimed to find three morphological types of A-RGCs: two in the inner IPL and one in the outer IPL. The two On cells were distinguished by the density of their dendrites and not their stratification layer in the IPL. Kong et al. (2005) found four large RGC types through morphological clustering analysis and specifically questioned whether clusters 8 or 11 were the On A-RGCs. Unfortunately, it is as difficult to draw conclusions from these studies as it is to completely reconcile them with each other. We should be particularly careful in light of the recent report on the nasal-to-temporal gradient of the On-Sustained A-RGCs that was not taken into account in this earlier morphological work[34]. Our findings distinguish On-Transient from On-Sustained A-RGCs based on physiology alone and thus we do not address the morphology of these two types.

In addition to morphological diversity, physiological diversity was also noted in the mouse A-RGCs since the beginning of their characterization. In figure 2, Pang et al. (2003) shows a histogram of the measured inhibitory chloride current amplitudes and comments on how it varied across the tested population (n=23). The only difference they noticed was in the frequency of light-evoked spikes. It is possible the On-Transient and -sustained cells we see possess the same morphology, but receive different levels of inhibition.

Many reports provide evidence for morphological and physiological diversity in the mouse A-RGCs. Unfortunately, none of those reports except one verify the targeted RGCs as alpha by staining for neurofilament[34]. The decisive answer will come from patching On-Transient cells, filling them with dye, staining for neurofilament, and reconstructing their morphology in relation to the stratification pattern of the starburst amacrine cells. A thorough comparison of lamination and dendritic branching patterns with matching data from On-Sustained cells will resolve any morphological differences. Ultimately one would like a transgenic mouse line specific to the individual On-Transient and On-Sustained populations. Then it could be assessed whether each population evenly tiles the retina in a mosaic, as shown for the Off-Transient A-RGCs, to constitute separate types of RGCs[28]. Here we provided the starting point for future work by presenting diversity in the On A-RGCs. Our unexpected finding of On-Transient A-RGCs reestablishes symmetry in the mouse A-RGC population.

3.5.2 Unique Spike Shape of the Alpha Retinal Ganglion Cells

No previous reports have made mention of the irregular spike shape of the A-RGCs. This is in part due to few studies of the A-RGC extracellular responses. Our observations from recording the extracellular action potentials of the A-RGCs to light stimuli indicate unique spike-generation machinery of these cells. We claim that the mouse A-RGCs make dendritic action potentials during normal function. Based on the periodicity of the prepotentials, even in the absence of a full spike, we believe the origin of regular firing for the A-RGCs may reside in the dendrites. A number of experiments can be done to check our hypothesis that the prepotential is of dendritic origin. Blocking

somatic spikes with QX-314 added to patch pipette or hypolarization of the soma during voltage clamp can test whether the prepotential persists without somatic spiking[51]. Multiple sites of spike generation can be investigated by calculating the interspike interval histograms to look for the absence of a refractory period[50]. Interestingly, the existence of the prepotential on all of the A-RGCs suggests the process of spike generation is shared across the four types.

Regardless of the origin, the prepotential on the action potential provides further validation that the On-Transient cells are part of the A-RGC class. Additionally, the spike shape is another criterion for determining whether a randomly patched cell is an A-RGC. Previous work from our lab on other genetically identified cell types, including the W3, J-RGC, and all four types of On-Off direction selective RGCs, did not see the A-RGC spike shape with a prepotential[36,56]. All of the RGCs we randomly patched during the course of these experiments also did not have such a spike shape ($n \approx 10$). It is worth noting that the exact size and position of the prepotential varied from cell to cell. This may be due to a number of reasons including the absolute temperature of the bath, but one possibility in particular may be the relative location of the patch pipette. Considering the large size of the A-RGC somata, if the pipette is further from the axon initial segment (AIS), and therefore closer to the dendritic input, the prepotential should be more clear. It will be interesting to see whether further investigation into the spiking machinery of the A-RGCs provides additional insight into their biophysics or criterion for their classification within and outside of the A-RGCs.

3.6 References

1. Boycott, B. B. & Wassle, H. The Morphological Types Of Ganglion Cells of the Domistic Cat's Retina. *J. Physiol.* **240,** 397–419 (1974).

2. Cajal, S. R. y. La rétine des vertébrés. *Cellule* **9,** 119–257 (1893).

3. Völgyi, B. Tracer Coupling Patterns of the Ganglion Cell Subtypes in the Mouse Retina. *J. Comp.* **512,** 664–687 (2009).

4. Coombs, J., van der List, D., Wang, G.-Y. & Chalupa, L. M. Morphological properties of mouse retinal ganglion cells. *Neuroscience* **140,** 123–136 (2006).

5. Peichl, L. E. O. Alpha Ganglion Cells in Mammalian Retinae: Common Propoerties, Species Differences, and Some Comments on Other Ganglion Cells. *Vis. Neurosci.* **7,** 155–169 (1991).

6. Peichl, L., Ott, H. & Boycott, B. B. Alpha ganglion cells in mammalian retinae. *Proc. R. Soc. Lond. B. Biol. Sci.* **231,** 169–97 (1987).

7. Wassle, H., Peichl, L. & Boycott, B. B. Morphology and topography of on- and off-alpha cells in the cat retina. *Proc. R. Soc. Lond. B. Biol. Sci.* **212,** 157–175 (1981).

8. Wässle, H., Peichl, L. & Boycott, B. Dendritic Territories of Cat Retinal Ganglion Cells. *Nature* **292,** 344–5 (1981).

9. Straznicky, C., Vickers, J. C., Gábriel, R. & Costa, M. A neurofilament protein antibody selectively labels a large ganglion cell type in the human retina. *Brain Res.* **582,** 123–8 (1992).

10. Peichl, L. E. O. Alpha and Delta Ganglion Cells in the Rat Retina. *J. Comp. Neurol.* **286,** 120–139 (1989).

11. Peichl, L. E. O., Buhl, E. H. & Boycott, B. B. Alpha Ganglion Cells in the Rabbit Retina. **41,** (1987).

12. Manookin, M. B., Beaudoin, D. L., Ernst, Z. R., Flagel, L. J. & Demb, J. B. Disinhibition combines with excitation to extend the operating range of the OFF visual pathway in daylight. *J. Neurosci.* **28,** 4136–4150 (2008).

13. Zhang, J., Li, W., Hoshi, H., Mills, S. L. & Massey, S. C. Stratification of alpha ganglion cells and ON/OFF directionally selective ganglion cells in the rabbit retina. *Vis. Neurosci.* **22,** 535–549 (2005).

14. Wassle, H., Koulen, P., Brandstatter, J. H., Fletcher, E. L. & Becker, C.-M. Glycine and GABA receptors in the mammalian retina. *Vision Res.* **38,** 1411–1430 (1998).

15. Zaghloul, K. a, Boahen, K. & Demb, J. B. Different circuits for ON and OFF retinal ganglion cells cause different contrast sensitivities. *J. Neurosci.* **23,** 2645–2654 (2003).

16. Zaghloul, K. a, Boahen, K. & Demb, J. B. Contrast adaptation in subthreshold and spiking responses of mammalian Y-type retinal ganglion cells. *J. Neurosci.* **25,** 860–868 (2005).

17. Zaghloul, K. a, Manookin, M. B., Borghuis, B. G., Boahen, K. & Demb, J. B. Functional circuitry for peripheral suppression in Mammalian Y-type retinal ganglion cells. *J. Neurophysiol.* **97,** 4327–4340 (2007).

18. Vardi, N., Masarachia, P. J. & Sterling, P. Structure of the starburst amacrine network in the cat retina and its association with alpha ganglion cells. *J. Comp. Neurol.* **288,** 601–611 (1989).

19. Weick, M. & Demb, J. B. Delayed rectifier K channels contribute to contrast adaptation in mammalian retinal ganglion cells. *Neuron* **71,** 166–179 (2011).

20. Murphy, G. J. & Rieke, F. Network variability limits stimulus-evoked spike timing precision in retinal ganglion cells. *Neuron* **52,** 511–524 (2006).

21. Peichl, L. & Wassle, H. Morphological Identification of on- and off-centre brisk transient (Y) cells in the cat retina. *Proc. R. Soc. Lond. B. Biol. Sci.* **212,** 139–153 (1981).

22. Muller, J. A. Y. F. & Dacheux, R. F. Alpha ganglion cells of the rabbit retina lose antagonistic surround responses under dark adaptation. 395–401 (1997).

23. Luan, L. *et al.* Y-like retinal ganglion cells innervate the dorsal raphe nucleus in the Mongolian gerbil (Meriones unguiculatus). *PLoS One* **6,** e18938 (2011).

24. Demb, J. B., Zaghloul, K. & Sterling, P. Cellular basis for the response to second-order motion cues in Y retinal ganglion cells. *Neuron* **32,** 711–21 (2001).

25. Pang, J. J., Gao, F. & Wu, S. M. Light-evoked excitatory and inhibitory synaptic inputs to ON and OFF alpha ganglion cells in the mouse retina. *J Neurosci* **23,** 6063–6073 (2003).

26. Petrusca, D. *et al.* Identification and characterization of a Y-like primate retinal ganglion cell type. *J. Neurosci.* **27,** 11019–27 (2007).

27. Crook, J. D. *et al.* Y-cell receptive field and collicular projection of parasol ganglion cells in macaque monkey retina. *J. Neurosci.* **28,** 11277–91 (2008).

28. Huberman, A. D. *et al.* Architecture and activity-mediated refinement of axonal projections from a mosaic of genetically identified retinal ganglion cells. *Neuron* **59,** 425–438 (2008).

29. Huberman, A. D. & Niell, C. M. What can mice tell us about how vision works? *Trends Neurosci.* **34,** 464–73 (2011).

30. Van Wyk, M., Wässle, H. & Taylor, W. R. Receptive field properties of ON- and OFF-ganglion cells in the mouse retina. *Vis. Neurosci.* **26,** 297–308 (2009).

31. Margolis, D. J. & Detwiler, P. B. Different mechanisms generate maintained activity in ON and OFF retinal ganglion cells. *J. Neurosci.* **27,** 5994–6005 (2007).

32. Schubert, T. *et al.* Connexin36 mediates gap junctional coupling of alpha-ganglion cells in mouse retina. *J. Comp. Neurol.* **485,** 191–201 (2005).

33. Qiao, M., Sanes, J. R. & Duan, X. *In preparation*.

34. Bleckert, A., Schwartz, G. W., Turner, M. H., Rieke, F. & Wong, R. O. L. Visual space is represented by nonmatching topographies of distinct mouse retinal ganglion cell types. *Curr. Biol.* **24,** 310–5 (2014).

35. Buffelli, M. *et al.* Genetic evidence that relative synaptic efficacy biases the outcome of synaptic competition. *Nature* **424,** 430–434 (2003).

36. Zhang, Y., Kim, I.-J., Sanes, J. R. & Meister, M. The most numerous ganglion cell type of the mouse retina is a selective feature detector. *Proc. Natl. Acad. Sci. U. S. A.* **109,** E2391–8 (2012).

37. Enroth-Cugell, C. & Robson, J. The Contrast Sensitivity of Retinal Ganglion Cells of the Cat. *J. Physiol.* **187,** 517–552 (1966).

38. Enroth-Cugell, C. & Freeman, A. The Receptive-field spatial structure of cat retinal Y cells. *J. Physiol.* 49–79 (1987).

39. Victor, J. D. & Shapley, R. M. The nonlinear pathway of Y ganglion cells in the cat retina. *J. Gen. Physiol.* **74,** 671–89 (1979).

40. Peichl, L. & Wässle, H. The structural correlate of the receptive field centre of alpha ganglion cells in the cat retina. *J. Physiol.* **341,** 309–24 (1983).

41. Kim, I.-J., Zhang, Y., Meister, M. & Sanes, J. R. Laminar restriction of retinal ganglion cell dendrites and axons: subtype-specific developmental patterns revealed with transgenic markers. *J. Neurosci.* **30,** 1452–1462 (2010).

42. Bender, K. J. & Trussell, L. O. The physiology of the axon initial segment. *Annu. Rev. Neurosci.* **35,** 249–65 (2012).

43. Kole, M. H. P. & Stuart, G. J. Signal processing in the axon initial segment. *Neuron* **73,** 235–47 (2012).

44. Fjell, J., Dib-Hajj, S., Fried, K., Black, J. a. & Waxman, S. G. Differential expression of sodium channel genes in retinal ganglion cells. *Mol. Brain Res.* **50,** 197–204 (1997).

45. Boiko, T. *et al.* Functional specialization of the axon initial segment by isoform-specific sodium channel targeting. *J. Neurosci.* **23,** 2306–13 (2003).

46. Wollner, D. a & Catterall, W. a. Localization of sodium channels in axon hillocks and initial segments of retinal ganglion cells. *Proc. Natl. Acad. Sci. U. S. A.* **83,** 8424–8 (1986).

47. Fried, S. I., Lasker, A. C. W., Desai, N. J., Eddington, D. K. & Rizzo, J. F. Axonal sodium-channel bands shape the response to electric stimulation in retinal ganglion cells. *J. Neurophysiol.* **101,** 1972–87 (2009).

48. Llinas, R. & Nicholson, C. Electrophysiological Properties ofDendrites and Somata in Alligator Purkinje Cells. *J. Neurophysiol* 532–551 (1971).

49. Schwindt, P. & Crill, W. Local and Propagated Dendritic Action Potentials Evoked by Glutamate Iontophoresis on Rat Neocortical Pyramidal Neurons. *J. Neurophysiol.* **77,** 2466–2483 (1997).

50. Oesch, N., Euler, T. & Taylor, W. R. Direction-selective dendritic action potentials in rabbit retina. *Neuron* **47,** 739–50 (2005).

51. Velte, T. J. & Masland, R. H. Action Potentials in the Dendrites of Retinal Ganglion Cells. *J. Neurophysiol.* **81,** 1412–1417 (1999).

52. Van Wart, A., Trimmer, J. S. & Matthews, G. Polarized Distribution of Ion Channels within Microdomains of the Axon Initial Segment. 339–352 (2007).

53. Weber, P. *et al.* Mice Deficient for Tenascin-R Display Alterations of the Extracellular Matrix and Decreased Axonal Conduction Velocities in the CNS. *J Neurosci* **19,** 4245–4262 (1999).

54. Sun, W., Li, N. & He, S. Large-scale morphological survey of mouse retinal ganglion cells. *J. Comp. Neurol.* **451,** 115–26 (2002).

55. Badea, T. C. & Nathans, J. Quantitative analysis of neuronal morphologies in the mouse retina visualized by using a genetically directed reporter. *J. Comp. Neurol.* **480,** 331–51 (2004).

56. Duan, X., Krishnaswamy, A., De la Huerta, I. & Sanes, J. R. Type II Cadherins Guide Assembly of a Direction-Selective Retinal Circuit. *Cell* **158,** 793–807 (2014).

Chapter 4: The Responses of Mouse Alpha Retinal Ganglion Cells to Manipulated Natural Movies

4.1 Introduction

Much of what we know about the visual system has been discovered by driving neural responses with artificially produced visual stimuli. Such laboratory-generated stimuli, such as drifting gratings, are common in part because they are easily parameterized. By varying one parameter at a time and repeating the stimulus, the neural responses driven by specific stimulus features can be readily isolated. While such routine laboratory stimuli are useful to understand response properties of the retina, the majority of visual stimuli we personally encounter in our day-to-day interactions with the world are fundamentally different. Natural scenes tend to be more complex and they are dominated by high-order correlations in space and time. Only in rare cases can natural movies be reproduced with simple stimuli, such as a dark bird against a bright sky is approximated by a black dot on a white background. The complex structure of natural scenes makes it difficult to interpret the origin of neural responses unlike in the case of parameterized laboratory stimuli. Therefore, instead of directly driving neural responses with natural movies, some studies have drawn inspiration from natural vision, such as by reproducing saccadic eye movements, to probe visual responses[1–5]. Other studies have focused on specific features of visual scenes, such as the prevalence of dark contrasts or scale invariance, to explain response properties[6–12]. To investigate the responses of the A-RGCs to natural scenes, we chose to "parameterize" natural stimuli by performing spatial manipulations on movies motivated by the center-surround organization of retinal receptive fields. We could then compare the A-RGC responses to the original and manipulated movies to gain a sense of the relative importance of various components of the natural movie to the neural output.

The choice of what constitutes a natural stimulus is unfortunately somewhat arbitrary because the characteristics of visual environments vary. Some effort has been made to standardize stimuli, but for now the field of visual neuroscience has no defining rigorous criterion[13]. We chose to use two movies: a human simulation of what a mouse may see outdoors and a recording in an indoor arena from a small camera attached to a mouse's head. Both are meant to closely approximate the input to the photoreceptors under self-motion with the former at higher spatial and temporal resolution with the latter incorporating natural movements of the mouse. This approach to use movies from "critter-cams" has been utilized to study the retina at least once before with the so-called W3 RGCs[14]. The W3 cells, the smallest RGCs in the mouse retina, showed markedly different responses to artificial and natural stimuli. The cells responded robustly to the standard moving spot experimental stimulus, but rarely responded to movies of retinal input dominated by global-motion[14]. Examples such as this are a reminder that to fully understand the function of the retina, it is important to test responses to stimuli that mimic ones in the natural world.

We took advantage of the recently reported KCNG4^{Cre} transgenic mouse line that selectively labels the A-RGCs in the ganglion cell layer when crossed with the *Thy1-STOP-YFP* fluorescent reporter[15–17]. Importantly, all A-RGCs recorded responded robustly to our chosen natural movies that were dominated by global motion. Additionally the On-Sustained and Off-Sustained responses nearly perfectly mirrored each other indicating the A-RGCs continuously encode natural scenes. We also found the visual responses, across the A-RGC population, to change surprisingly little when

stimulated with the manipulated movies. Based on this, we propose that the A-RGCs may perform simple spatial processing on visual input under natural conditions.

4.2 Comparison of alpha retinal ganglion cell responses to original and manipulated natural movies

Using the KCNG4^{Cre} transgenic mouse line, we targeted the fluorescently labeled A-RGCs with patch electrodes for cell-attached recording of extracellular action potentials. After a brief characterization of the cell type, we began to stimulate the cells with natural movies. We chose two movies to show to the retina: one a human approximation of what a mouse may experience in the outside world and the second a "mouse cam" recording from a mouse's head while moving freely in an arena (Figure 4.1). The mouse cam movie differs from the so-called simulated mouse movie by containing the natural statistics of mouse head movement.

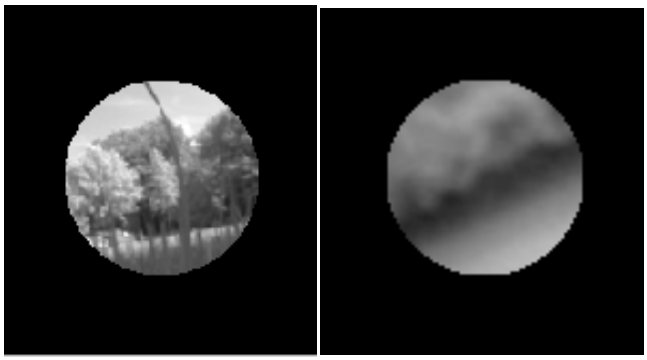

Figure 4.1: The first frames from the simulated mouse (left) and mouse cam (right) natural movies covered with a 1000 µm circular mask. For clarity, the area outside of the movie is shown in black in the figure, but in the experiment it was grey. The mouse cam movie was recorded at lower spatial and temporal resolution due to weight constraints limiting the choice of camera.

Our general approach was to manipulate these movies and calculate how much the A-RGC responses changed under the new stimulus conditions. The similarity of the responses allowed us to gain a sense for the relative importance of altered components of the visual scene in shaping the output of the cell. We determined the A-RGC spiking responses by showing multiple (6-8) repetitions of both movies and calculating the peristimulus time histogram (PSTH) by binning at twice the stimulus frame rate. To assess the degree of similarity under the two conditions, we calculated the average correlation coefficient across single trials. This gave us an unbiased, quantitative way to assess the similarity of the alpha RGC responses under the two stimulus conditions.

We performed four primary manipulations to each frame of the natural movies. The first was to blur the movie to replicate the effect of the optics of the mouse eye. The second was to rotate the movie by 180 degrees. The third was to partly, or completely, remove spatial information in the RGC surround. The last manipulation was to average the pixels in the receptive field center (Figure 4.2).

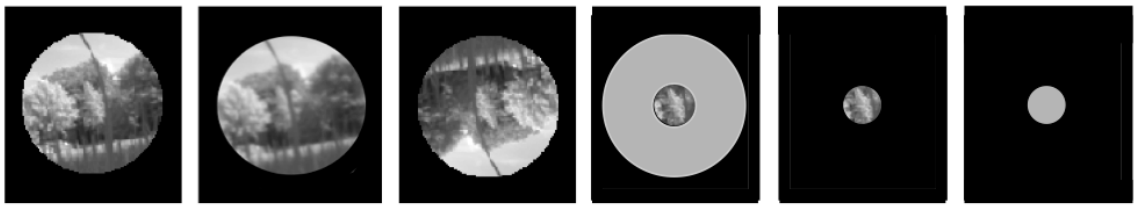

Figure 4.2: Example frames from each of the manipulated simulated mouse natural movies. The original stimulus with a mask of R = 500 µm is on the far left. Moving to the right, the stimuli become progressively less similar to the original. The second stimulus is blurred to approximate mouse optics and the third is the original movie rotated by 180 degrees. The fourth and fifth stimuli have manipulated surrounds while keeping the center the same as the original (R = 125 µm). The surround is either averaged for each frame or removed entirely, respectively. The last stimulus on the far right is the average of the central pixels for each frame. For clarity, the area outside of the movie is shown in black in the figure, but in the experiment it was grey.

4.2.1 A-RGC responses to original natural movies

To assess the degree of similarity between the original and manipulated movies, we first needed to measure the responses to the original movie. It is well known that RGCs, and neurons in general, respond to stimuli with a certain level of stochasticity. Thus, repeats of the same stimulus will elicit slightly different neural responses. To quantify the similarity of the responses to the original movie, we compared single spike trains from multiple repetitions of the same stimulus. In practice, the spike trains were binned at twice the stimulus frame rate, 33 ms, and the average Pearson's correlation coefficient was calculated across repetitions. We chose the bin width to be of the same order of magnitude as the A-RGC response latency. By correlating the individual spike trains, rather than the average response, we captured the intrinsic noise of the cell. Thus when we compared spike trains from different stimulus conditions, we could assess how much of the variation resulted from the change in stimulus and how much resulted from innate neural noise. On average, individual spike trains from a single cell to the original movies were between 80 – 90% correlated across trials under both the simulated mouse and mouse cam movies. This indicated a baseline 10-20% decrease in correlation comparing any two spike trains, of the same cell, due to intrinsic neural noise. We visualized the level of noise by plotting the standard error of the mean along with the average firing rate (Figure 4.3). Each graph was color coded to indicate the A-RGC type; Red = Off-Transient, blue = Off-Sustained, green = On-Transient, and black = On-Sustained. The average correlation across cells to trials of the same stimulus for the Off-Transient, Off-Sustained, On-Transient, and On-Sustained A-RGC were 81±5%, 86±4%, 85±6%, and 89±4%, respectively. For example, we could not expect the average

correlation coefficient between spike trains from different stimuli to be more than 86% for the Off-Sustained A-RGCs. Therefore, we assessed the response similarity under different stimuli by the ratio of the correlation between different stimuli to the correlation within the same stimulus, i.e. 86% for the Off-Sustained, rather than by the absolute correlation values (see Chapter 2 for more detail).

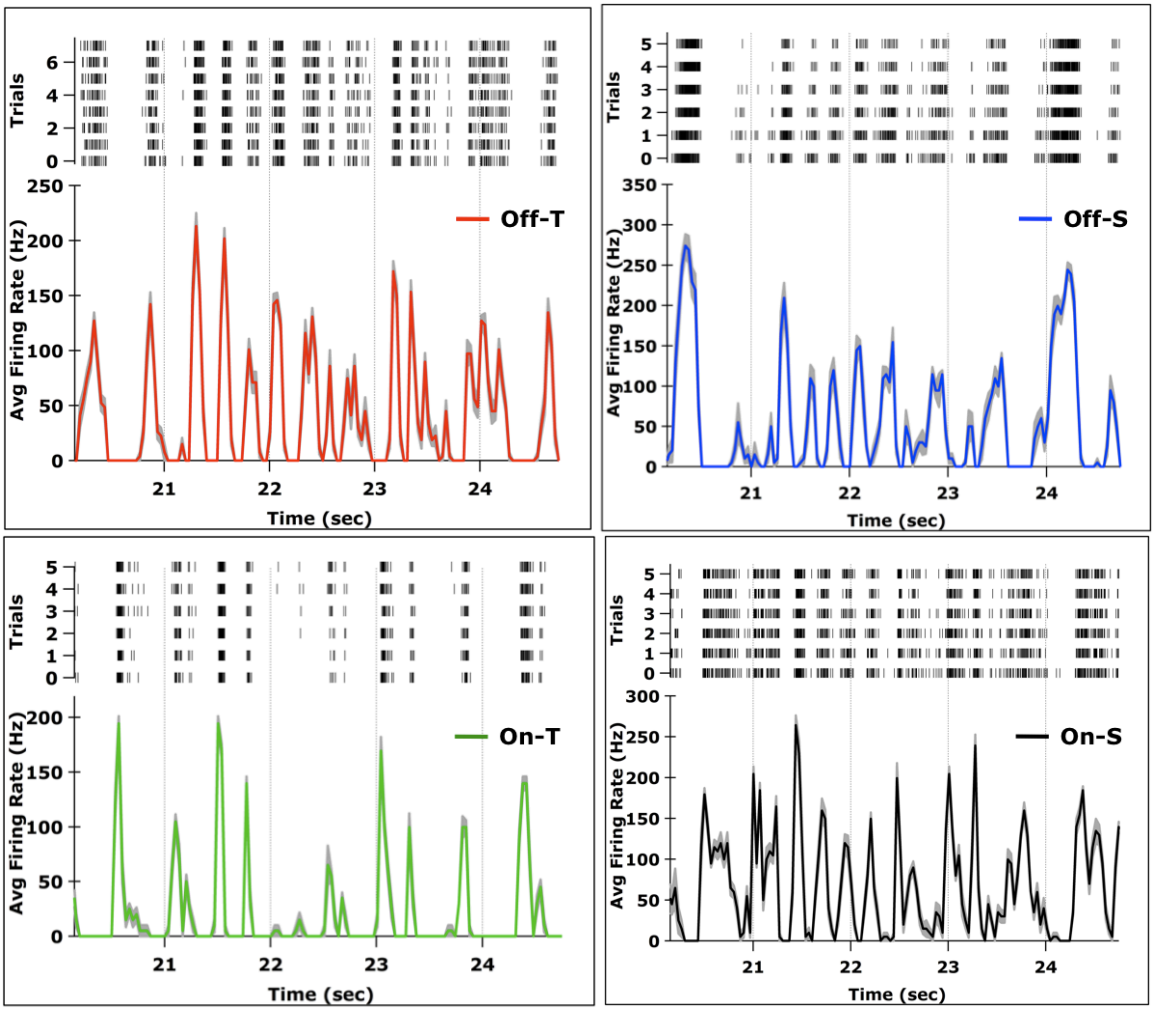

Figure 4.3: Example responses from each of the A-RGCs to the same portion of the simulated mouse natural movie. A raster graph for each repeat of the stimulus is at the top with the average response histogram at the bottom (33 ms bins)

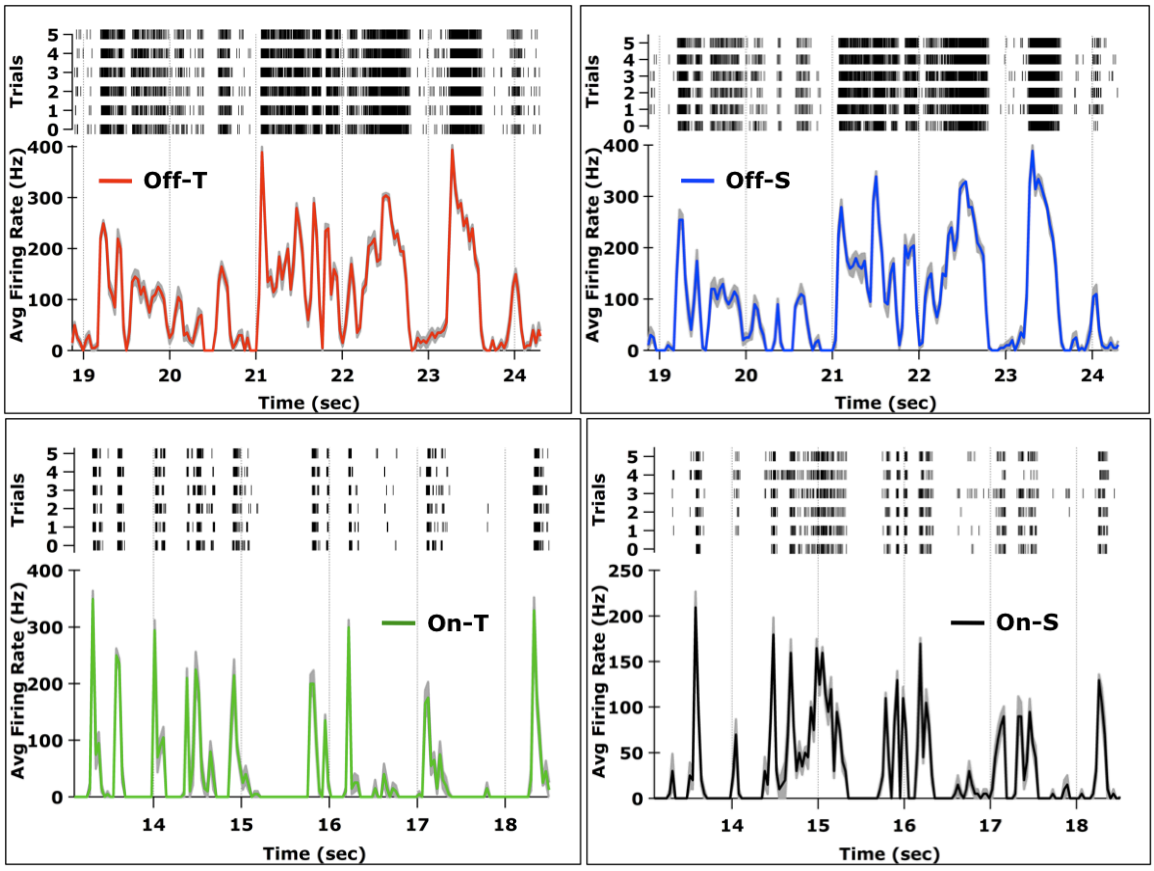

Figure 4.4: Example responses from each of the A-RGCs to the same portion of the "mouse cam" natural movie for the Off and On cells, respectively. A raster graph for each repeat of the stimulus is at the top with the average response histogram at the bottom (33 ms bins). The Off-Transient responses are subtly more transient than the Off-Sustained.

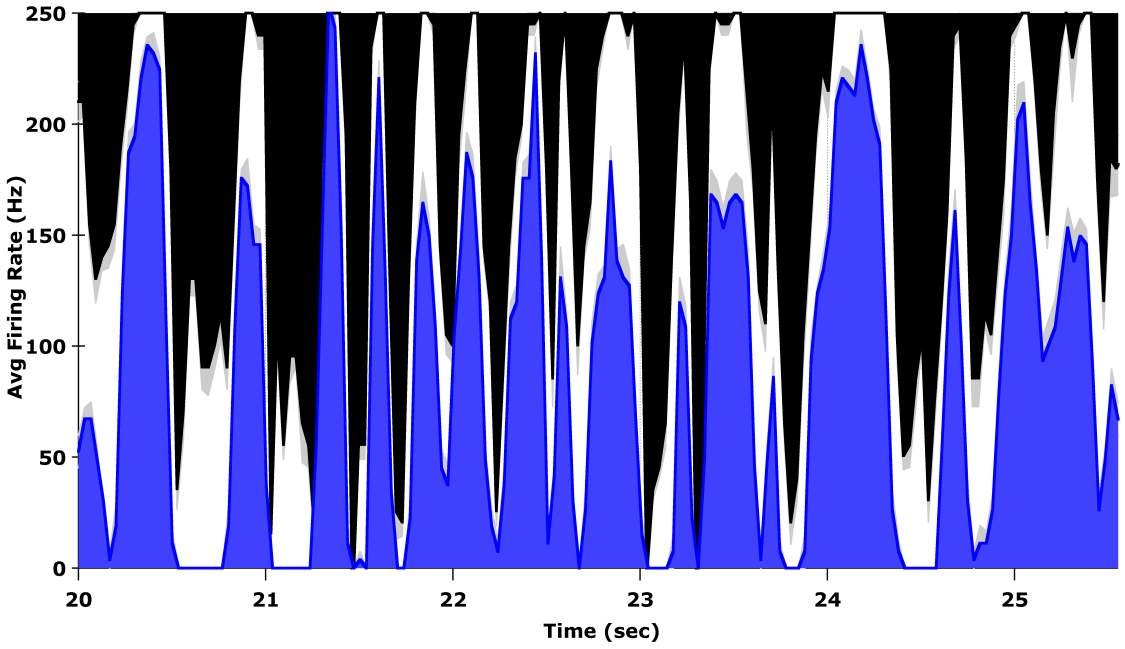

Figure 4.5: Off-Sustained (blue) and On-Sustained (black) A-RGCs responses to the simulated mouse movie mirror each other.

4.2.2 Movie blurred to approximate distortion by mouse optics

Recognizing that the spatial resolution of our natural movies taken with cameras and shown to the retina *in vitro* may deviate from actual stimuli that fall on the retina, we blurred the simulated mouse movie to account for the optics of the mouse eye. Though the literature claims that mice are both myopic and hyperopic, the reported modulation transfer functions of the mouse eye in all reports are similar[18,19]. We chose to filter the movie based on the worst possible estimate of mouse optics. The modulation transfer function we used included all aberrations, such as defocus and astigmatism (Figure 4.6). 50% modulation transfer amounted to 6.3 cycles per alpha RGC receptive field. Thus, the movie was blurred on the scale of 20 um.

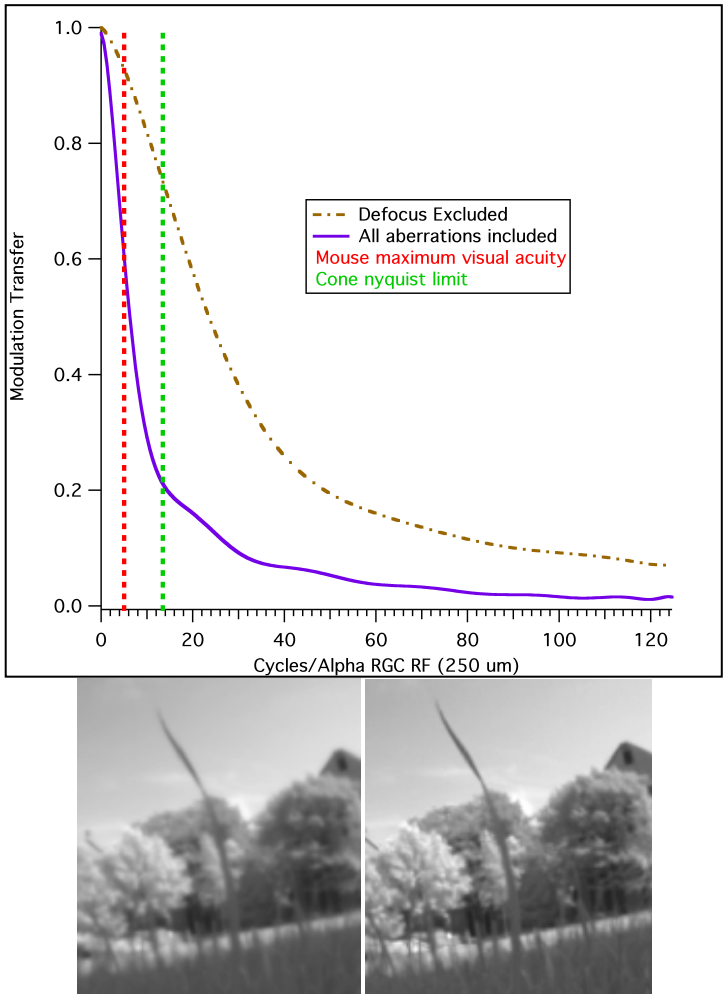

Figure 4.6: Modulation transfer function used to filter the simulated mouse natural movie (top). The curves were reproduced from Geng et al. (2011) and the purple used as the "worst case" to approximate the blur of the mouse optics. Examples frame from the blurred movie (bottom, left) and the original movie are shown below (bottom, right).

The responses of the A-RGCs to the blurred movie were highly correlated to the responses of the unmodified movie. For each RGC type, the correlation was above 70%. The responses to the original and blurred movies for the Off- and On-Transient A-RGCs were each 75±10%. For the Off-Sustained and On-Sustained A-RGCs, the correlations were 99±3% and 98±5%, respectively. It is unsurprising that removing high frequency information had little effect on the Off-Sustained cells considering they have receptive fields with the lowest spatial resolution. It is less expected that the responses of the On-Sustained cells, with robust responses to gratings with ~30 um bars, were equally unaffected. This may be because the blurring of the movie was on the scale of 20 um and thus at the limit of their spatial resolution. The same is true for the transient A-RGCs. Therefore, the "worst case" blur of the image on the retina either had no effect, in the case of the sustained cells, or a minimal effect leaving the majority of the light responses intact, for the transient cells.

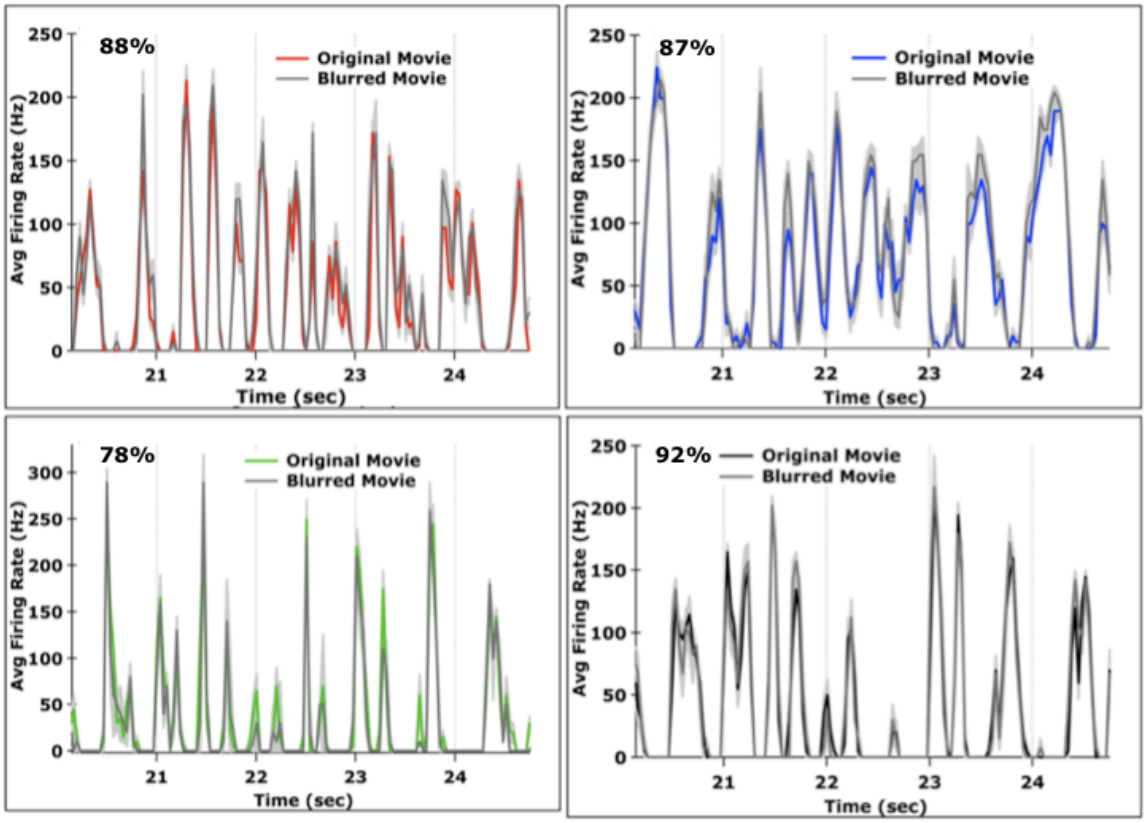

Figure 4.7: Comparison of average responses to original and blurred simulated mouse movie. The correlation between the original and blurred movies for the particular data in each panel is given in the upper left hand corner. Red = Off-Transient, blue = Off-Sustained, green = On-Transient, and black = On-Sustained. Dark grey are the responses from each cell to the manipulated movie.

4.2.3 Movies rotated by 180 degrees

Based on their responses to moving spots, we claimed the A-RGCs to be responsive to motion, but not direction selective (see Chapter 3, Figure 3.10). Therefore, we expected the responses of the A-RGCs to be mostly unaffected by rotation of the natural movies. To test this, we recorded the responses of the A-RGCs to both movies rotated by 180 degrees.

As predicted from the moving spot stimuli, the majority of the alpha responses were shared between the responses to the original and manipulated movies. On average, the responses to the original and rotated movies were 70-99% correlated for both the simulated mouse and mouse cam movies.

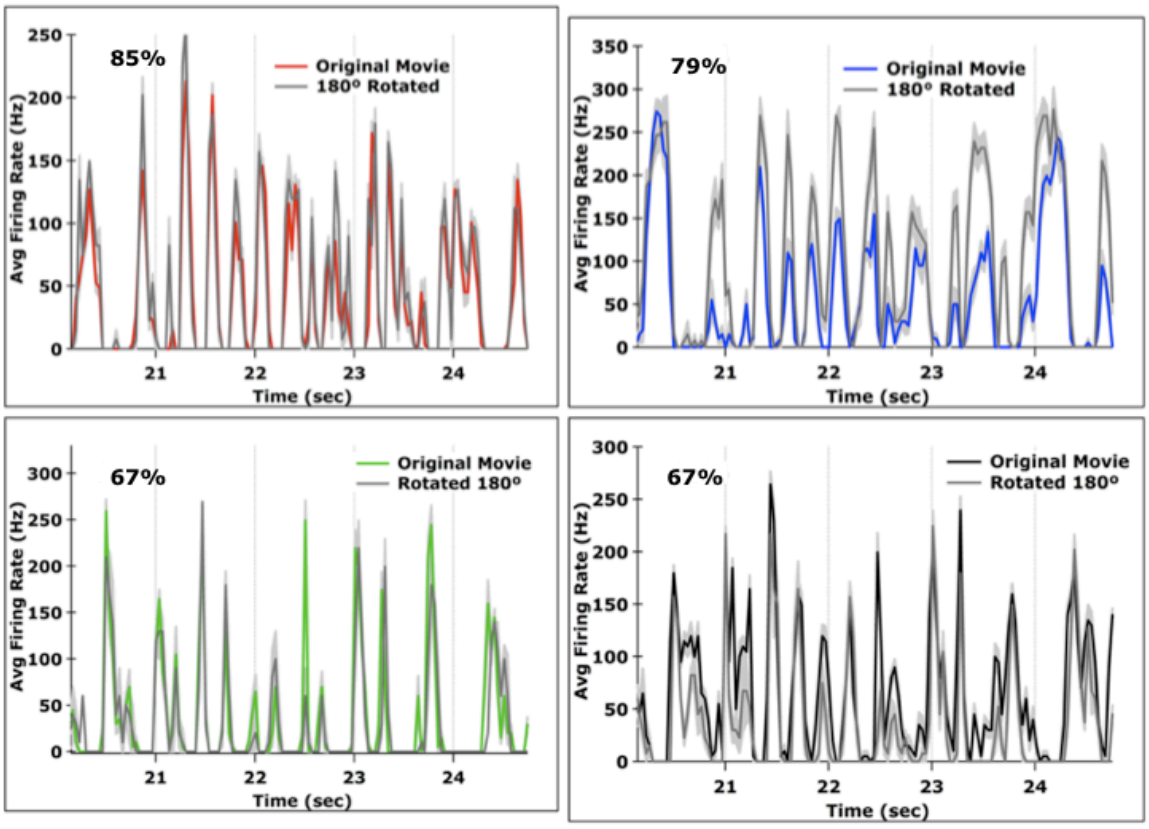

Figure 4.8: Example responses to the original and 180 degree rotated simulated mouse movie for each A-RGC type. The correlation between the original and rotated movies for the particular data in each panel is given in the upper left hand corner. Red = Off-Transient, blue = Off-Sustained, green = On-Transient, and black = On-Sustained. Dark grey are the responses from each cell to the manipulated movie. The significant deviation of the rotated response magnitude for the Off-Sustained example was not systematic. Sometimes the magnitude of the A-RGC responses would change over time and the change was particularly dramatic for some Off-Sustained cells.

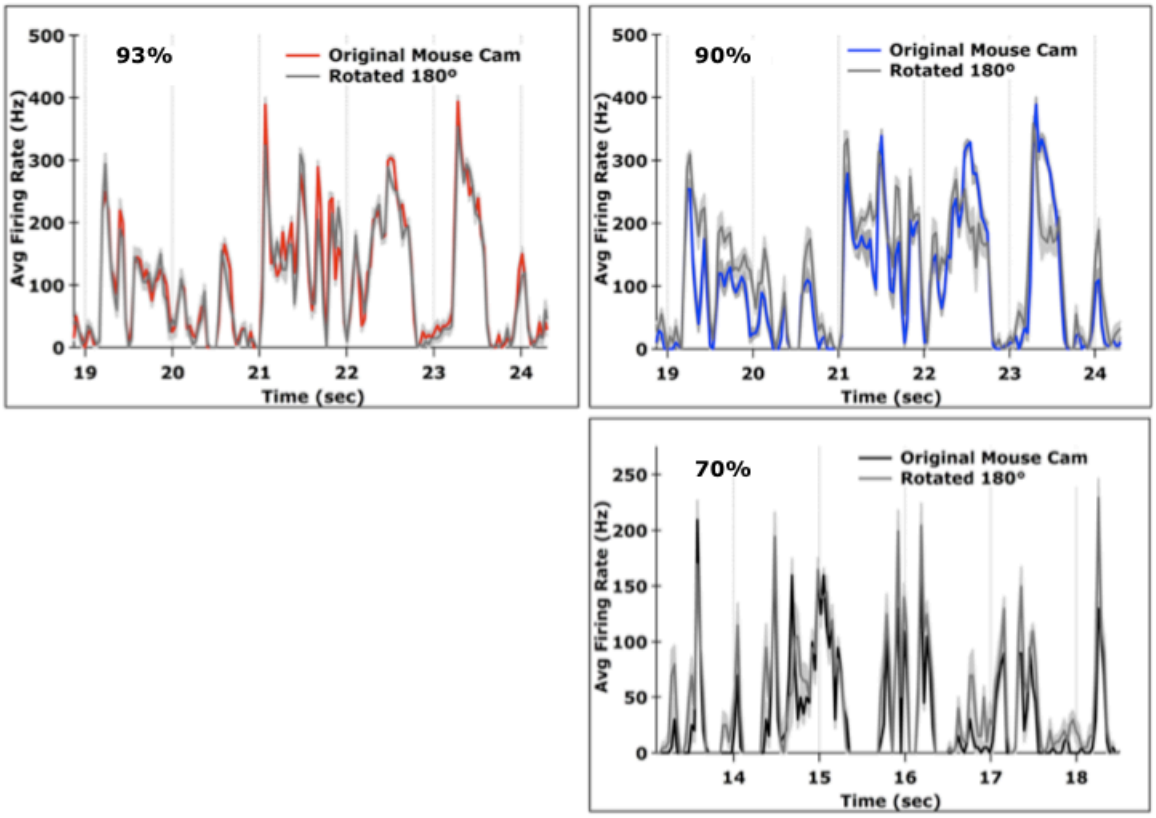

Figure 4.9: Comparison of average responses to original and 180 degree rotated mouse cam movie. The correlation between the original and rotated movies for the particular data in each panel is given in the upper left hand corner. Red = Off-Transient, blue = Off-Sustained, green = On-Transient, and black = On-Sustained. Dark grey are the responses from each cell to the manipulated movie.

Across all A-RGC types, the Off-Transient responses were the least effected by the stimulus rotation with average response correlations of 89±2% and 91±7%, respectively, to the simulated mouse and mouse cam movies (Figures 4.8 & 4.9). The similarity in responses for the Off-Sustained RGCs was more variable depending on the stimulus. Again to the simulated and mouse cam movies, the responses were 78 and 99±3% correlated with the original. The significant deviation of the rotated response magnitude in Figure 4.8 for the Off-Sustained example was not systematic. Thus, both the Off-Transient and Off-Sustained cells were largely unaffected by the rotation of the movie. This suggests that our claim from moving spots, that the A-RGCs are not direction selective, is also true under more natural stimuli. The same trend holds for the On A-RGCs. The On-Sustained cells were 88±6% and 82±8% correlated, respectively, for the simulated and mouse cam movies. The On-Transient cells were the least correlated, ~70%, but with fewer examples.

By comparison, responses of non-alpha direction selective RGCs showed no similarity (0% correlation) under the original and rotated simulated mouse movie (Figure 4.10). Even the responses of a non-direction selective, non-alpha Off RGC were only 50% similar under the two stimuli (data not shown). Therefore compared to other types of RGCs, the responses of all the A-RGCs seem to be less sensitive to stimulus rotation. As found using moving binary spot stimuli, the A-RGCs are not selective to motion in a particular direction and this property holds under more natural stimulus conditions.

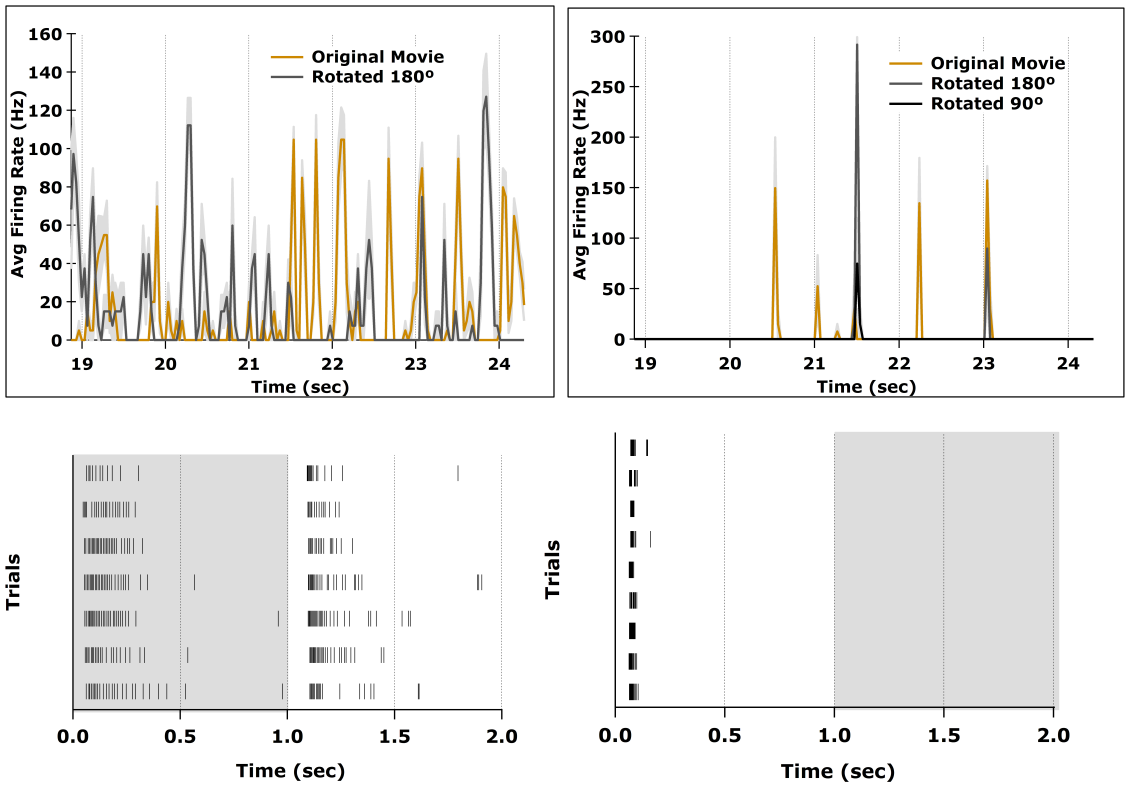

Figure 4.10: Responses from two non-alpha, direction selective cells to the original and rotated simulated mouse movie. Example responses to flashing spots are in the lower raster graphs. The responses of the On-Off DS-RGC (left) and On DS-RGC (right) to the rotated movie are 0% correlated with the original (n=3).

4.2.4 Movies with averaged or removed surrounds

Encouraged by the similarity between the original and rotated movie responses, we started gauging the importance of various regions of the A-RGC receptive fields in generating the output to natural movies. We started by manipulating the surround. Considering the comparatively weak surrounds of the A-RGCs to flashing binary spots (Chapter 3, Figure 3.8, top), we wondered how much the stimulus in the surround influenced the responses to more natural stimuli[14]. To test this we used two stimuli: one with an averaged surround and one with the movie restricted to the center of the receptive field (D = 200 - 250 um). In the first stimulus, we took a flat average of the classical surround (i.e. the entire masked movie) for each frame. The values for the average we obtained when weighting the surround based on the difference of Gaussian fit to the spatial receptive field were essentially the same across cells (data not shown). In the second stimulus, the movie in the surround was replaced with solid grey (Figure 4.2). The first stimulus tests the computation of spatial information in the surround. If spatial summation in the surround is highly nonlinear, averaging the surround should greatly affect the responses from the A-RGCs. Alternatively, the responses should also vary if the neurons average the surround differently than our estimate. We found the responses to the original movie and the movie with the averaged surround to be very similar across the population of A-RGCs. This indicates either that the spatial summation of light across the receptive field surround is fairly linear, or that the surround has little influence on the overall responses. The responses of all the A-RGCs to the manipulated simulated mouse movie, with the exception of the On-Transient that were not tested, were 86-99% correlated with the original. Under the mouse cam stimulus, the entire Off population was

essentially unaffected by the manipulation with correlations of 99±3% to the original. The On-Sustained responses to both the simulated and mouse cam movies changed by the same amount (86±8% correlated to the original). In general, averaging the surround affected the A-RGC responses by less than 15%.

The second manipulation to the surround, removing it entirely, directly tested how much the stimulus in the surround influenced the neural output under these two natural movies. With both the simulated mouse and the mouse cam movies restricted to the center of the receptive field (D = 200 - 250 μm), the correlation to the original data was above 70% for each A-RGC type. The responses of Off- and On-Sustained cells were the least affected by removing the surround and were 80-90% correlated with the original. The Off- and On-Transient cells were more variable. Under the simulated mouse movie, the Off-Transient responses were only 74±3% similar, but under the mouse cam they were 93±7% similar. The opposite trend was true for the On-Transient responses that were 82% and 72% correlated, respectively. In general, the surround seemed to have a relatively minor influence on the final responses of the A-RGCs to these natural movies.

By comparing the difference in responses between the two stimuli with manipulated surrounds, we could speculate on the computation performed by the A-RGC surround. If the similarity in responses dropped between these two manipulations, it suggested that a linearly summed surround shaped the output of the A-RGCs. On the other hand, if averaging and removing the surround decreased the response similarity by the same amount, this indicated the input in the surround was nonlinearly summed or that we did not capture the actual A-RGC surround weighting with our estimate. The responses of the Off- and On-Sustained A-RGCs were equally influenced by both

manipulations. This result suggested any drop we saw in response correlation was due to a non-linearly summed or poorly estimated surround. Again, the surround stimulus was calculated by a flat average, but no difference was seen when using the weighting for the surround obtained by the difference of Gaussian fit to the spatial receptive field. Specifically, the sustained A-RGCs were 85% correlated, or higher, to the original responses when the surround was manipulated, suggesting the surround influenced ~15% of the responses to these movies. The two stimulus conditions cannot be compared for the On-Transient A-RGCs, but their responses were comparable to the On-Sustained suggesting nonlinear surround computation for the majority of the A-RGCs. The results were different for the Off-Transient cells. Under both natural movies the correlation across the two surround manipulations dropped by 7%. This correlation drop indicated that two surround mechanisms might have been active in the Off-Transient A-RGCs to both linearly and nonlinearly average the surround. Overall, A-RGC nonlinear subunits primarily drove the influence from the surround, or our understanding of the underlying computation was lacking, with the exception of the Off-Transient cells that appeared to be more complicated.

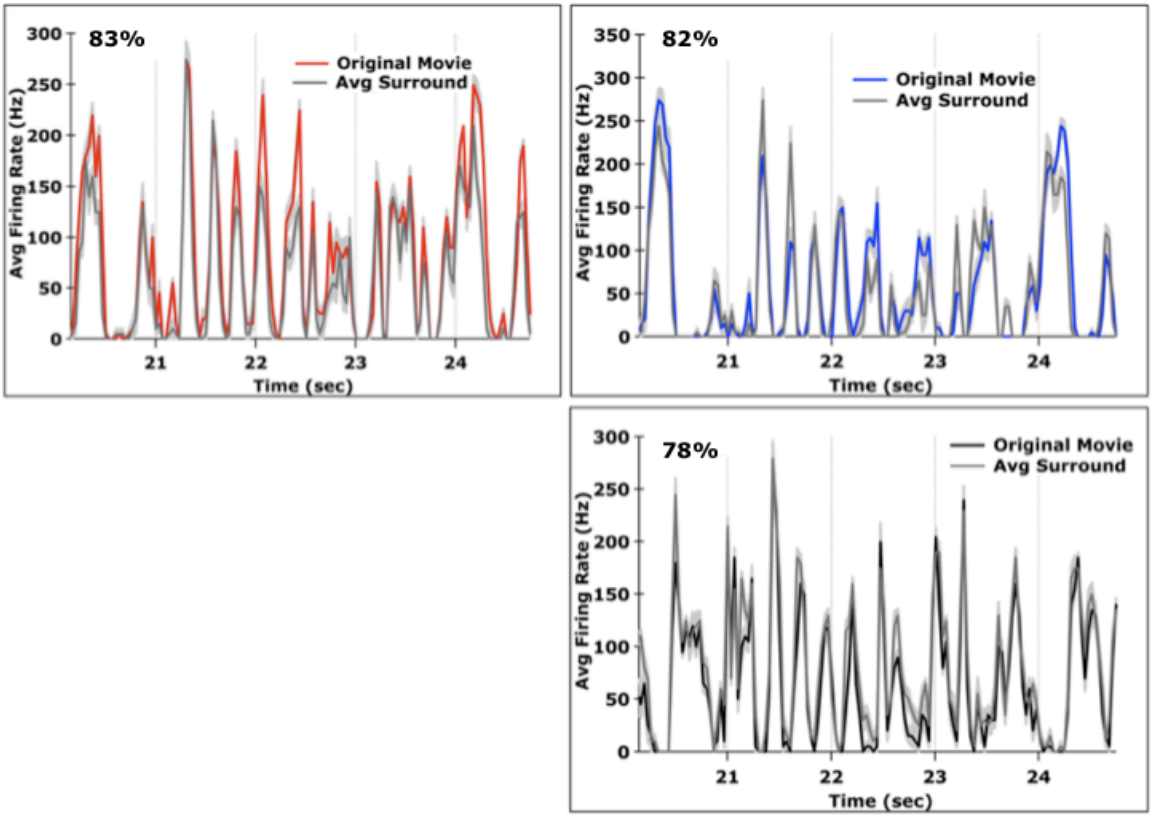

Figure 4.11: Comparison of average responses to original and simulated mouse movie with an averaged surround. The correlation between the original and manipulated movies for the particular data in each panel is given in the upper left hand corner. Red = Off-Transient, blue = Off-Sustained, green = On-Transient, and black = On-Sustained. Dark grey are the responses from each cell to the manipulated movie.

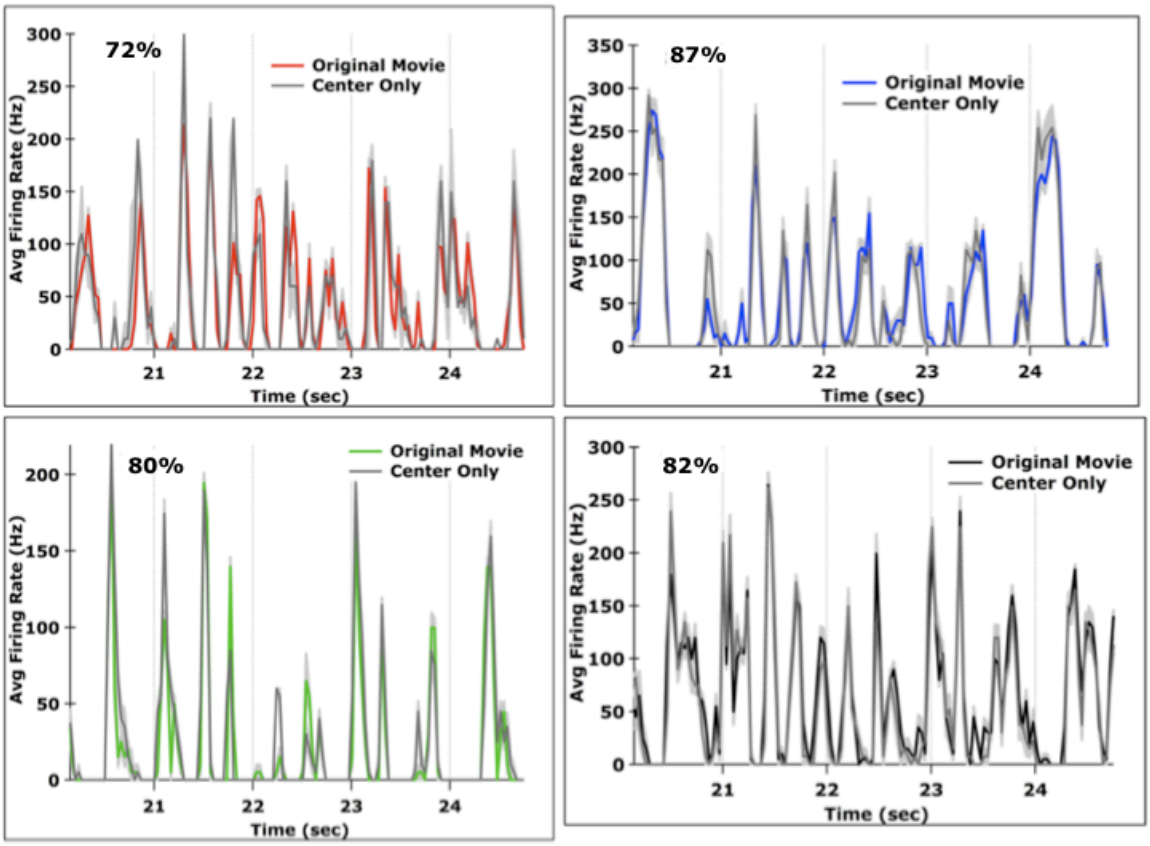

Figure 4.12: Comparison of average responses to original (R = 500 um) and simulated mouse movie in the center of the receptive field (R = 125 um). The correlation between the original and central movies for the particular data in each panel is given in the upper left hand corner. Red = Off-Transient, blue = Off-Sustained, green = On-Transient, and black = On-Sustained. Dark grey are the responses from each cell to the manipulated movie.

The responses of non-alpha RGCs to the simulated mouse movie with a removed surround were less correlated to their original responses than the A-RGCs (Figure 4.12). The correlations ranged from 0-49% similarity with the original. Therefore, the similarity in the A-RGC responses to the original and manipulated movies were consistently higher than randomly selected murine RGCs (Figure 4.13).

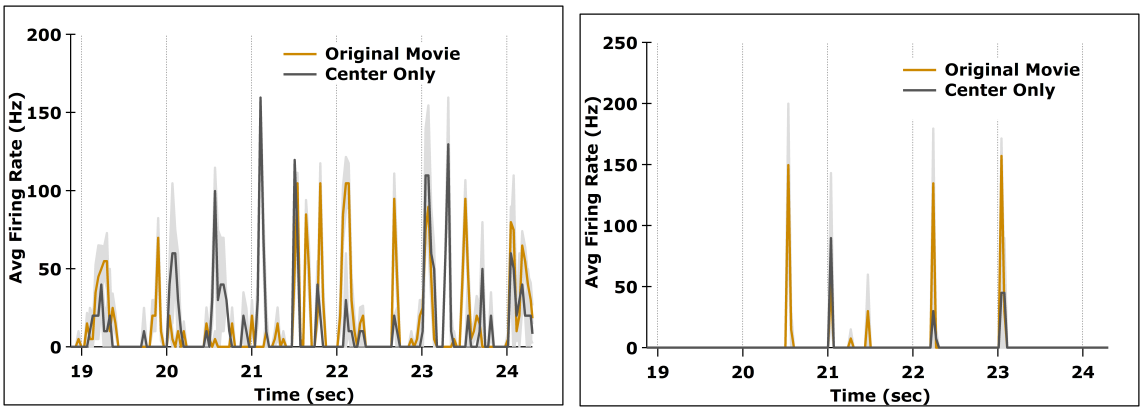

Figure 4.13: Example responses from non-alpha RGCs to the original (R = 500 µm) and center only (R = 200-250 µm) simulated mouse movie. These are the same On-Off (left) and On (right) cells from Figure 4.10.

4.2.5 Movies obtained by averaging the central pixels of the original movie

Since removing the surround from the movies left over 70% of the A-RGC responses to the original movie intact, we tested the final and most extreme of the movie manipulations: averaging the movie pixels in the receptive field center. Specifically, we took a flat average of the pixels in the center, within a 250 μm mask, for each frame (Figure 4.2). This manipulation discarded nearly all the spatial information in the stimulus considering the surround had already been replaced by a grey annulus. In this new stimulus, the average luminance across the receptive field center remained unchanged from the original, but the fine spatial information was lacking. Based on an earlier finding that A-RGCs nonlinearly sum light input across their receptive field centers (see Chapter 3, Figure 3.6), we expected that removing the fine spatial information from the stimulus would dramatically change their responses.

Comparing the original responses of the A-RGCs to those from these extremely simplified versions of the natural movies, we were surprised to find them quite similar. Each RGC type had a correlation with the original responses above 65%. Consistent with their spatially low-resolution receptive fields, the responses of the Off-Sustained RGCs under the new stimulus were the most similar. Their responses to the simulated mouse and mouse cam movies were 79% and 99% correlated, respectively. Unexpectedly, the response correlations for the other three alpha RGC types were no less than 65% (Figure 4.14). The On population showed roughly the same response similarity with ~82% and ~70% correlated responses to the simulated mouse and mouse cam movies, respectively. This result was unanticipated considering the On A-RGCs were shown to have spatially nonlinear receptive fields down to ~30 μm bars. The similarity of the Off-Transient cell

responses differed across the two movies with either an average 68% or 99% correlation, respectively, depending on stimulating with the simulated mouse or mouse cam movie. In general, the time course and gain of the responses changed under stimulation with the averaged central pixel movies. The timing of each peak in firing rate was later by one bin (~33 ms), the peak firing rates were higher, and firing rate dropped off at the same rate making the peaks under the average central pixel movies sharper (Figures 4.14 & 4.15). The sharper peaks were seen across all A-RGC types and for both the simulated mouse and mouse cam natural movies regardless of the order of presentation of stimuli during the experiment (Figure 4.16).

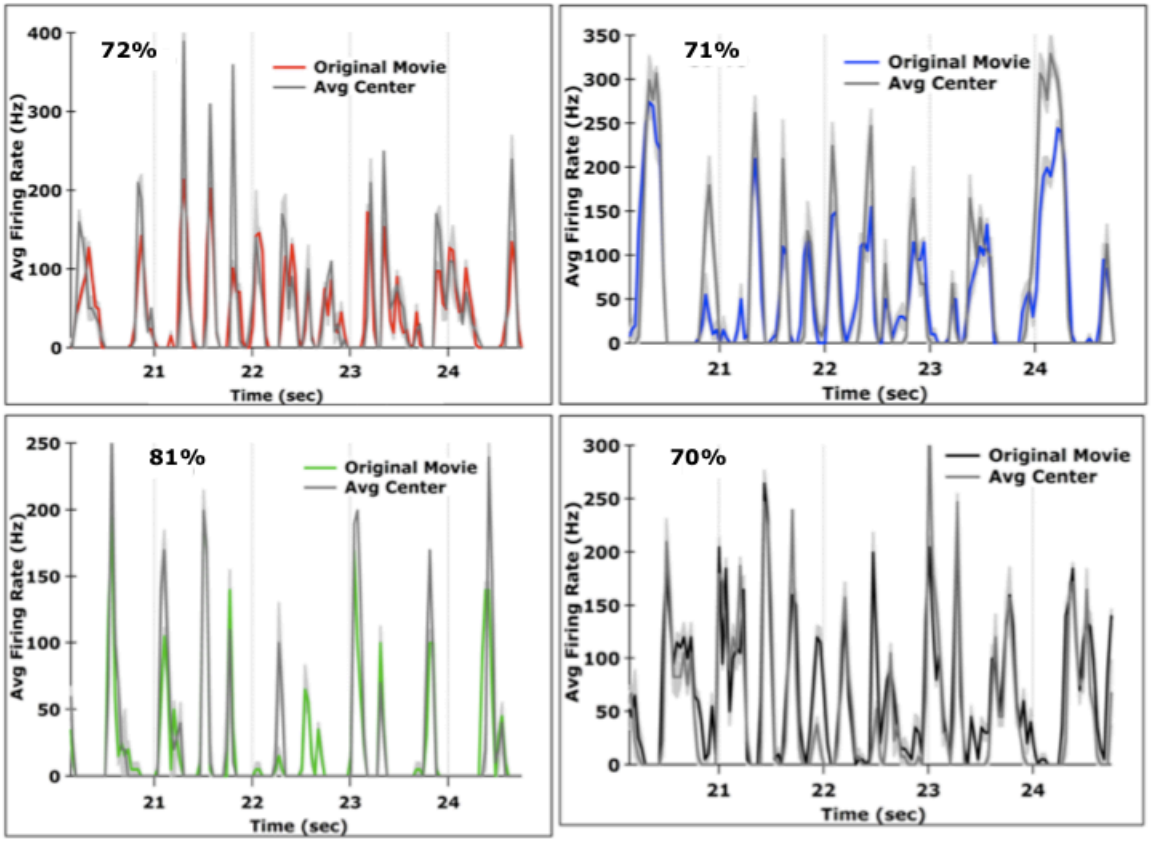

Figure 4.14: Comparison of average responses to original and simulated mouse movie with the central pixels of each frame averaged. The correlation between the original and manipulated movies for the particular data in each panel is given in the upper left hand corner. Red = Off-Transient, blue = Off-Sustained, green = On-Transient, and black = On-Sustained. Dark grey are the responses from each cell to the manipulated movie.

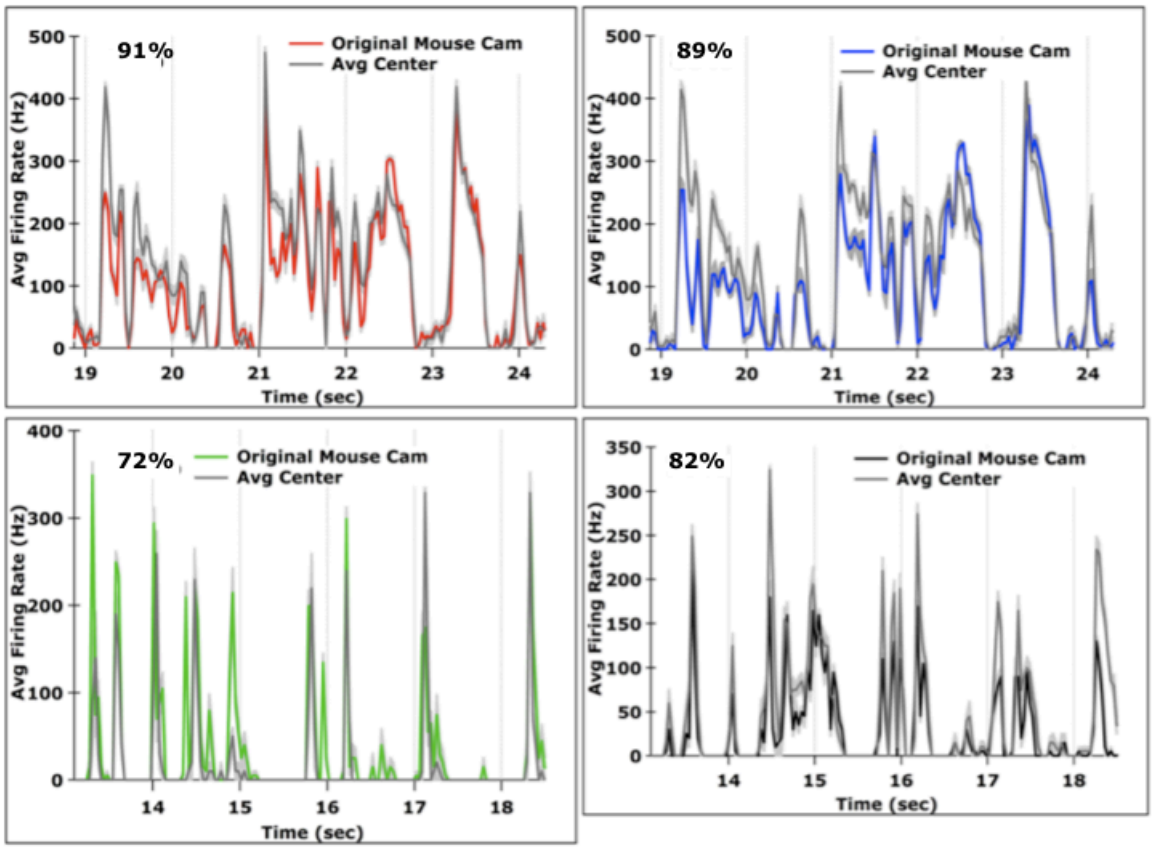

Figure 4.15: Comparison of average responses to original and "mouse cam" movie manipulated by averaging the central pixels of each frame. The correlation between the original and averaged center movies for the particular data in each panel is given in the upper left hand corner. Red = Off-Transient, blue = Off-Sustained, green = On-Transient, and black = On-Sustained. Dark grey are the responses from each cell to the manipulated movie.

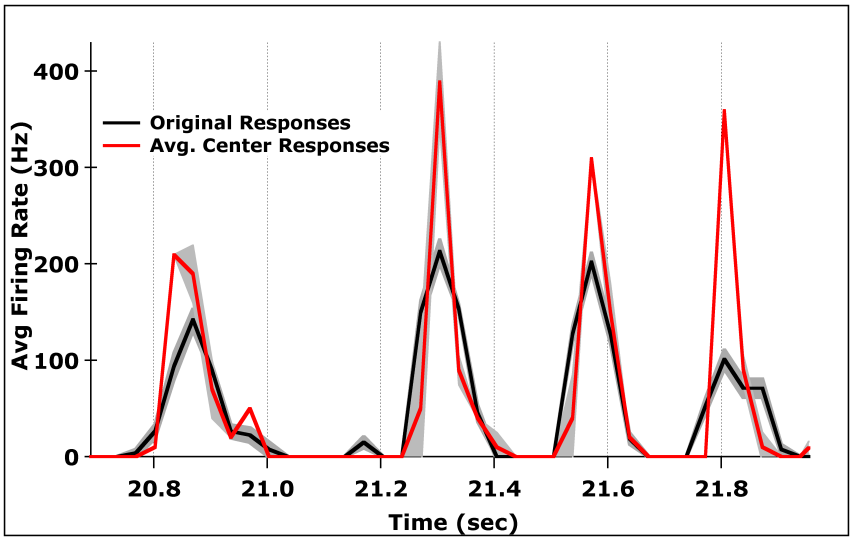

Figure 4.16: Off-Transient A-RGC responses to the averaged center movie are sharper and slightly delayed relative to the original movie responses.

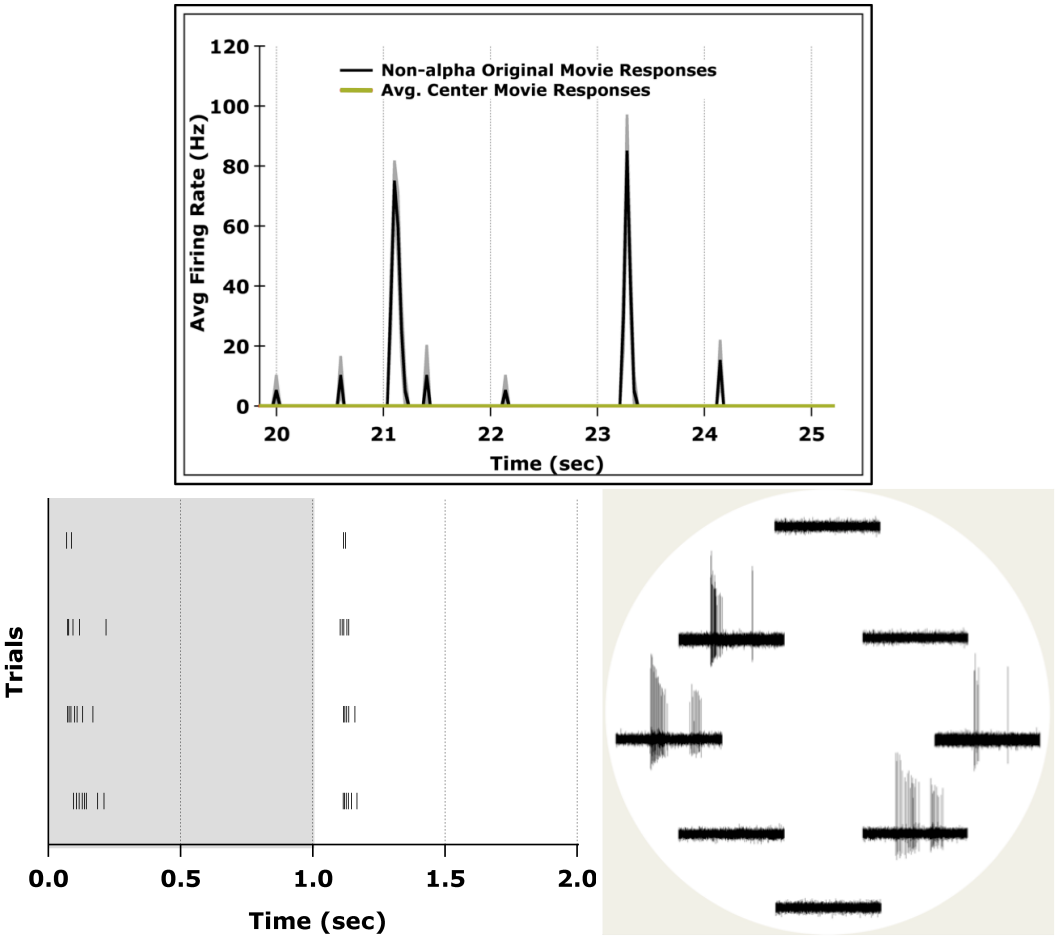

Figure 4.17: Example responses of an On-Off direction selective cell to the original (black) and averaged center (gold) simulated mouse movies. The responses to the original movie are sparser than those of the A-RGCs and they disappear entirely for the averaged center movie (top). In general, this cell performs computations different from the A-RGCs as seen in the On-Off (bottom left) and direction selective (bottom right) responses.

For all the A-RGCs, the similarity in responses to the manipulated versions of the original movies was greater than the similarity in responses for non-alpha RGCs under the same stimulus conditions (Figure 4.18). This indicated that the A-RGCs performed more simple computations on these natural movies than other RGC types. Additionally, the decrease in correlation between the responses to differing movies was often roughly the same as the correlation within repeats of the original movie (Figure 4.18, y-axis). Overall, based on the high degree of similarity between the responses to the original and averaged center movies, the majority of the responses of the entire A-RGC population to the simulated mouse and mouse cam natural movies depended on the average stimulus in the receptive field center.

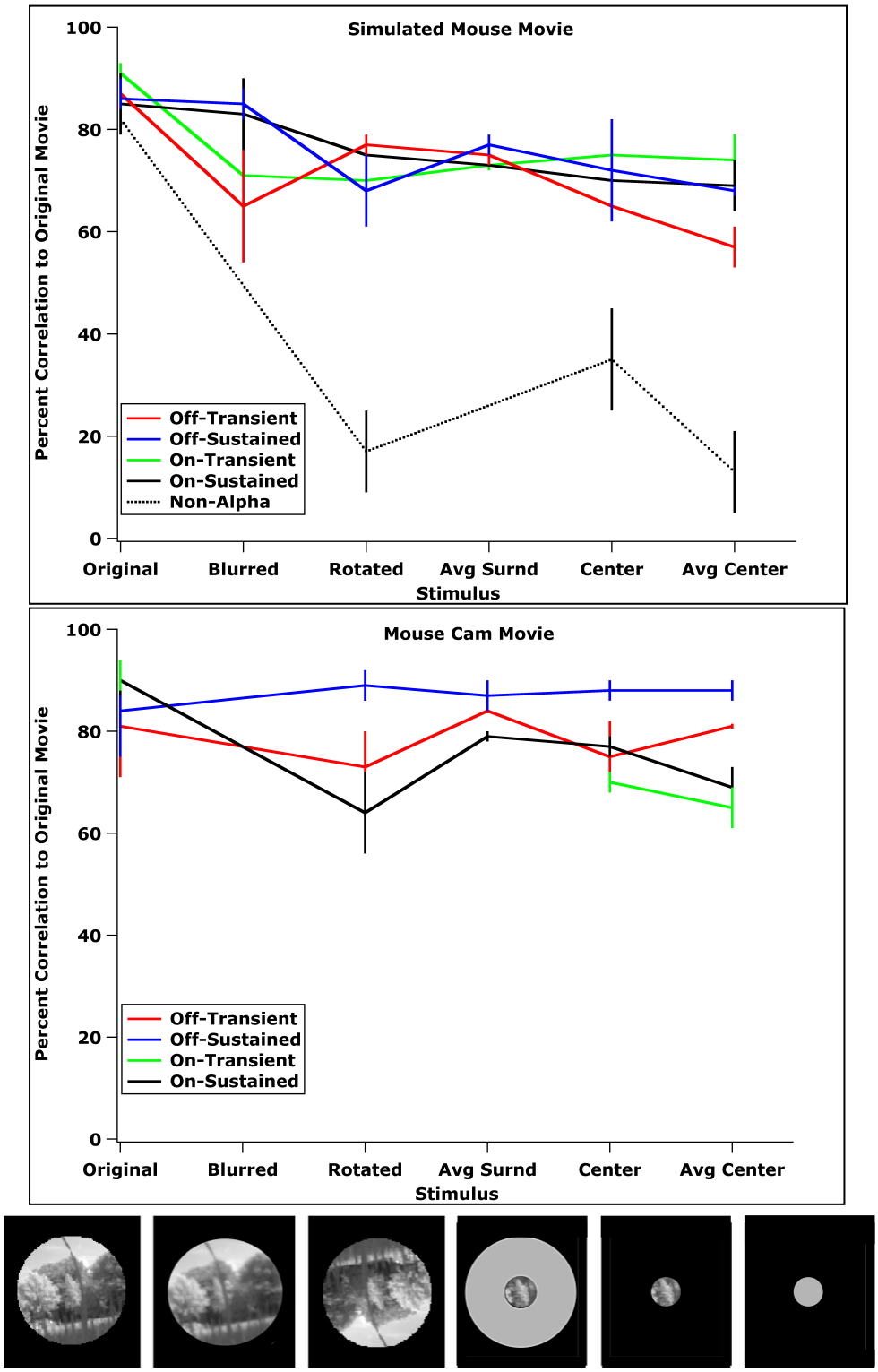

Figure 4.18: Summary of the single trial correlations across stimulus conditions for the original simulated mouse (top) and mouse cam (bottom) movies. The stimuli on the x-axis are organized such that the ones further from the origin have less in common with the original movie.

4.3 Discussion

The two principal results from this work are that the alpha retinal ganglion cells (A-RGCs) respond well to movies of self-motion and that those responses predominantly persist under stimulation with movies that have been crudely manipulated.

The entire population of A-RGCs responded robustly to the simulated mouse and mouse cam movies. Though these movies differed in important ways, they were both mainly dominated by self-motion rather than motion of external objects in the visual field. All the A-RGCs responded roughly 50% of the time during both movies. When considering the combined firing rate of the Off- and On-Sustained A-RGCs, they essentially contributed to the encoding of the visual stimulus at every point in time (Figure 4.5). By comparison, the non-alpha RGC responses to the same movie were far less frequent (Figure 4.10). This comparison suggests that the A-RGCs are very active during natural mouse vision and that upstream computations in the brain may involve combining input from multiple of the A-RGC types.

We probed the important aspects of various spatial elements of the stimulus to the alpha RGC responses by comparing the responses to original and manipulated movies. The correlations across stimulus conditions reported here were likely underestimates. The movie repetitions were not interleaved and thus responses may also have become less correlated due to changes in time and not only due to the change in stimulus. The first blurring manipulation suggested that distortions from the optics of the mouse eye were not the limiting factor in A-RGC driven natural vision, particularly when considering the blurring we performed overestimated the optical distortions. We included defocus and we did not consider the distance of objects when performing the manipulation, meaning all

detail on the order of 20 μm, or 0.66 degrees, was blurred. The Off- and On-Sustained A-RGCs were completely unaffected by the blurring of the stimulus and over 74% of the Off- and On-Transient A-RGC responses remained. The minimal influence of the blurring on the neural responses was consistent with spatial summation of areas greater than 20 μm as seen previously (see Chapter 3, Figure 3.6).

Similar to our results suggesting a small role of optical blurring in the visual responses of the A-RGCs, we found a relatively minor influence of the A-RGC surround on neural output. This claim is based on finding the majority of the A-RGC responses remained after the surround manipulations. Additionally, with the exception of the Off-Transient cells, the A-RGCs perform a weighting of the surround other than flat or Gaussian, or nonlinear subunits drive the influence from the surround. This claim is based on the findings that averaging the surround and removing it entirely influenced the A-RGC responses by the same magnitude. The lower correlations often found for the On-Transient cells may be due to having fewer samples. Our experience places the On-Transient A-RGCs as a minority of the On population (25%) and therefore we recorded from fewer of them in general. Overall, these results suggest that the A-RGC surround is nonlinearly summed and that the role of the surround is relatively minor compared to the receptive field center for the neural responses to these two natural movies.

Not only did the A-RGCs respond robustly to manipulated movies, unlike some non-alpha RGCs, they retained the bulk of their responses under the most crude of manipulations: averaging the pixels in the receptive field center. Though this finding suggested that fine spatial information in the receptive center was not the primary component of these natural movies driving the A-RGCs, eliminating this information did

have noticeable effects on the neural outputs. Across all four A-RGC types, the same general peaks in firing rate were present under both conditions, but under the averaged center movie, the peaks were often later by ~10 ms and sharper (Figure 4.16). This suggested that nonlinear summation within the receptive field was important to the absolute timing and magnitude of the responses. The importance of the nonlinear subunits can be imagined by considering the responses of an Off-Transient A-RGC, assuming identical subunits tiling the receptive field center, under stimulation with the original movie and averaged center movie. Under the original movie, local nonlinear subunits likely drove RGC firing when only the local intensity of interest resembled the preferred stimulus. In the case of the averaged center movie, a dark object moving into the center would more slowly change the local intensity. This "blurred" entry of the dark object would result in a delay in the subunit response. Additionally, for the same subunit response as to the original movie, the entire stimulus would need to resemble the preferred stimulus and would likely drive the entire center at the same time to result in a larger overall response. Therefore, local nonlinear subunits may slightly speed up and broaden responses from the A-RGC.

We have established a baseline level of understanding for the neural responses of A-RGCs to natural movies. This study was limited to stimulating with two movies at a single light level. It is known that the statistics of natural movies can change drastically depending on the environment and recently it was reported that the surround strength of the sustained A-RGCs changes depending on the background light level[20]. Under the conditions tested, the surround had a relatively weak influence on the overall A-RGC responses. This left the bulk of the responses driven by the center that appears to perform

simple computations on our two natural movies. Overall, we found the A-RGCs to respond robustly to movies of self-motion and for those responses to be primarily driven by coarse spatial information in the receptive field center. These results will better inform further studies of RGCs under more natural stimuli by allowing a comparison with the A-RGCs.

4.4 References

1. Roska, B. & Werblin, F. Rapid global shifts in natural scenes block spiking in specific ganglion cell types. *Nat. Neurosci.* **6,** 600–8 (2003).

2. Baccus, S. a, Olveczky, B. P., Manu, M. & Meister, M. A retinal circuit that computes object motion. *J. Neurosci.* **28,** 6807–6817 (2008).

3. Olveczky, B. P., Baccus, S. a & Meister, M. Segregation of object and background motion in the retina. *Nature* **423,** 401–408 (2003).

4. Rucci, M., Iovin, R., Poletti, M. & Santini, F. Miniature eye movements enhance fine spatial detail. *Nature* **447,** 851–854 (2007).

5. Gollisch, T. & Meister, M. Rapid neural coding in the retina with relative spike latencies. *Science* **319,** 1108–1111 (2008).

6. Ruderman, D. L. Origins of Scaling in Natural Images. *Vision Res.* **37,** 3385–3398 (1997).

7. Ratliff, C. P., Borghuis, B. G., Kao, Y., Sterling, P. & Balasubramanian, V. Retina is structured to process an excess of darkness in natural scenes. (2010).

8. Laughlin, S. A simple coding procedure enhances a neurons' information capacity. *Z. Naturforsch* **36,** 910–912 (1981).

9. Tadmor, Y. & Tolhurst, D. J. Calculating the contrasts that retinal ganglion cells and LGN neurones encounter in natural scenes. *Vision Res.* **40,** 3145–57 (2000).

10. Atick, J. & Redlich, A. What Does the Retina Know about Natural Scenes? *Neural Comput.* **4,** 196–210 (1992).

11. Atick, J. J. & Redlich, A. N. Towards a Theory of Early Visual Processing. *Neural Comput.* **2,** 308–320 (1990).

12. Borghuis, B. G., Ratliff, C. P., Smith, R. G., Sterling, P. & Balasubramanian, V. Design of a neuronal array. *J. Neurosci.* **28,** 3178–89 (2008).

13. Betsch, B. Y., Einhäuser, W., Körding, K. P. & König, P. The world from a cat's perspective--statistics of natural videos. *Biol. Cybern.* **90,** 41–50 (2004).

14. Zhang, Y., Kim, I.-J., Sanes, J. R. & Meister, M. The most numerous ganglion cell type of the mouse retina is a selective feature detector. *Proc. Natl. Acad. Sci. U. S. A.* **109,** E2391–8 (2012).

15. Duan, X., Krishnaswamy, A., De la Huerta, I. & Sanes, J. R. Type II Cadherins Guide Assembly of a DirectiOn-Selective Retinal Circuit. *Cell* **158,** 793–807 (2014).

16. Qiao, M., Sanes, J. R. & Duan, X. *In preparation*.

17. Buffelli, M. *et al.* Genetic evidence that relative synaptic efficacy biases the outcome of synaptic competition. *Nature* **424,** 430–434 (2003).

18. Artal, P., Tejada, P. H. De, Tedó, C. M. & Green, D. G. Retinal image quality in the rodent eye. 597–605 (1998).

19. Geng, Y. *et al.* Optical properties of the mouse eye. **2,** 597–605 (2011).

20. Farrow, K. *et al.* Ambient illumination toggles a neuronal circuit switch in the retina and visual perception at cone threshold. *Neuron* **78,** 325–38 (2013).

Chapter 5: Simple Models Successfully Predict the Responses of the Alpha Retinal Ganglion Cells to Natural Movies and Artificial Stimuli

5.1 Introduction

A central goal of visual neuroscience is to delineate the relationship between sensory input and neural output. The ultimate target is to correctly predict the neural activity to any visual stimulus. One way to achieve this goal is to build a model that specifies the mathematical relationship between visual input and neural output. Visual processing begins at the retina where photoreceptors convert photons to electrical signals. Considerable computations are then performed on the stimuli by the circuitry of the retina before the visual information is sent to the brain through the axons of the retinal ganglion cells (RGCs)[1–4]. Therefore if we hope to extract the neural computations performed at each stage of the visual system, we need a complete description of the relationship between visual input and ganglion cell neural output. A number of approaches to modeling the retina have been successful over decades of research and we chose one particular modeling formalism for predicting RGC output called the linear-nonlinear (LN) model. The two key components in this approach are a linear filter and a nonlinear transformation[5–10]. The linear filter replicates the spatio-temporal receptive field of the cell and the nonlinearity typically mimics the process of spike generation. Models combining these components, LN cascade models, are the most commonly used models for describing the early areas of the visual system (Figure 5.1). Therefore, in an effort to understand retinal transformations between visual input and neural output, we utilized LN modeling techniques to predict the responses of one of the most thoroughly studied RGCs, the alpha retinal ganglion cells (A-RGCs).

For the retina in particular, a successful modeling approach has been to package the individual computations of the LN model into plausible circuit elements. This is

reasonable because the general retinal circuitry is known. In this context, each element in the model represents a specific computation performed by neurons in the retina. There are three main building blocks typically utilized for such schematic circuits. First, the raw stimulus is fed to bipolar subunits that represent the linear, spatiotemporal filter of the neuron (Figure 5.1: "B"). Moreover, the bipolar-to-ganglion and ganglion-to-brain synapses are static nonlinearities that often describe how the output is transformed into a firing rate (Figure 5.1: "Oval rectifying function"). Lastly, the pooling of synaptic inputs in the RGC is mimicked by a weighted summation of the rectified bipolar subunit signals (Figure 5.1: Input to "G"). This circuit element approach produced models that were easy to interpret, realistic, and captured the mathematical transformation performed by the retinal wiring. Crucially, a number of computations in the retina have already been successfully explained using this approach[4,11,12]. We designed our models of the A-RGCs using the circuit element framework of the LN model to tie the components of successful models to their potential biological implementations.

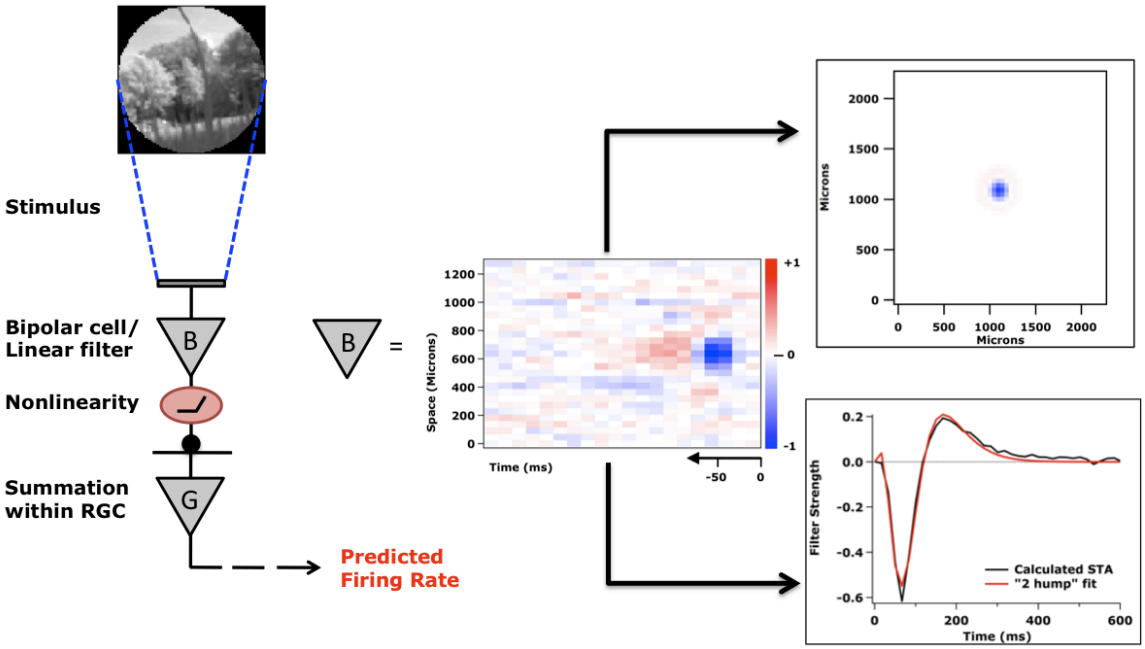

Figure 5.1: Schematic for the linear-nonlinear (LN) cascade model drawn using circuit elements. In this formalism specific computations are assigned to particular neurons within retinal circuitry. The input stimulus is filtered in space and time by the bipolar cell ("B"). The filtered stimulus is rectified by synaptic transmission of the signal to the RGC ("G") represented by a static nonlinearity ("Piecewise function inside oval"). The bipolar cell represents the full spatio-temporal filter.

One reason for the popularity of the LN model has been its ease of use when paired with white noise stimulation [7]. White noise stimuli include no spatiotemporal correlations and are often generated by pulling independent values from a Gaussian distribution. This kind of stimulus is useful for calculating receptive field parameters of a cell because of its fairly flat spatial and temporal spectrums[7,13,14]. Thus, the parameters for the LN model including the spatio-temporal receptive field and, in simple cases, the static nonlinearity can be directly calculated from neural data to greatly reduce the number of free parameters and enhance ease of analysis. We utilized white-noise stimuli to probe the receptive field properties of the A-RGCs and to ask the level of model complexity required to successfully predict their responses. By calculating the typical spatio-temporal filters along with nonlinearities across spatial components of the receptive field, we informed the structure of our models. This approach allowed us to assemble the LN model from the A-RGC responses and build up further models based on spatial receptive field properties.

To address the question of where on the spectrum of complexity models successfully predicting A-RGC responses fall, we started from the most simple model for RGCs: the LN model. We chose to bypass the simpler model for visual responses consisting of only a linear filtration stage. Purely linear models of neural responses to visual stimuli have been successful in rare cases when predicting the graded output of cone photoreceptors[6,15], but when modeling downstream neurons, like RGCs, it is necessary to include a nonlinear stage after the linear filter. At the most fundamental level, a rectification of the RGC input is required because the neural output is in the form of action potentials. The RGC firing rate cannot fall below zero and cells typically

possess baseline firing rates < 20 Hz with maximal firing rates exceeding a few hundred Hertz. An explanation of this behavior requires a nonlinear transformation. Beyond the simplicity and biological underpinnings of the LN model, many other RGC modeling studies found the framework to successfully reproduce neural responses[1,9,16–18]. Therefore, we chose the LN model as our standard model for explaining A-RGC visual responses.

Thus far, we have only mentioned white noise stimuli because when paired with the LN model, the approach has proven very useful to probe the computations performed by the early stages of the visual system. Unfortunately, many of the properties of white-noise stimuli that make them computationally attractive are not true of more natural stimuli. In the end, it is important to remember an ultimate goal is to link neural activity to naturally occurring stimuli. Thus, a sufficient model of visual processing should correctly predict the responses to natural stimuli in addition to the typical stimuli used in the laboratory. Very few models of the early visual system, including the retina, lateral geniculate nucleus (LGN), and primary visual cortex (V1), have been subjected to this ultimate test[13]. To date there are no reports of models successfully predicting retinal responses to natural movies. The closest instance was in modeling the output of primate RGCs to spatially uniform natural light sequences[19]. All other models of retinal processing have been tested on artificial stimuli such as white noise, textures, high-contrast gratings, and moving spots [3,6,7,16,20–25]. In the feline LGN and primate V1, some linear-nonlinear models derived from artificial stimuli have been successfully tested on natural movies[26–28]. If we hope to fully connect naturalistic visual input with brain activity, successful models for predicting the output of the retina to natural movies must

be established. Therefore after developing models for the A-RGC responses to white-noise stimuli of increasing complexity, we fit those same models to responses from natural movies (Figure 5.2). By comparing the receptive field parameters optimized during the model fitting and the final firing rate prediction, we assessed both the similarity of A-RGC visual stimuli processing under the two stimulus conditions and whether the same models were sufficient to describe responses under multiple stimulus environments.

To systematically build and assess models of increasing complexity in predicting A-RGC responses to stimuli of growing spatial intricacy, we created a table of stimuli verses models (Figure 5.2). Some compartments of the table were not filled in and other compartments were expanded to include various simplifications. By utilizing the models and experimental stimuli in Figure 5.2, we found the A-RGC processing of visual input to remain fairly constant across the stimulus conditions and that the simple models could successfully predict responses to white-noise and natural movie stimuli.

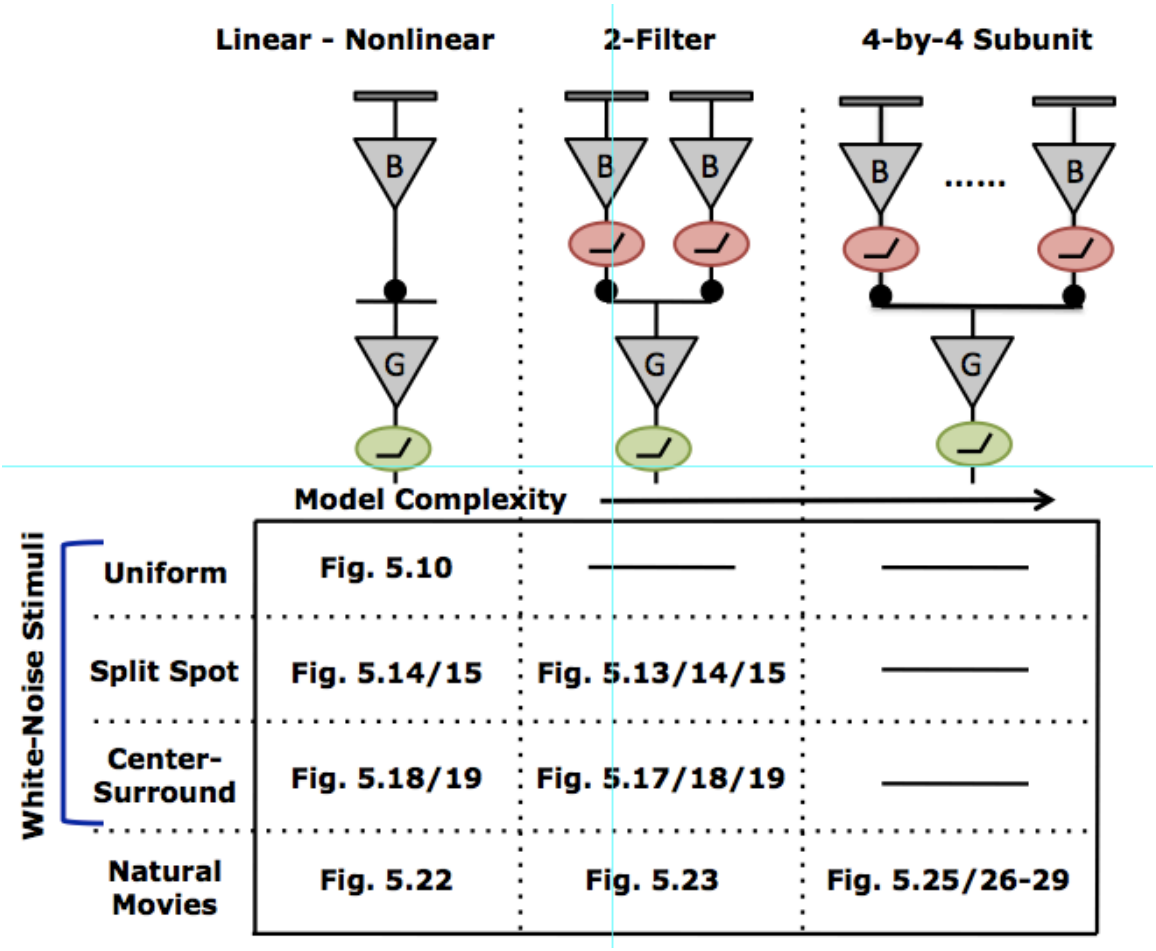

Figure 5.2: Diagram of the experimental stimuli and computational models used to assess the computations performed by the A-RGCs. When moving along the modeling axis from left to right, the number of model components increases, but the type of components remains unchanged. Similarly, the number of spatial components in the stimuli shown to the A-RGCs increases from top to bottom.

5.2 Definitions of model terminology

Receptive field: The region of visual field over which a visual neuron responds to stimuli[29,30]

Spatio-temporal receptive field: An estimate of how the neuron weights different spatial and temporal components of the stimulus. The spatio-temporal receptive field is a linear filter that describes the preferred stimulus of a visual neuron. An image that closely matches the filter will produce a large response. Often the receptive field is assumed to be separable in space and time and thus approximated by the multiplication of a spatial receptive field and temporal kernel:

$$F(x,t) \approx X(x)T(t) \qquad \text{(Eqn. 1)}$$

Reverse-correlation: An umbrella term for calculating receptive fields by correlating recorded spike trains with the white-noise stimulus sequence[31].

Spike triggered average (STA): A reverse-correlation method that calculates the average stimulus that produced a spike. Receptive fields can be calculated as the STA from a random noise stimulus that is constructed to have zero mean[32].

Difference of Gaussians: The typical parameterization of the spatial receptive field for a retinal ganglion cell is by a difference of Gaussian functions. The first term embodies the excitatory center and the second gives the inhibitory surround. A_{cen} sets the amplitude, σ_{cen} determines the width, and r_o defines the coordinates of the center Gaussian. Equivalent parameters specify the surround Gaussian.

$$X(r) = A_{cen} \exp\left[\frac{-(r - r_{o\_cen})^2}{\sigma_{cen}^2}\right] - A_{srnd} \exp\left[\frac{-(r - r_{o\_srnd})^2}{\sigma_{srnd}^2}\right] \qquad \text{(Eqn. 2)}$$

Temporal kernel: A linear filter that represents the impulse response function for a neuron. The duration of the kernel reflects the memory of a neuron. In practice, the kernel is the temporal weighting function plotted in reverse.

"2 hump model": The parameterization of the temporal kernel is by a difference of gamma functions. Temporal kernels are typically biphasic and so each term sets one of the "humps" by specifying the shape n and decay time τ with amplitude ratio a.

$$T(t) = (t/\tau_1)^{n_1} e^{-n_1(t/\tau_1 - 1)} - a(t/\tau_2)^{n_2} e^{-n_2(t/\tau_2 - 1)} \qquad \text{(Eqn. 3)}$$

Linear-nonlinear model: A common formalism for modeling the responses of retinal ganglion cells. The stimulus input is first filtered by a linear stage then passed through a static nonlinearity. The average firing rate of the neuron is specified by the nonlinear transformation of the filtered stimulus.

Filtering/Convolution: The first stage of the linear-nonlinear model is to convolve, or filter, the stimulus by the receptive field. For our models, we only convolve in the temporal domain. The time-dependent filtered stimulus is calculated by weighting the spatially weighted stimulus with the temporal kernel at each point in time. The filtering stage is important because the firing rate at any point in time depends not only on the current stimulus, but the stimulus in the recent past as determined by the length of the temporal kernel.

Nonlinearity: An instantaneous function that transforms the filtered stimulus into a firing rate. The nonlinearity can be approximated from the data by plotting the neural firing rate versus the filtered stimulus and fitting a smooth function[7,17]. The nonlinearity can also be calculated from Bayes rule as the frequency of spike-triggered stimuli divided by the frequency of all stimuli[32]. The simplest nonlinearity parameterization is by piecewise

rectification, but in model fitting it is often preferred to use a smooth function such as a log-sigmoid (Eqn. 4). In equation 4, the nonlinear output is a function of the linear prediction and the maximum firing rate K, gain g, and threshold θ.

$$N(r) = K/(1 + e^{-g(r-\theta)}) \quad \text{(Eqn. 4)}$$

Optimization: Each model was fit to the data by finding parameters that calculated a firing rate prediction that most closely matched the average firing rate of the RGC. The spike trains were binned at twice frame rate of the stimulus (33 ms). The parameters were found using the Levenberg-Marquardt algorithm for least squares fitting in IGOR (Wavemetrics, Inc). In practice we always started fitting the model from reasonable initial guesses for the parameters. When fitting the temporal kernel, the initial parameters were calculated from equation 3.

Goodness-of-fit: The model performance was assessed by calculating the similarity between the model prediction and RGC responses. A number of metrics can be used to make this comparison and we chose to evaluate the correlation between the data and the fit.

Correlation: Pearson's correlation coefficient was calculated to assess the goodness-of-fit of the model prediction. The correlation we quote is the average correlation of the prediction of the model with each binned spike train repetition of the stimulus. We also calculated the intrinsic noise of the RGC by correlating the same individual repetitions to the same stimulus.

Overfitting: A common concern when fitting a model to any kind of data is the possibility of having too many parameters such that you end up fitting the noise along with the signal. To guard against this possibility, the standard method is to the fit the model to one

set of data, i.e. the training dataset, and test the model on a separate set of data, i.e. the testing dataset. We followed this method and all correlation values quoted are comparing the model prediction to the testing dataset.

5.3 The first stage of the linear-nonlinear model: The linear filter

As described above, the basic LN model consists of a linear filter and a static nonlinearity (Figure 5.1). To begin modeling using this framework, we first needed a measure of the A-RGC's linear spatio-temporal filters. Below are the results of experiments, without specific definitions of terms, probing these receptive field properties. (See section 5.2. for details on terminology and methods Chapter 2 for further explanation.)

5.3.1 Raw spatio-temporal receptive fields

The spatio-temporal receptive field was calculated for each neuron using the standard reverse-correlation technique[7]. The A-RGCs displayed temporally biphasic behavior and showed center-surround antagonism typical of ganglion cells[17]. The biphasic time course for an Off-Transient A-RGC can be clearly seen in Figure 5.3, left. Approximately 33 ms before time zero, i.e. the time of the spike, the temporal receptive field negatively peaks, as expected for an Off cell. Before that time, there is a positive peak in the receptive field. Thus this neuron responds most strongly for a stimulus that transitions from light to dark. The spatial extent of the preferred stimulus can be seen on the y-axis. The receptive field center, i.e. the negative peak in time, is ~230 μm across. Flanking both above and below the blue center are red regions indicative of surround

antagonism. The same pattern is seen for an On-Sustained A-RGC, but with reversed polarity of preferred stimulus (Figure 5.3, right). These spatio-temporal receptive fields represent the linear filters of the A-RGCs.

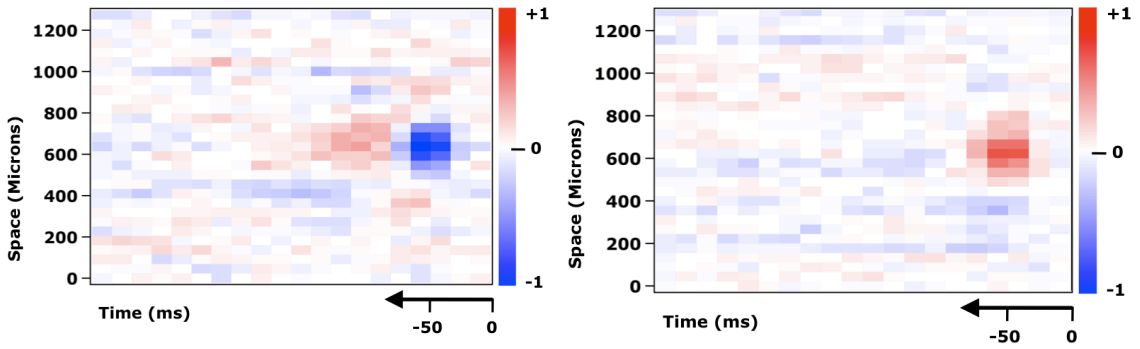

Figure 5.3: Sample spatio-temporal receptive fields for an Off-Transient (left) and On-Sustained (right) A-RGC. The receptive fields were measured with checkerboard white-noise and calculated as the spike-triggered average stimulus. They were spatially integrated over one dimension to display the center-surround antagonism and the biphasic time course.

For the purposes of modeling and noise reduction, it was useful to describe receptive fields in terms of a few parameters. We assumed the spatio-temporal receptive fields to be separable in space and time and thus mathematically described by a direct product of a purely spatial receptive field and temporal kernel. We chose to parameterize the spatial portion with the standard 2-dimensional difference of Gaussians model[33–35] and the temporal kernel using the "2-hump model" comprised of a difference of gamma functions[17,36]. The next sections specify our procedure of receptive field parameterization to provide intuition for the linear stage in our models of A-RGC responses.

5.3.2 Spatial receptive field parameterization

We calculated spatial receptive fields from the same data in Figure 5.3 by plotting the spike-triggered average stimulus as a function of space for each time frame preceding the spike. By averaging the frames corresponding to the temporal peak, we obtained nice center-surround receptive fields for each A-RGC type (Figure 5.4). We parameterized these images using a difference of Gaussians to reduce noise in the estimate of the spatial receptive field (Figure 5.5).

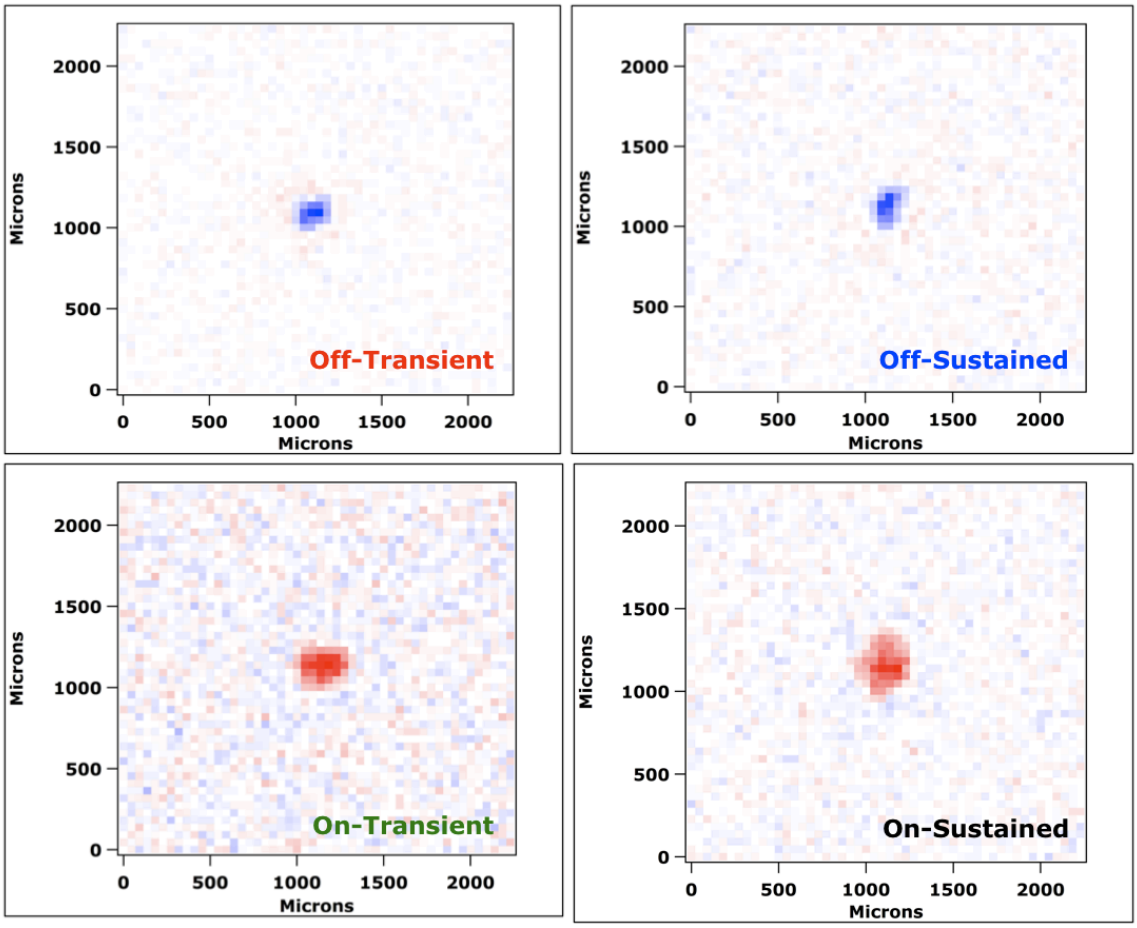

Figure 5.4: Raw spatial receptive fields for the A-RGCs calculated by averaging the frames of the temporal peak. The color scale is the same as in Figure 1: Red = +1, White = 0, Blue = -1.

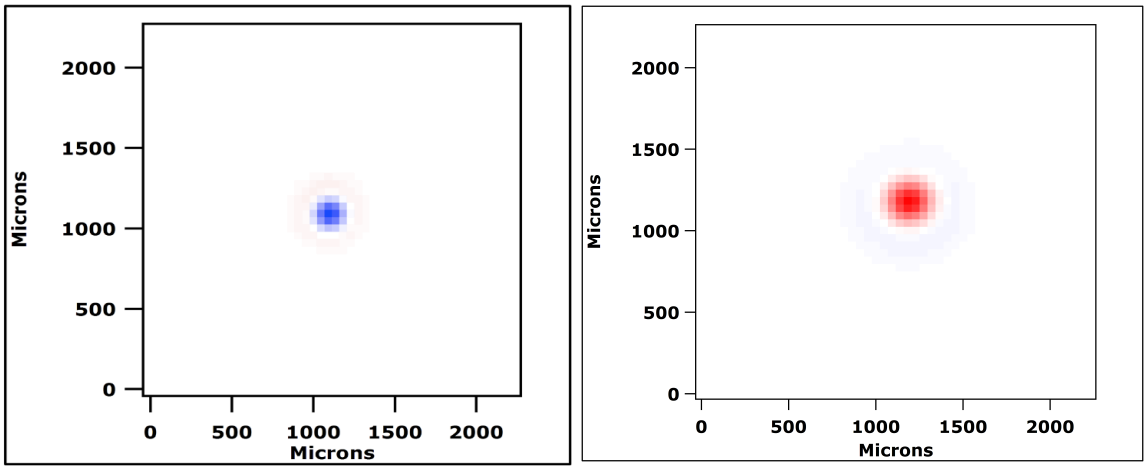

Figure 5.5: Example fits of checkerboard spatial receptive fields from Figure 5.4 with a difference of Gaussians for an Off-Transient (left) and On-Sustained (right) A-RGC.

When checkerboard STAs were not available, we approximated the spatial receptive field by fitting a difference of Gaussians to the peak firing rate vs radius curve (Figure 5.6). The A-RGC responses to spots of increasing radius contained the same essential spatial information as the checkerboard STAs except for the exact coordinates of the cell's position. In practice the exact coordinates were not required because all stimuli were centered over the RGC at the beginning of the experiment. The receptive field size was calculated from Figure 5.6 as the radius where the curve reached a maximum value. The influence of surround suppression was visualized by how much that maximum value decreased as the radius increased. In Figure 5.6 an Off-Transient and On-Transient A-RGC show the different extremes for center receptive field size and surround strength. The difference of Gaussian parameterization of the spatial receptive field produced good fits in both cases. The final spatial filter was obtained by rotating the center and surround Gaussian curves around the y-axis.

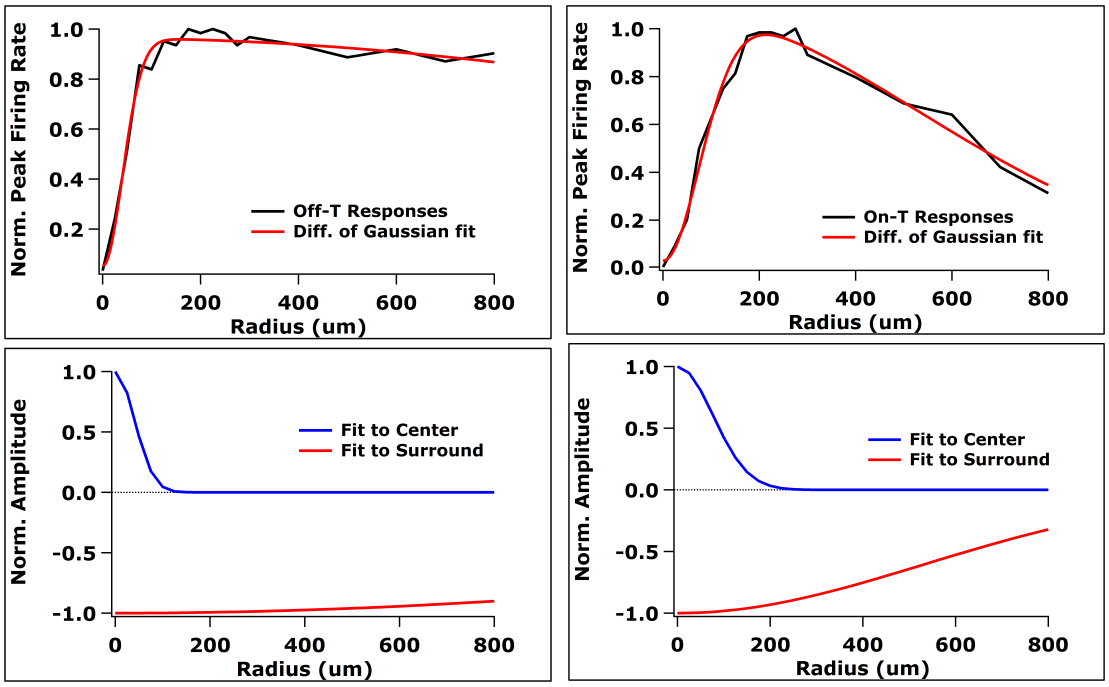

Figure 5.6: Difference of Gaussian fit to receptive field mapping curve via the growing spot sequence (Top; Black = Normalized firing rate; Red = Difference of Gaussian fit). The calculated center (blue) and surround (red) Gaussian curves captured the spatial receptive field properties for centers of varied size and surrounds of different strengths.

By fitting either the checkerboard spatial receptive field or the responses to spots of increasing diameter, we obtained an estimate of the spatial receptive field for every A-RGC. We next needed to define the temporal receptive field to completely parameterize the linear portion of the LN model.

5.3.3 Temporal receptive field parameterization

As described above, we parameterized the spatial receptive field by assuming the spatio-temporal receptive field to be separable in space and time. In reality, the spatio-temporal receptive fields were not truly separable because the spatial center and surround possessed different temporal dynamics. Therefore to properly estimate the time course of a neural response, it was necessary to consider the center and surround kernels independently. The temporal kernels represented the impulse response function of a cell and were calculated by reverse correlation with a white-noise stimulus (Figure 5.7). The A-RGCs showed center-surround antagonism typical of RGCs by their surrounds preferring stimuli of opposite polarity the center (Figure 5.7). The surrounds also tended to peak later than the center by ~20 ms. It should be noted that the temporal kernels could also explain a number of response properties of the A-RGCs. For example, the Off-Transient cells had the weakest surround, which was reflected in the magnitude of their surround filter (Figure 5.7, upper left). Also, the two kernels for the transient cells were more biphasic than the sustained cells as was expected by their brief light responses.

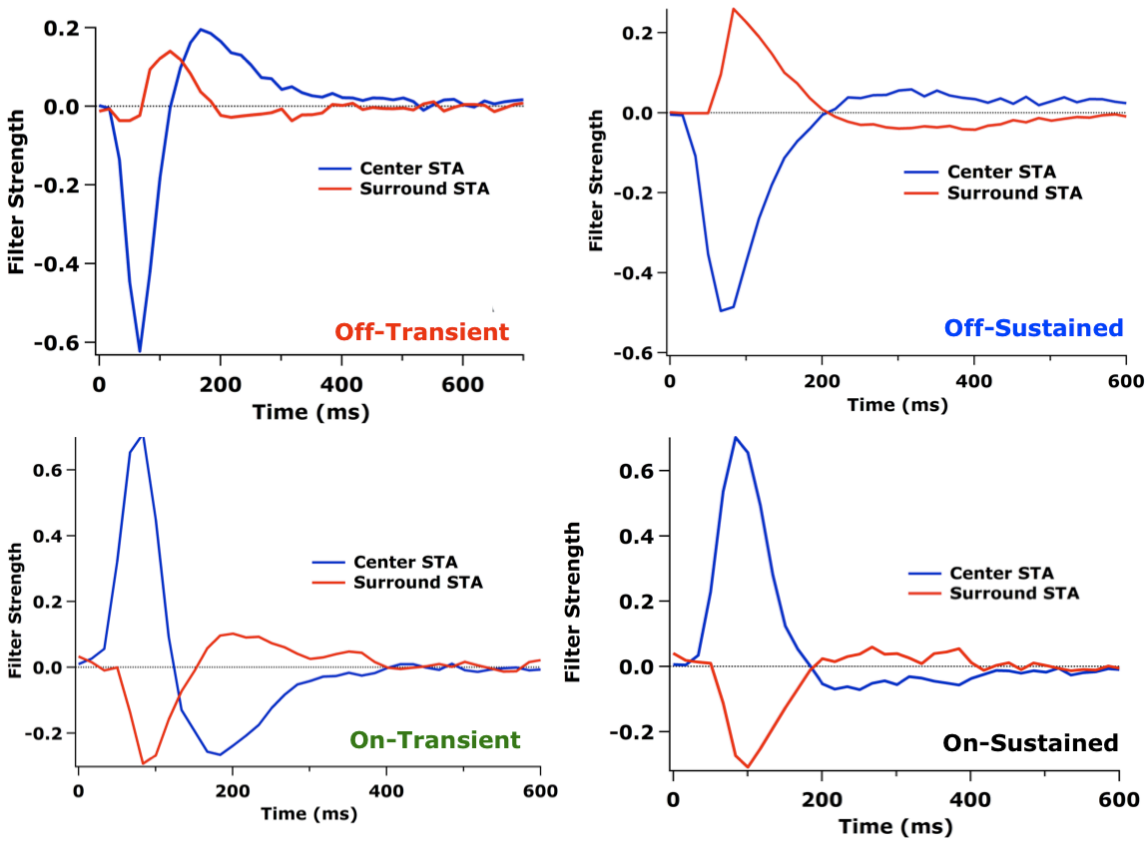

Figure 5.7: Raw temporal kernels for the A-RGCs calculated by reverse-correlation of the spike train with a white-noise stimulus. The stimulus consisted of a spot over the receptive field center (200-250 um diameter) and an independently flickering annulus in the surround (Inner diameter = 200-250 µm; Outer diameter = 1000 µm). Similar filters could also be obtained by averaging the time course for the pixels in the checkerboard spatial receptive field center and surround.

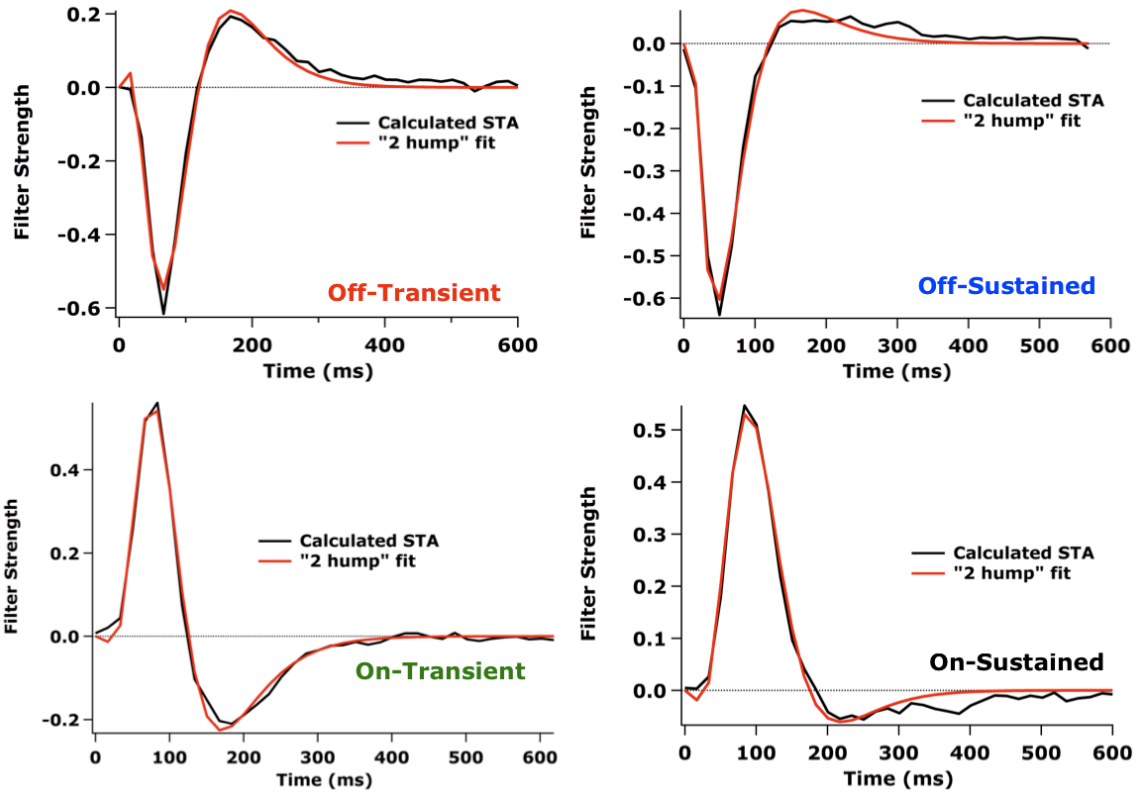

Figure 5.8: The "2 hump" model was sufficient to fit the A-RGC temporal kernels and reproduce the filter shape. The fitting equation was provided in section 5.2.

To reduce noise and the number of model parameters, we fit the calculated temporal spike-triggered averages (STAs) with a "2 hump" model. We consistently obtained satisfactory fits of the original center and surround kernels with this parameterization (Figure 5.8). By using the accepted methods of reverse-correlation, spatial difference-of-Gaussian parameterization, and temporal "2 hump" parameterization, we successfully estimated the spatio-temporal receptive fields of the A-RGCs by separately fitting the spatial and temporal components independently. The parameterization allowed for the reduction of noise in our approximation of the linear filter and, in later models for natural movie responses, was used to determine starting parameters for fitting the first stage of the LN model.

5.4 Completing the linear-nonlinear model with the threshold nonlinearity

The second stage of the LN model was a thresholding nonlinearity that transformed the linear prediction into a firing rate (Figure 5.1). The form of this nonlinearity was determined in previous work either through direct calculation or during model fitting. The nonlinearity was often calculated by plotting the firing rate as a function of the filtered stimulus, i.e. the input to the ganglion cell. The resulting curve gives the lookup table for the RGC output given any value of the range of stimuli tested. This simple LN model with a single calculated nonlinearity was typically sufficient to predict RGC responses to a spatially uniform stimulus[9,16]. For consistency across all models of increasing spatial complexity, we parameterized and fit the nonlinearity to the data. We chose to use a log-sigmoidal parameterization (Eqn 4) of the nonlinearity with three parameters: maximum firing rate (K), gain (g), and threshold (θ). Our standard LN

model kept the parameters calculated for the linear filter fixed and fit the three nonlinearity parameters (Figure 5.2). We referred to this model with three parameters as the LN model and it served as the standard to which all subsequent models were compared. Therefore with our above estimation of the linear filter, we were prepared to fit the LN model to A-RGC responses to spatially uniform white-noise stimuli and begin filling in the stimuli versus model table in Figure 5.1.

5.4 Predicting neural response to uniform white-noise stimuli using the linear-nonlinear model

Our first test of the standard LN model was to predict the responses of the A-RGCs to a spatially uniform spot flickering over the receptive field center. This kind of simple, uniform visual stimulus was standard for modeling the responses of RGCs[6,18,37]. Thus, we expected this first modeling attempt to predict the A-RGC responses fairly well and that was indeed what we found. The average correlation between the model prediction and single spike trains from repeats of the stimulus were, on average, above 80% for all the A-RGCs. Figure 5.9 (left) gives an example of the single spike trains (top raster), the average firing rate (bottom, black, peristimulus time histogram (PSTH)), and the model prediction (bottom, red, PSTH) for an On-Sustained A-RGC. The goodness of fit for this particular dataset was 90% as assessed by the average correlation between the fit and the single trial repetitions. The fit (red) captures the fluctuations in A-RGC firing rate very well by overestimating and underestimating the peak firing rates roughly equally. This can be more easily visualized by plotting the actual nonlinearity from the data (black) with the nonlinearity found by the model (Figure 5.9, right, red). The red

model output nicely follows the mean of the data, which indicates a proper parameterization of the A-RGC nonlinearity and therefore description of the firing rate. Additional fits to Off-Sustained and Off-Transient A-RGC responses to a spatially uniform stimulus by the LN model display the same behavior illustrating a successful match between cell type, model, and stimulus (Figure 5.10).

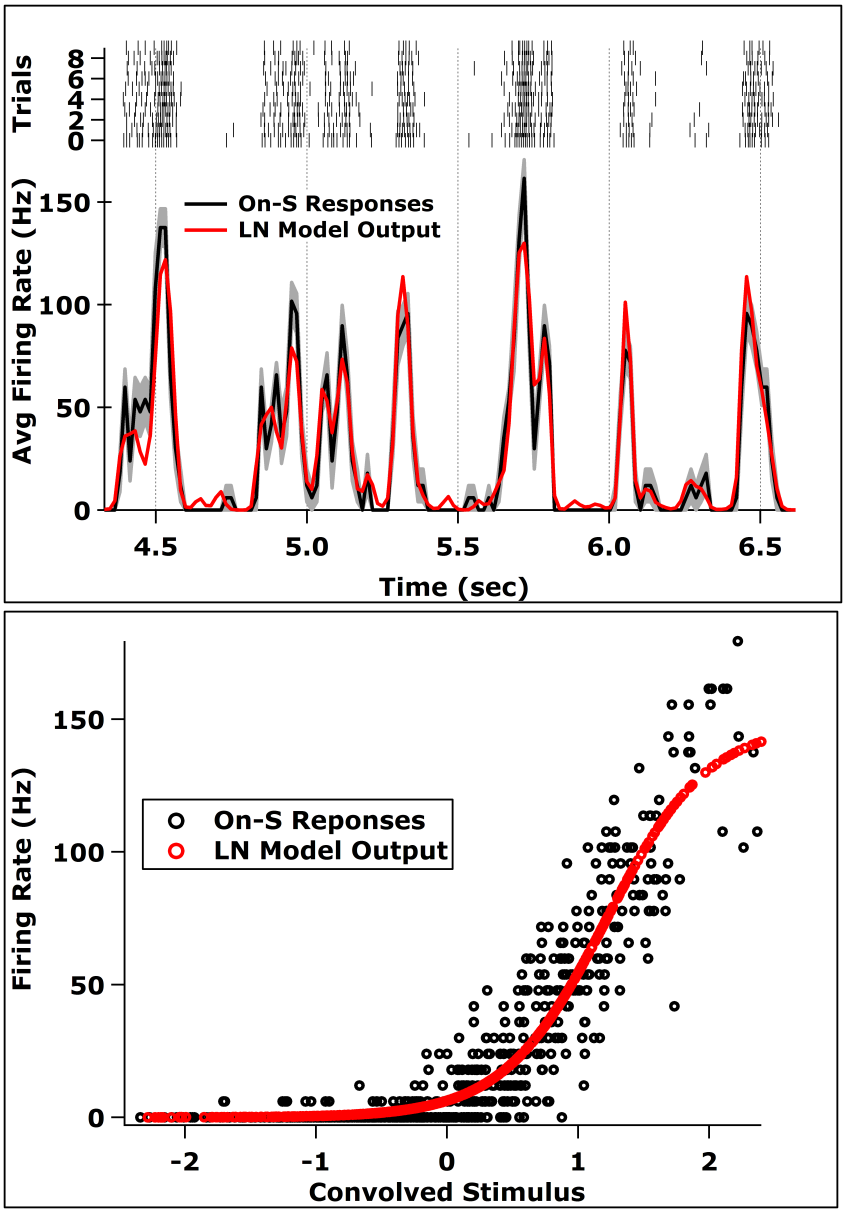

Figure 5.9: Responses, model prediction, and fitting parameters for an On-Sustained A-RGC to a spatially uniform spot (250 µm diameter) centered over the receptive field. A raster graph and summary PSTH (black) are plotted for a segment of the 10 second repeated stimulus. The grey is the standard error of the mean (SEM) of the visual responses. The average correlation between the model and individual spike trains is 90% (top). The nonlinearity found by the model closely approximates the thresholding used by the cell (bottom).

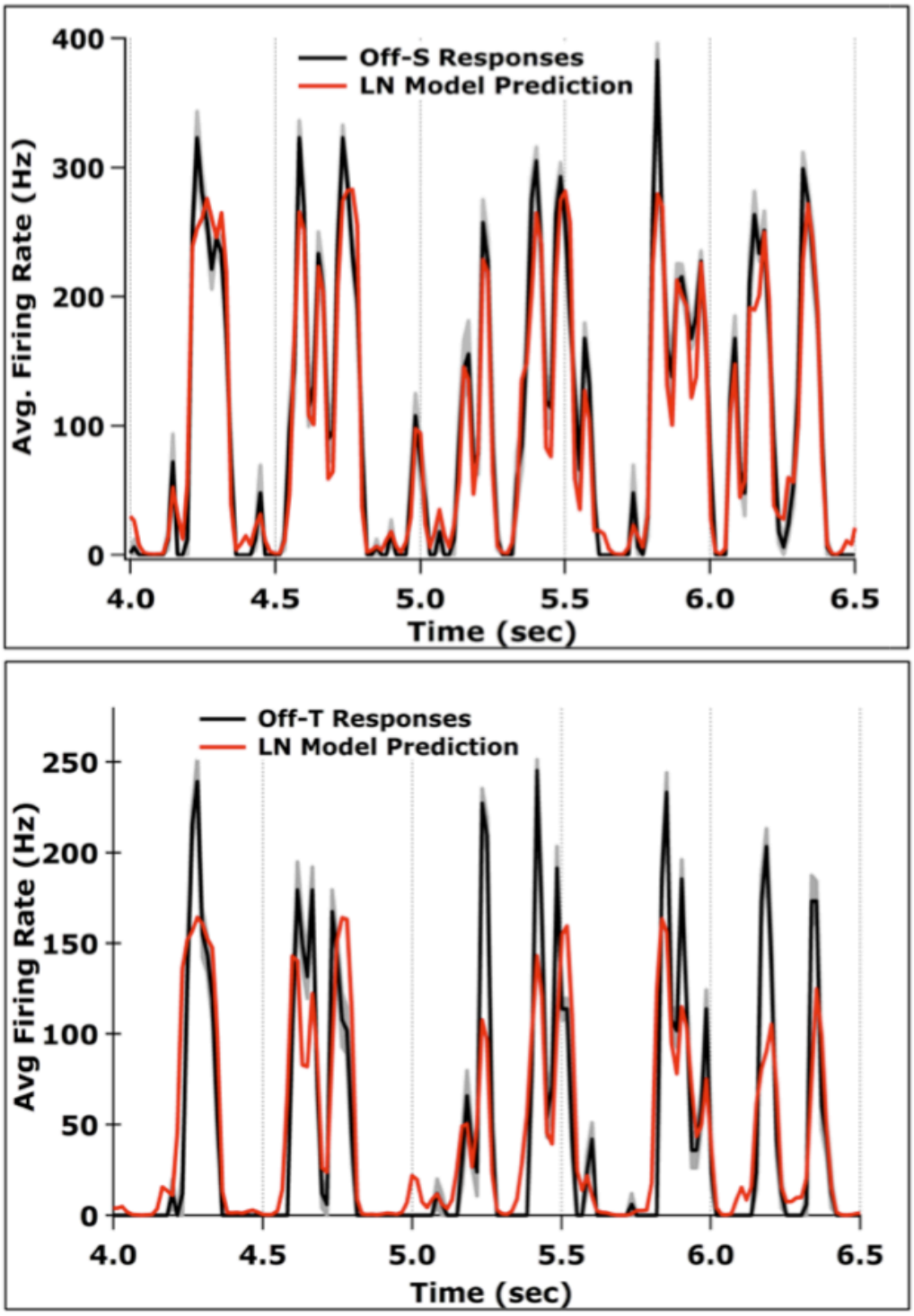

Figure 5.10: Example responses and standard LN model predictions for Off-Sustained (top) and Off-Transient (bottom) A-RGCs to the same segment of the spatially uniform white-noise stimulus. The black curve is the summary PSTH of the data, the grey is the standard error of the mean (SEM) calculated from the stimulus repeats, and the red is the model prediction. Off-Sustained: 92% average correlation. Off-Transient: 85% average correlation.

5.4.2 Split spot white-noise, 2-dimensional nonlinearities, and the "split" 2-filter model

To build upon our understanding of the A-RGC computations of visual stimuli, we continued to increase the complexity of the stimulus (Figure 5.1). When increasing the complexity and size of the stimulus, other nonlinearities may exist between different spatial components of the receptive field. We probed for these kinds of complex spatial processing of the A-RGCs by designing white-noise stimuli to force out any additional nonlinearities. We then used the information to design models of the A-RGCs to extend to spatially complex stimuli.

We first probed for nonlinear computation in the A-RGC receptive field center by stimulating with a white-noise spot that was split down the center into two halves (Figure 5.11). Each half flickered in a binary fashion independently at 60 Hz. We tested the nonlinear computation in the A-RGC center because the structure of the computation on spatially segregated visual input is important for building an appropriate model. If we were to find that the A-RGCs summed visual input linearly across their receptive field centers, the LN model would be sufficient to capture their visual responses. If instead the A-RGCs performed spatially nonlinear computation, a more suitable model would have local summation and rectification of visual input. We expected the latter scenario because A-RGC analogs in other mammals were found to locally sum and rectify visual input across their receptive fields. By stimulating with temporally independent, split spot white-noise of high contrast, we extracted any local nonlinear computations of that nature.

To differentiate between the described linear and nonlinear options, we plotted the 2D-nonlinearity of the neural responses. The 2D-nonlinearities for the split center white-

noise responses were analogous to the 1D-nonlinearity described above for a spatially uniform stimulus (Figure 5.9). In brief, we plotted the filtered stimulus from both spot halves on the x- and y-axes, respectively, and the firing rate on the z-axis (Figure 5.11). Thus, the color-coded surface plot served as the 2D-lookup table to estimate the output firing rate given any two inputs to the RGC from the split spot stimulus.

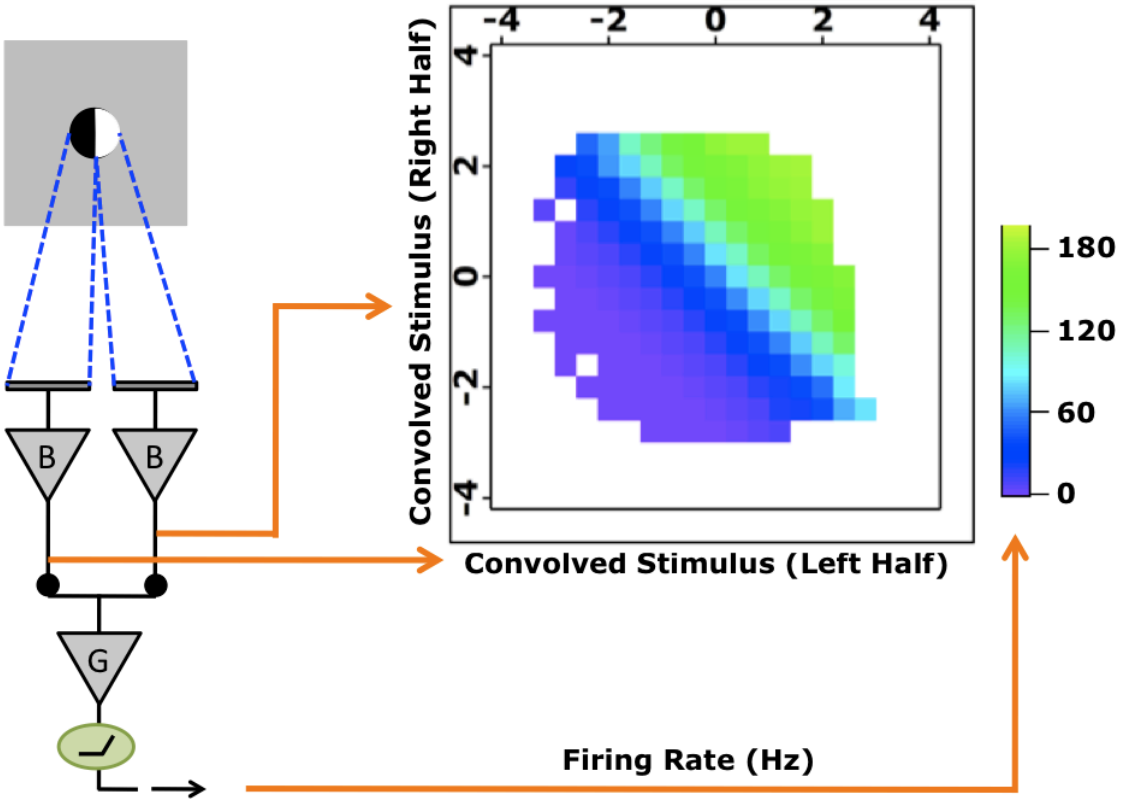

Figure 5.11: Diagram outlining the calculation of the 2D-nonlinearity from responses to the split spot white-noise stimulus. Here the LN model is shown with local spatial summation and the two visual channels are filtered and summed prior to rectification by the RGC.

The 2D-nonlinearity for each type of A-RGC tested displayed nonlinear spatial processing in the receptive field center (Figure 5.12). Nonlinear summation was clear because the signature of linear summation, straight contour lines across the 2D-nonlinearity, was missing. The shapes of the contours in the 2D-nonlinearities were all curved to some degree. Additionally, the shape of the nonlinearity was mostly symmetric around the diagonal indicating equivalent stimulus processing of each receptive field half. By stimulating with split spot white-noise, we confirmed our previous finding that the receptive field centers of the A-RGCs nonlinearly sum visual input (see Chapter 3, Figure 3.6).

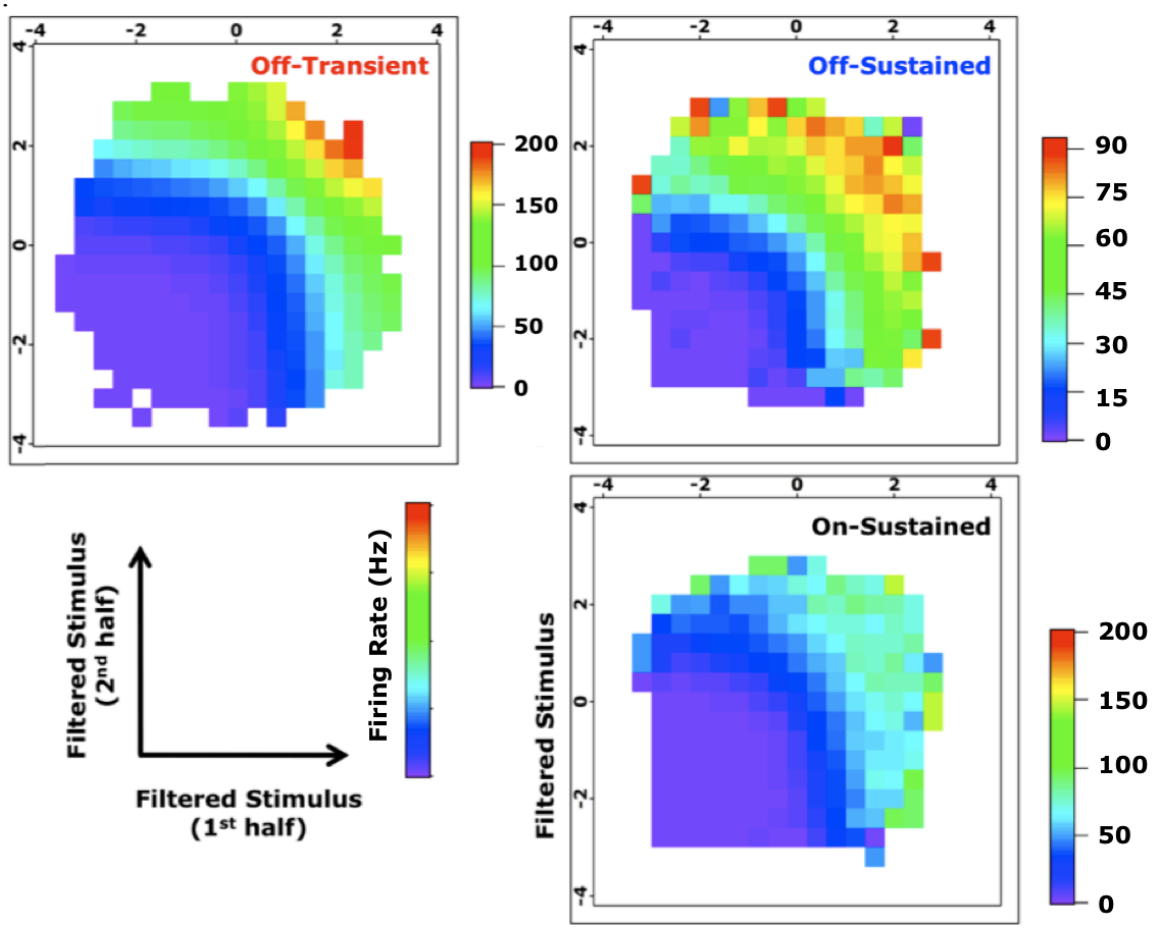

Figure 5.12: 2D-nonlinearites for the A-RGCs calculated from responses to split spot white-noise stimulation. The stimulus consisted of 600 sec of a split randomly flickering binary spot (200-250 µm diameter) centered over the receptive field. The x- and y-axes each represent a separate channel of the split spot stimulus that has been filtered by the respective temporal kernel. The temporal kernels were calculated through standard reverse-correlation techniques from the same data. The color scale for the z-axis indicates the firing rate that resulted from simultaneous input from the x and y stimulus channels.

Based on the indication of nonlinear spatial processing, we expanded the standard LN model to include local nonlinear subunits. To match the split center stimulus, we used a 2-filter model (Figure 5.13). This model possessed an additional filter and nonlinearity such that each half of the stimulus was separately filtered and rectified before summation within the RGC. This was in contrast to the LN model where the filtered stimuli were combined before rectification. Given the symmetry of the 2D-nonlinearities, we assumed processing of each stimulus half by equivalent bipolar cell types. This was reflected in the model by constraining the two bipolar terminal nonlinearities to be the same. A weighted sum of the stimulus channels was implemented through independent nonlinearity scaling factors. A final nonlinearity, representing the spike thresholding of the RGC, transformed the summed bipolar input into a firing rate. The performance of the new "split" 2-filter model was compared to the performance of the standard LN model to complete the second row for the split spot white-noise stimulus in Figure 5.1.

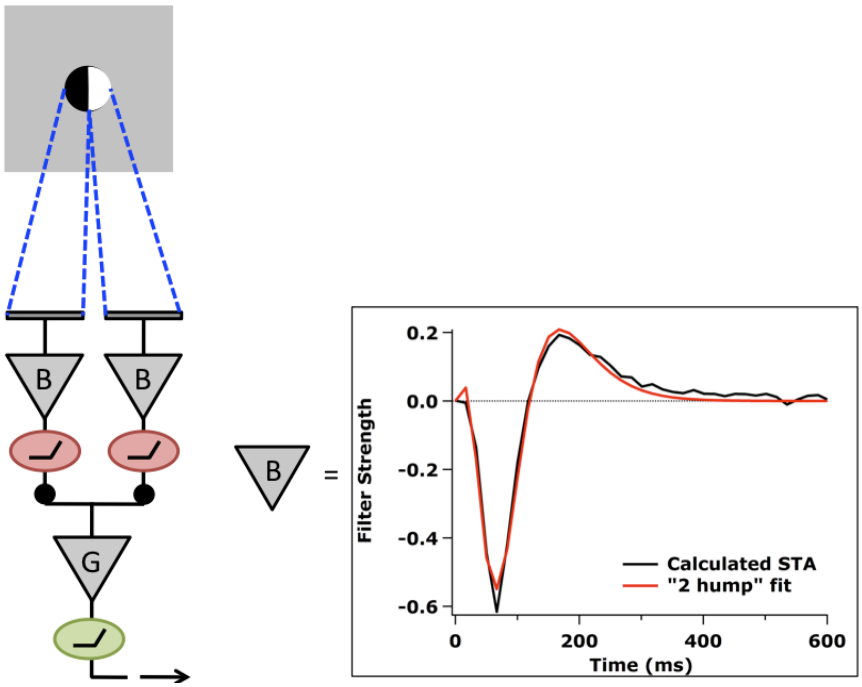

Figure 5.13: Two-filter "split" model designed to predict A-RGC responses to the split spot white-noise stimulus. The receptive field center is locally summed, filtered, and rectified ("B") before final summation and rectification within the ganglion cell ("G").

Overall, both the LN and "split" 2-filter models predicted the responses of the A-RGCs to repetitions of the split spot white-noise quite well. All model predictions for each cell type were over 70% correlated to the neural responses, but the 2-filter model consistently out performed the LN model by at least 2%. Even though the increase in model performance could potentially be explained by the 4 additional free parameters of the 2-filter model, the influence of the local rectification on the computation performed by the model was reflected in the 2D-linearities for the Off-Sustained responses in Figure 5.14. The LN model linearly summed light over the receptive field center to predict the neural output was whereas the 2-filter model independently rectified and summed the two stimulus channels. The former resulted in a linear transformation and the latter closely approximated the actual 2D-nonlinearity from the data. Therefore, the success of the "split" 2-filter model over the LN model was judged by both the replication of the 2D-nonlinearity and the similarity of the firing rate prediction. Similar successful firing rate predictions were also made for the other A-RGCs tested as seen by the additional example fits for the Off-Transient and On-Sustained cells (Figure 5.15).

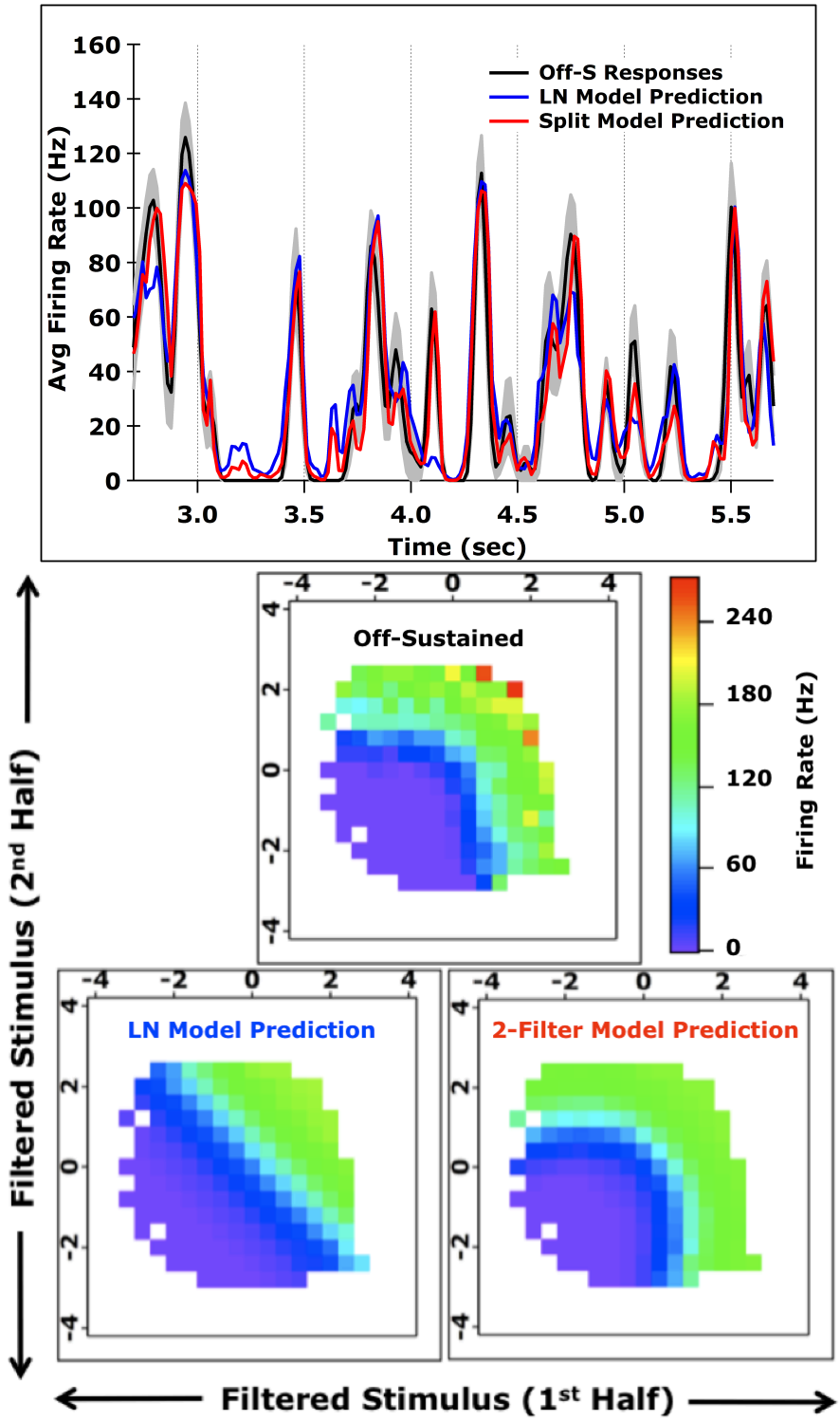

Figure 5.14: LN and 2-filter "split" model predictions of an Off-Sustained A-RGC's responses to split center white-noise. The correlation between the data and the fit improves by 5% from the LN to the split model (84% to 89%). The increased performance of the 2-filter model can be attributed to a closer approximation of the original 2D-nonlinearity (lower right) versus the LN model (lower left).

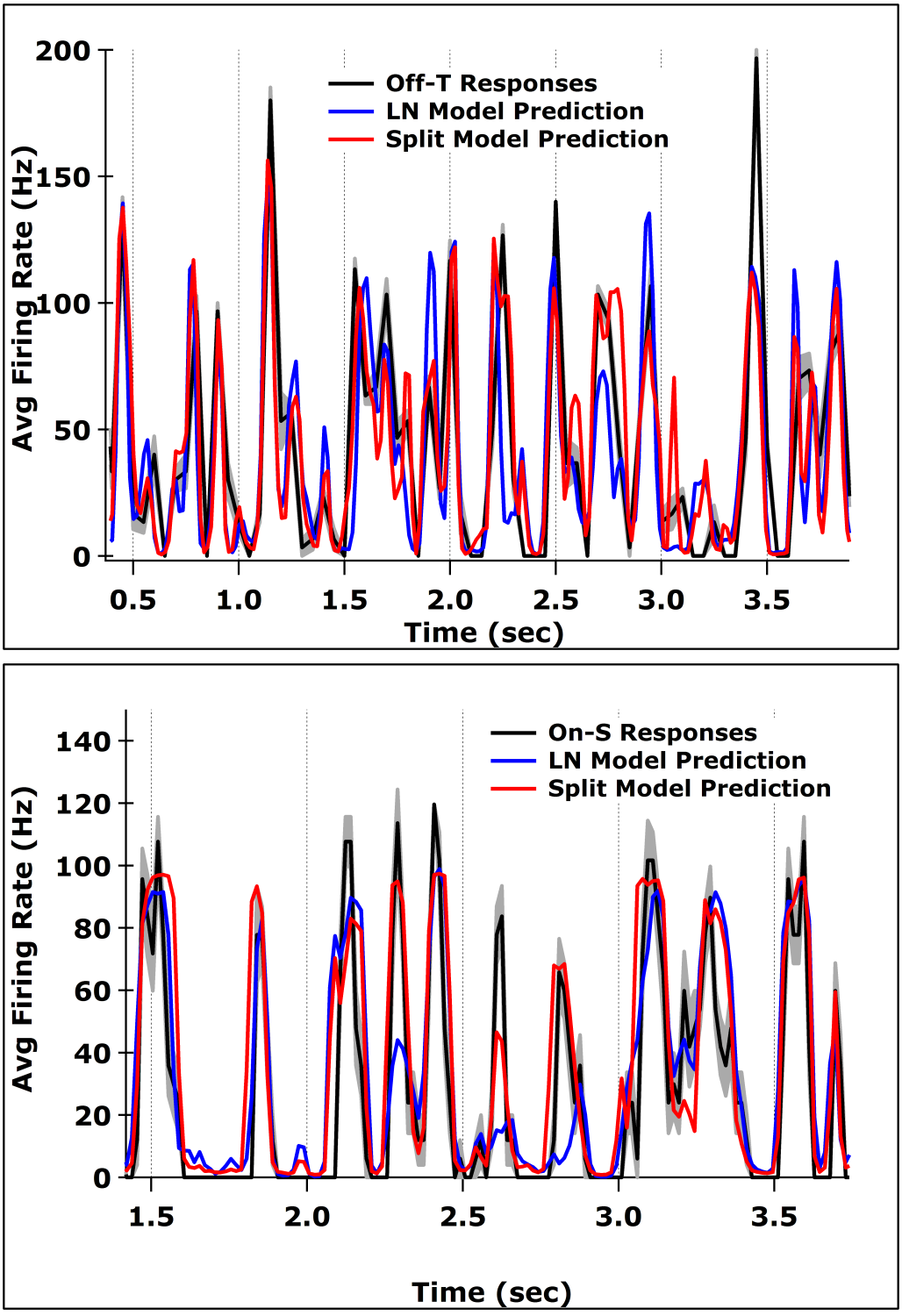

Figure 5.15: Examples of LN (blue) and "split" 2-filter (red) model predictions for Off-Transient (black, top) and On-Sustained (black, bottom) responses to split spot white-noise. For both examples, the correlation between the data and the fit improves by a few percent from the LN to the split model. Off-Transient: 77% to 80%. On-Sustained: 82% to 84%.

After successfully fitting the A-RGC responses to uniform and split-center white-noise, we have completed the top half of the proposed modeling in Figure 5.1. Thus far the LN model predictions to both sets of data have been 75-90% correlated, on average, with the single trial responses. Considering the average correlations across the A-RGC single trial responses fell between 88-94%, the LN model predictions were at most 20% less correlated than the data. We continued to probe the spatial nonlinearities of the A-RGCs by moving to the third stimulus: center-surround white-noise.

5.4.3 Center-surround white-noise, 2D-nonlinearities, and the "center-surround" 2-filter model

In a similar manner to probing the A-RGC visual processing in the receptive field center, we designed a stimulus to drive the center and surround components independently. Aware of nonlinear processing in the center, we were investigating the influence of the surround on the final firing rate. Analogous to the split center analysis, we plotted the 2D-nonlinearities calculated from the responses to the center-surround stimulus. The x-axis was the stimulus filtered by the center and the y-axis was the stimulus filtered by the surround (Figure 5.11). Due to the opposite polarity of the temporal kernels in the center and surround, the negative portion of the y-axis represented the preferred stimulus for the surround. Our convention was to keep the maximum firing rate in the top right corner.

We studied the shape of the 2D-nonlinearities to assess the level of influence of the surround as well as the mechanism. For example, if the surrounds were to have no influence and the firing rate was only driven by the stimulus in the center, the contours of

the 2D-nonlinearity would be parallel to the y-axis. Such behavior is similar to the 2D-nonlinearity for the Off-Transient cell type in Fig. 5.16. This finding agreed with our earlier result that the Off-Transient cells have the weakest surrounds of all the A-RGCs (see Chapter 3, Figure 3.8). For the rest of the A-RGCs, the shapes of the 2D-nonlinearities illustrated an impact of the surround (Figure 5.16). The shape of the On-Sustained 2D-nonlinearity suggested the surround input to the RGC was independently rectified because the center threshold increased during preferred stimuli in the surround, yet remained unchanged during non-preferred surround stimuli. The action of the surround was less clearly defined for the other two cell types: Off-Sustained and On-Transient. The surround could either be linearly or nonlinearly influencing the responses to the stimulus in the center. Based on these results, we designed a model to suit the center-surround white-noise responses.

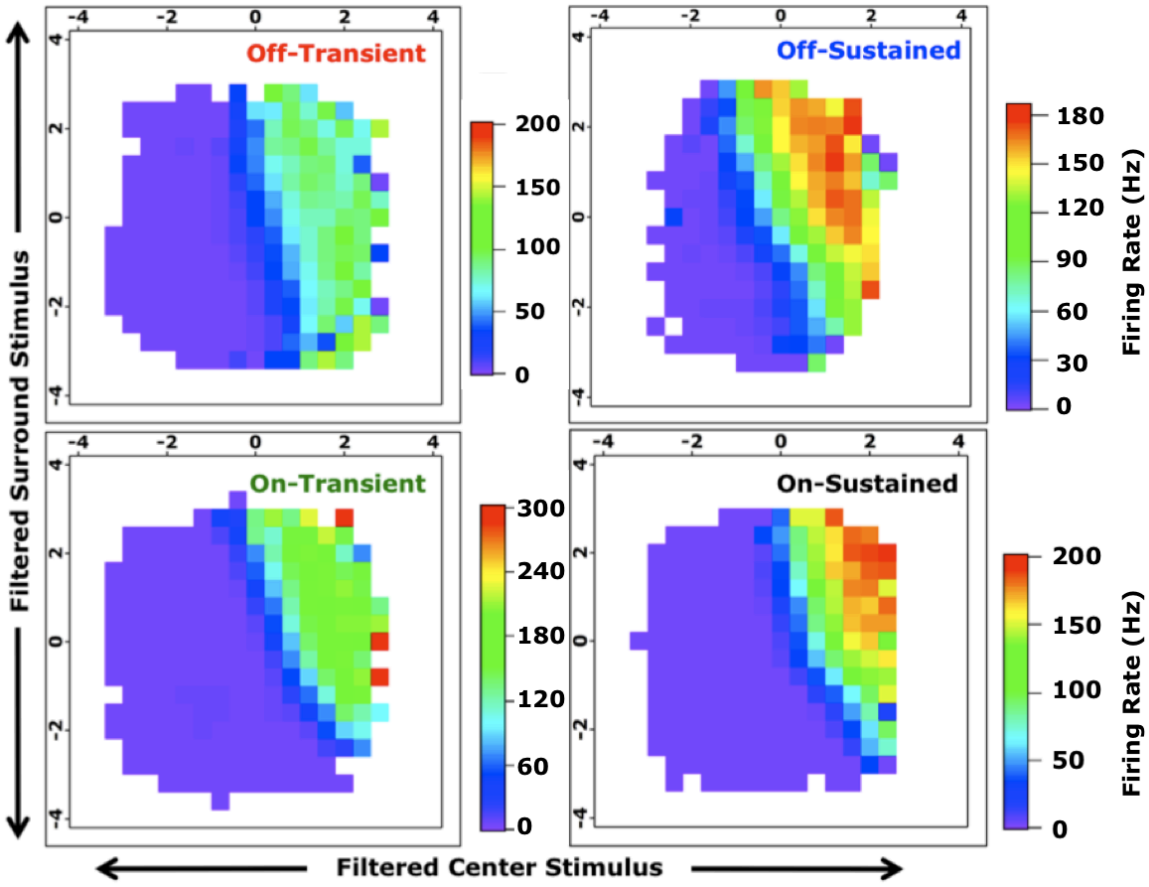

Figure 5.16: 2D-nonlinearites for the A-RGCs under center-surround white-noise stimulation. The stimulus consisted of 600 sec of random binary flicker centered over the receptive field center. One channel was restricted to the center (200-250 µm diameter) and the other to the surround (1000 µm diameter). No annulus separated the spatial components. The x- and y-axes represent a separate channel of the split spot stimulus that has been filtered by the respective temporal kernel. The temporal kernels were calculated through standard reverse-correlation techniques. The color scale for the z-axis indicates the firing rate that resulted from simultaneous input from the x and y stimulus channels.

Based on the shape of the 2D-nonlinearities from the center-surround white-noise responses, we implemented a modified version of the "split" 2-filter model (Figure 5.17). The structure and components of the model were same, but we adjusted the constraints on the parameters. In the case of the split-center stimulus, the two nonlinear channels in the center were assumed to be representing the computations performed by identical bipolar cells. Thus the subunit nonlinearities were constrained to have the same gain and threshold to minimize free parameters. To model the center-surround white-noise responses we allowed completely separate parameters for the two bipolar channel nonlinearities. To fill out the third row of Figure 5.1, we compared the predictive power of the LN model and the "center-surround" 2-filter model on the A-RGC responses to center-surround white-noise.

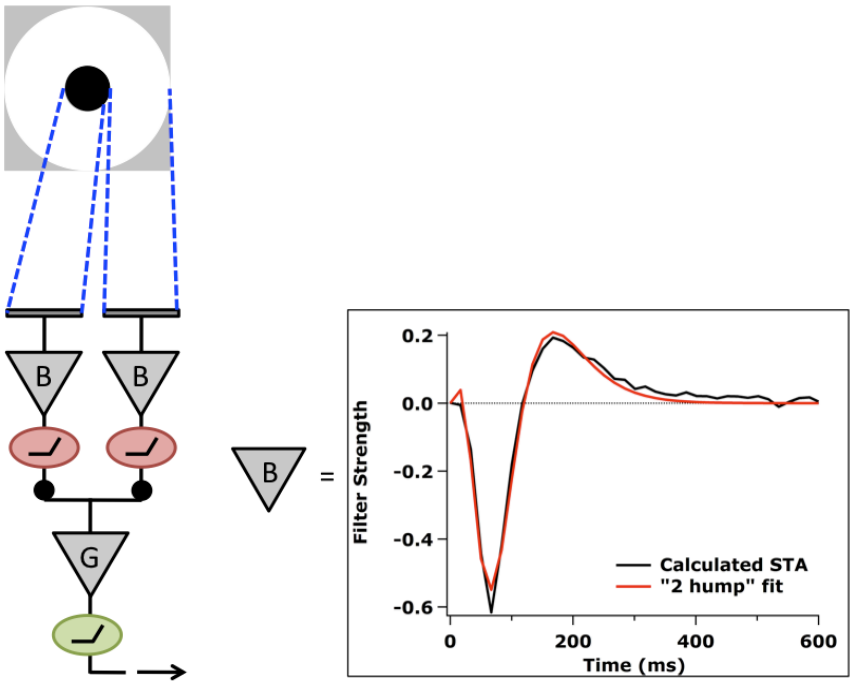

Figure 5.17: Diagram of the "center-surround" 2-filter model utilized to describe responses to the center-surround white-noise stimulus. The structure of the model is identical to the "split" 2-filter model in Figure 13 without any constraints on the parameters.

As with the previous responses to white-noise stimuli, the center-surround stimulus was reasonably predicted by the standard LN model that linearly summed the weighted center and surround (Figure 5.11). The average correlations between the predictions and the single trial repetitions were above 70% for all A-RGC types. Additionally, the 2-filter model that allowed the center and the surround to independently rectify their respective filtered stimuli, performed better than the LN model by ~8% average correlation (Figure 5.18). The computation of the "center-surround" 2-filter model also mimicked that of the On-Sustained A-RGC as illustrated in the similarity of the predicted 2D-nonlinearity with the one calculated from the data. The LN model poorly approximated the same center and surround computation. Similar behavior of the "center-surround" 2-filter model was seen for all of the A-RGCs (Figure 5.19). Therefore, the 2-filter model successfully reproduced the 2D-nonlinearity and improved upon the LN model prediction by including the nonlinear influence of the surround during the center-surround white-noise.

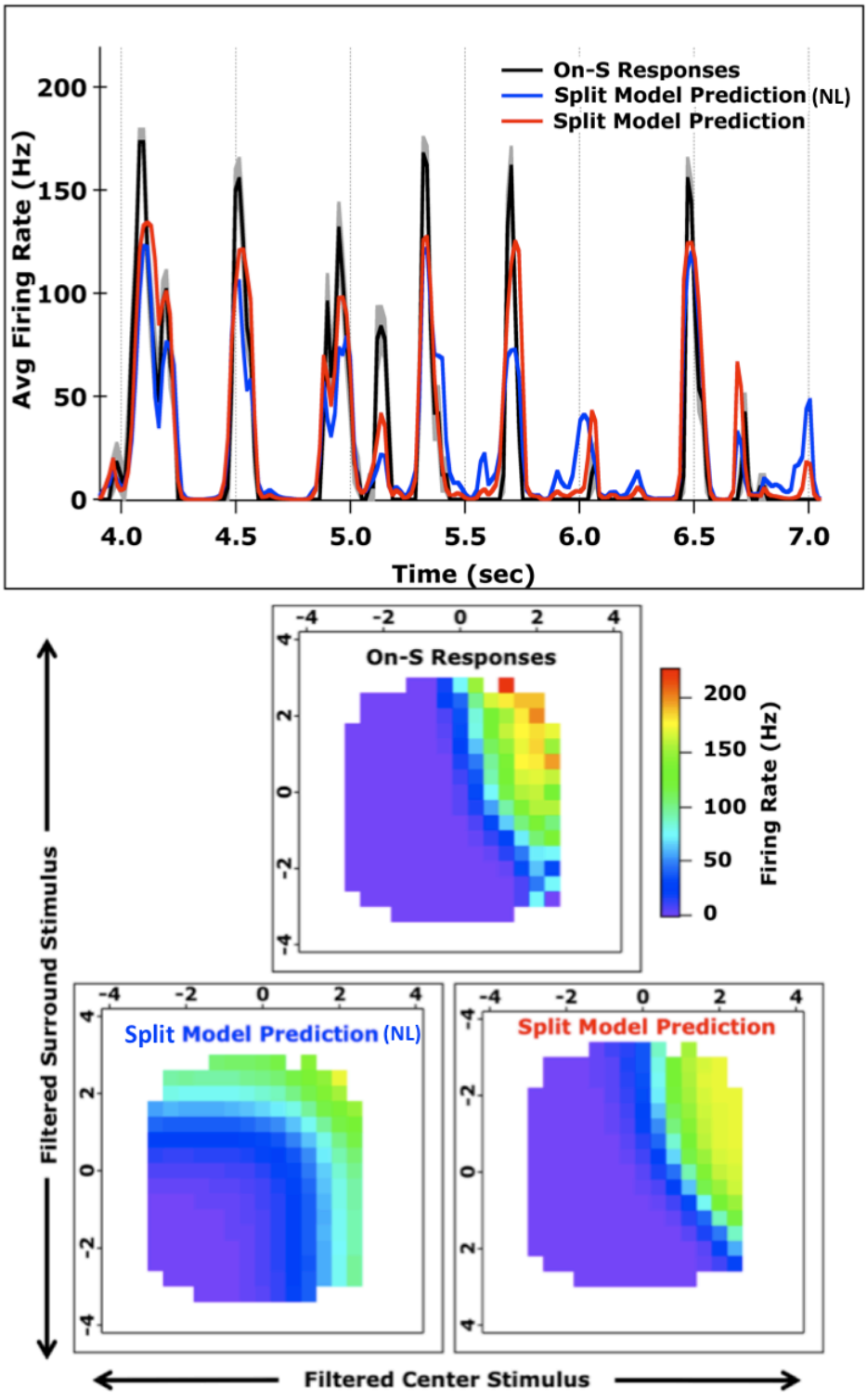

Figure 5.18: On-Sustained responses (black, top) to center-surround white-noise were well predicted by the 2-filter "split" model with independent center and surround nonlinearities (red). The 2-filter split model with nonlinearities forced to be the same (blue) predicted the peaks in the response reasonably well, but failed to reproduce the 2D-nonlinearity (bottom, left). Correlation improved from 81 to 84%.

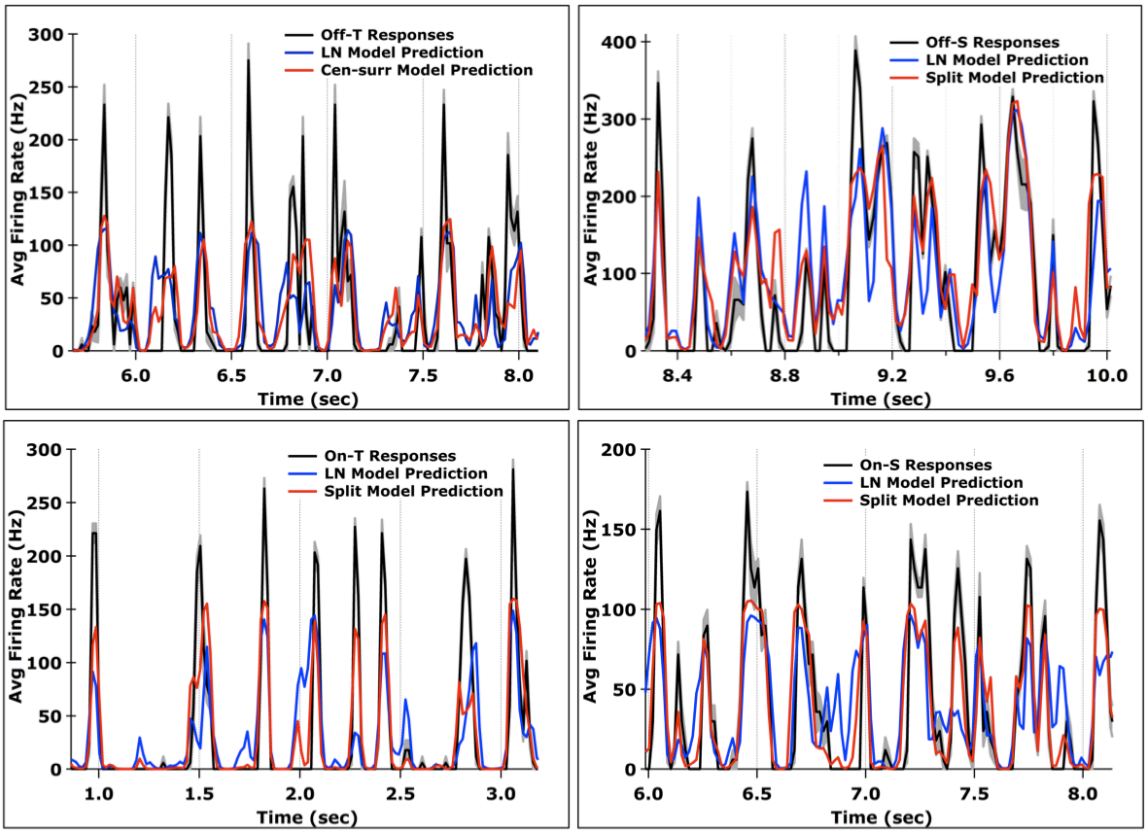

Figure 5.19: Average responses and model predictions by the LN and "center-surround" 2-filter model to center-surround white-noise stimuli for all A-RGCs. Both the LN model prediction (blue) and split model prediction (red) reasonably follow the data (black) within the SEM (grey). By eye, the LN model appears to deviate more from the data as verified by the average correlation to the data. Off-Transient: LN = 70%; Cen-surr = 76%. Off-Sustained: LN = 81%; Cen-surr = 88%. On-Transient: LN = 78%; Cen-surr = 87%. On-Sustained: LN = 74%; Cen-surr = 85%.

5.4.4 Summary of predicting responses to white-noise stimuli

We built models to explain the responses of the A-RGCs to white-noise stimuli of increasing complexity. These models increased in intricacy to match the spatial nonlinear computation of the A-RGCs and their performance was assessed by comparison with the standard LN model. The standard LN model consisted of a single linear filter, calculated by reverse correlation, and nonlinearity that approximated linear spatial summation. For all white-noise stimuli tested, this standard LN model predicted the neural responses quite well (Figure 5.20). The Off-Sustained A-RGC responses were the most consistently predicted by the LN model with no decrease in correlation as the stimulus complexity increased. On average, the Off-Transient A-RGC responses were the least well described by the standard LN model across all stimuli, but each model output was at least 70% correlated with the data. As expected from all the 2D-nonlinearities, allowing rectification of each independent stimulus channel with the 2-filter model increased the model performance to both the split center and center-surround white-noise stimuli (Figure 5.20). These models also had either 4 or 6 more free parameters than the LN model, but there was no chance of overfitting for any model because in each case the parameters were optimized on one portion of the dataset and tested on another (Figures 5.14 & 5.18). The 2-filter models also better replicated the spatial nonlinearities of the A-RGCs. The improved firing rate and nonlinearity predictions over the LN model showed the 2-filter models more correctly modeled the A-RGC computation on visual input. Overall, we found the responses of the mouse A-RGCs to white-noise stimuli to be well replicated by simple models of linear filters and sigmoidal nonlinearities.

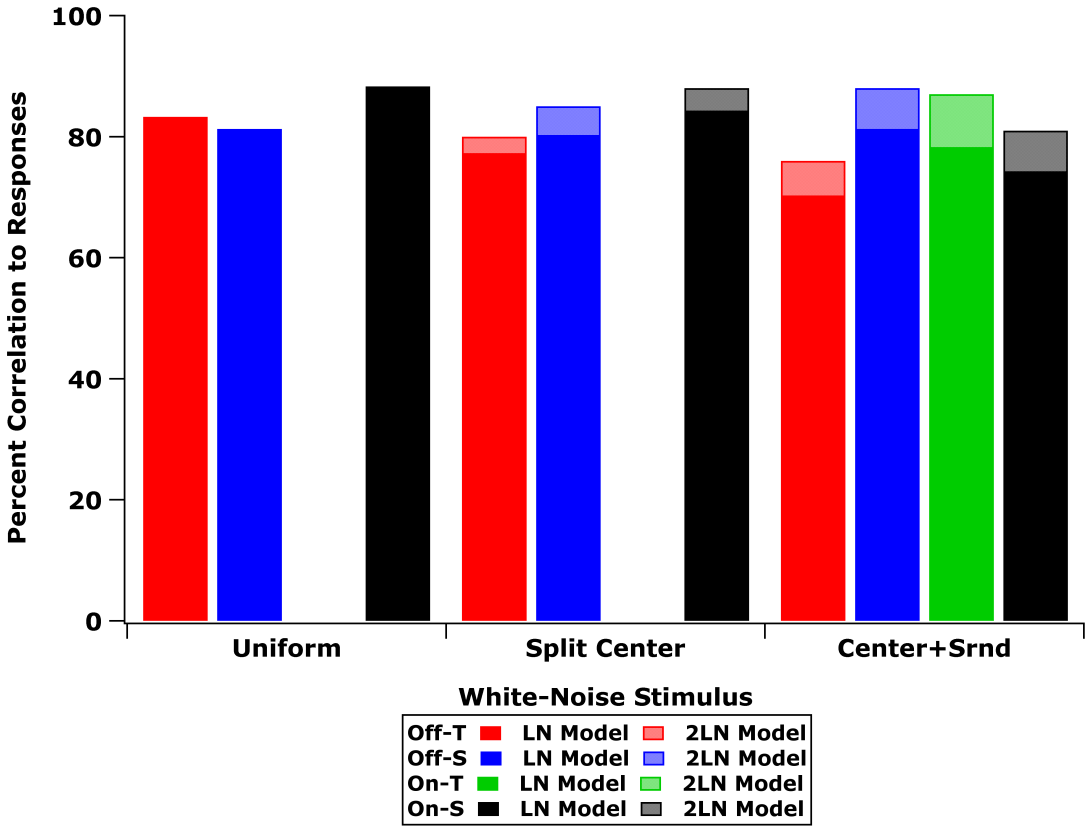

Figure 5.20: Summary of model performance in predicting A-RGC responses of white-noise stimuli of increasing complexity. The solid bars illustrate the performance of the LN model and the shaded bars show the increase in prediction correlation for the 2-filter model.

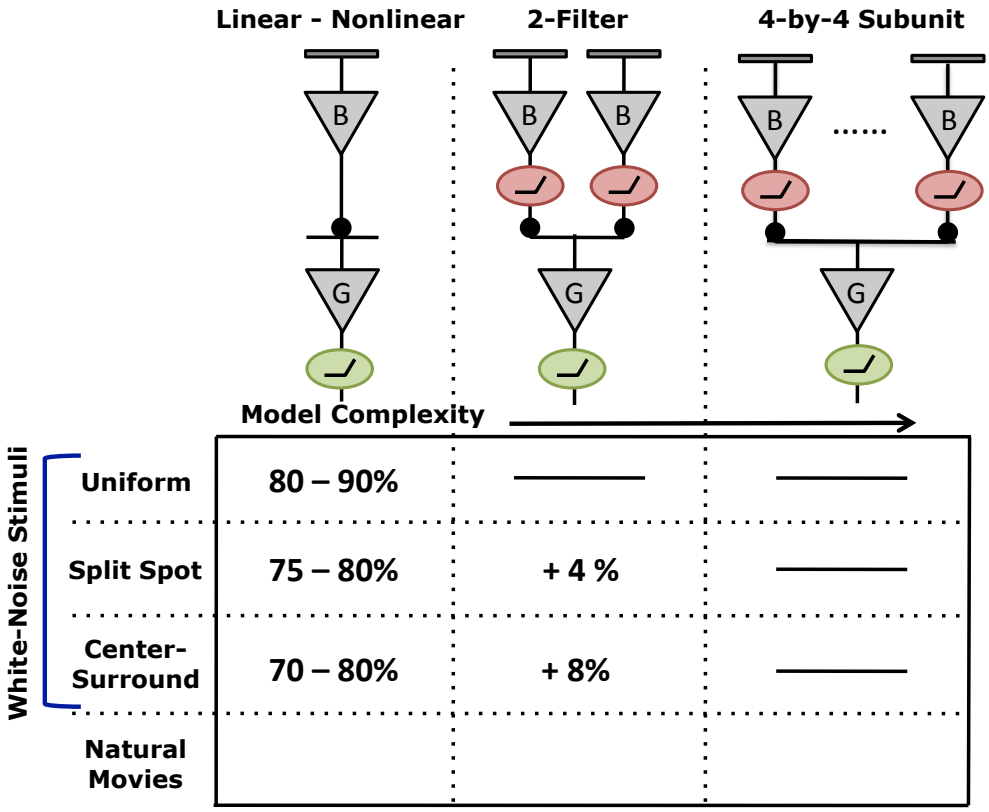

Figure 5.21: Summary of correlation values between data and model fit for responses of the A-RGCs to white-noise stimuli. The range under the linear-nonlinear model indicates the span of correlation values for the standard LN model across all 4 A-RGC types. The percent improvement indicated under the 2-filter model states the improvement in the two range values to fit the same data.

5.5 Predicting natural movie responses from models based on white-noise response properties

A sufficient model for the A-RGCs should predict their responses to any arbitrary visual input within the range of neural noise. In particular, we were interested in predicting natural movie responses to eventually link visual input, RGC pre-processing, brain activity, and motor output. We subjected our models built for responses to white-noise to the ultimate test of predicting responses to natural movies.

Our approach was to fill out the last row of the table in Figure 5.2. This consisted of applying models of increasing complexity to the same neural responses to establish the minimal number of components required to successfully reproduce the A-RGC responses to natural movies. The neural responses consisted of responses to two movies (~30 sec – 1 min long) in the receptive field center and surround (mask diameter = 1000 um). The same two movies, i.e. the simulated mouse and mouse cam movies, were used previously to investigate the relative importance of stimulus components to the A-RGC firing rate (see Chapter 4, Figure 4.1). Model performance was matched for both movie stimuli and so for clarity we only quoted the performance of the simulated mouse movie. We defined a successful firing rate prediction as one that differed from the A-RGC responses within intrinsic neural noise. The LN and "split" 2-filter models were tested in addition to a new model composed of nonlinear subunits in the receptive field center.

5.5.1 Performance of the linear-nonlinear model on predicting natural movie responses

We started by modeling the A-RGC responses with the simplest model for RGCs: the LN model. For the LN model we filtered the input stimulus of the training dataset with the spike-triggered average calculated by reverse correlation and passed that output

through a static nonlinearity. Above, we found this model to very successfully predict the responses of all the A-RGCs to a new spatially uniform stimulus and to reasonably predict the responses to more spatially complex white-noise stimuli. We also found earlier that the A-RGC responses to the original and manipulated movie of averaged central pixels were 70% similar, which suggested that these cells may be amenable to simple models (see Chapter 4, Figure 4.17). Based on the results from fitting white-noise responses and the similarity between the A-RGC responses to the original and manipulated movies, we hypothesized that the LN model would predict the responses to natural movies reasonably well. To test this hypothesis, we fit the natural movie responses with the LN model.

Just as for the white-noise stimuli, we convolved the movie with the measured spatio-temporal filter of the cell and rectified the filter output with a log-sigmoidal nonlinearity (Figure 5.1). The spatio-temporal filter was held constant, meaning this model again had three free parameters that were optimized during the fit: the nonlinearity gain, threshold, and peak firing rate (Eqn. 4). We found this standard LN model to predict the responses of the Off- and On-Sustained A-RGCs quite well. This assessment was based on the similarity of the model prediction to the A-RGC responses across repetitions of the same stimulus. For example, the On- and Off-Sustained A-RGC responses were ~85% correlated, on average, across single spike trains and the average similarity between the model output and the same single trial repetitions was 70-75%. On average the correlations between the predictions and the data were only 10-15% less than the similarity across trials (Figure 5.31). The Off- and On-Transient responses were consistently fit the worst by the LN model. On average their responses were 30-40% less

correlated than the single trial repetitions. Overall the predictions of the LN model with a fixed linear filter were at least 55% correlated to the A-RGC responses and in some cases the predictions were far better.

In the above standard LN model fitting, we kept the spatio-temporal filter measured from white-noise stimuli constant. Due to the differing statistics of white-noise and natural scenes, we acknowledged that the filtering properties of the A-RGCs may have changed under the two conditions. In an attempt to improve the predictions from the single filter LN model, we decided to optimize the temporal component of the receptive field. In practice, we kept the spatial receptive field fixed and chose starting parameters for the temporal kernel by fitting the STA with the "2 hump model"[17]. Fitting the temporal kernel added an additional 5 free parameters on top of the 3 parameters for the nonlinearity and this modification increased the prediction power of the single filter model. The model predictions of the Off- and On-Sustained A-RGC responses improved by 10-15%. This jump in performance put the error of the model prediction within the range of the intrinsic noise of the cell. The average correlation between single trial repetitions for the sustained cells was 85±4% and the average correlation between the repetitions and model prediction was 84±2%. Therefore the model reproduced the firing rate of the neuron within the biologically acceptable limits of the sustained A-RGCs. The model performance for the Off- and On-Transient responses also improved when fitting the temporal kernel. The prediction power with the modified standard LN model was roughly equivalent to the sustained A-RGC predictions under the standard model. The Off-Transient predictions were 13% and the On-Transient predictions were 20% less correlated than the data repetitions.

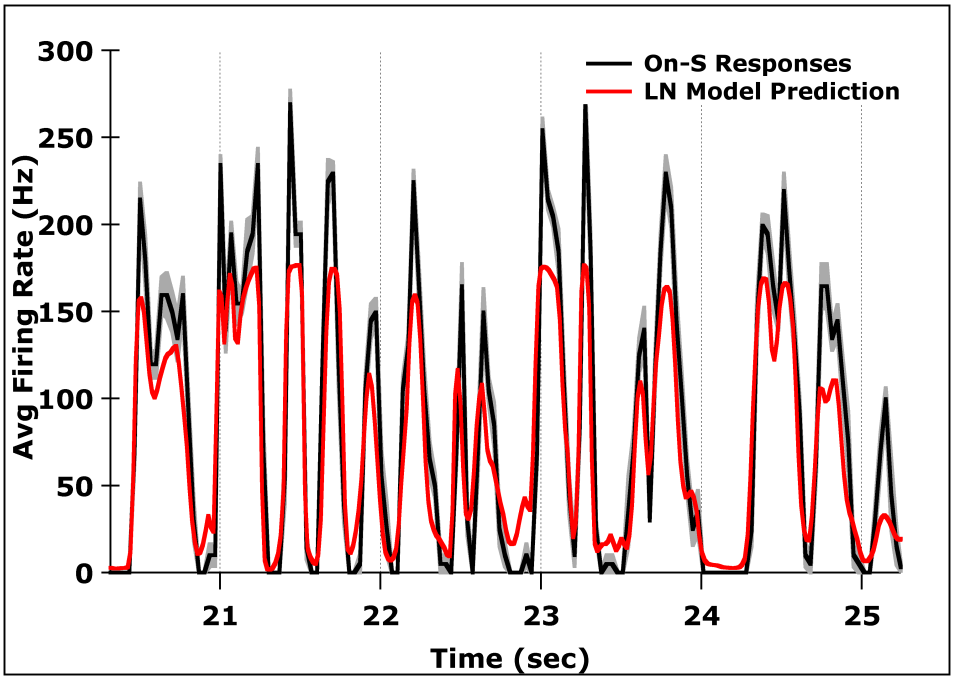

Figure 5.22: LN model prediction for an On-Sustained A-RGC's responses to the simulated mouse natural movie. In this example the temporal kernel and nonlinearity were optimized by the fitting algorithm. The correlation between the data and the fit was 87%.

We tested one final simplification of the LN model by assuming that the A-RGC spatial receptive field averaged across the pixels in the center. The motivation for this simplification came from our earlier observation of A-RGC responses to modified natural movies (see Chapter 4, Figure 4.17). For the same movies used in modeling, the majority (~70%) of the A-RGC responses to the original movie (1000 μm diameter mask) were retained when shown the same movie of only the average of the central pixels (200-250 μm diameter mask). The model for this fit was identical to the previous model, except instead of calculating the model input for each cell by filtering the movie with the spatial receptive field, the model input was the averaged movie stimulus we used during the movie manipulations. For all the A-RGCs, taking a flat average versus a weighted average of the pixels did not affect the model performance. If anything, the predictions using the flat averaged input were better than the weighted input by a few percent.

In summary, the standard LN model predicted the natural movie responses of the A-RGCs quite well. By modifying the model to fit the temporal kernel, this model with a single filter and nonlinearity was sufficient to predict the responses of the sustained A-RGCs within intrinsic biological noise. Unexpectedly, these predictions were generated by taking a flat average of the central pixels for each frame and the model performance did not improve with an input generated by filtering the movie with the spatial receptive field. Unlike for white-noise stimuli of increased complexity, the LN model was sufficient for predicting the majority of the responses to complex natural movies. This result indicated the computations performed by the A-RGCs under our natural movie stimuli were simpler than under the white-noise.

5.5.2 Performance of the split center model on predicting natural movie responses

The addition of a second independently flickering white-noise channel to generate the split spot white-noise required further model components to match the performance of the LN model to spatially uniform stimuli. This requirement was unsurprising considering the nonlinear addition of the stimulus illustrated by the 2D-nonlinearities (Figure 5.12). By adding a second, identical channel to locally rectify the new half of the stimulus, we improved on the LN model prediction by 2-9%. Based on this result, we hypothesized that applying the 2-filter "split" model to the natural movie responses would also improve upon the performance of the LN model. To generate the input for the split center model, we arbitrarily divided the center of the natural movie (250 μm diameter) into two halves (Figure 5.23). The average of the pixels in each half was either weighted based on the calculated spatial receptive field or computed as the flat average.

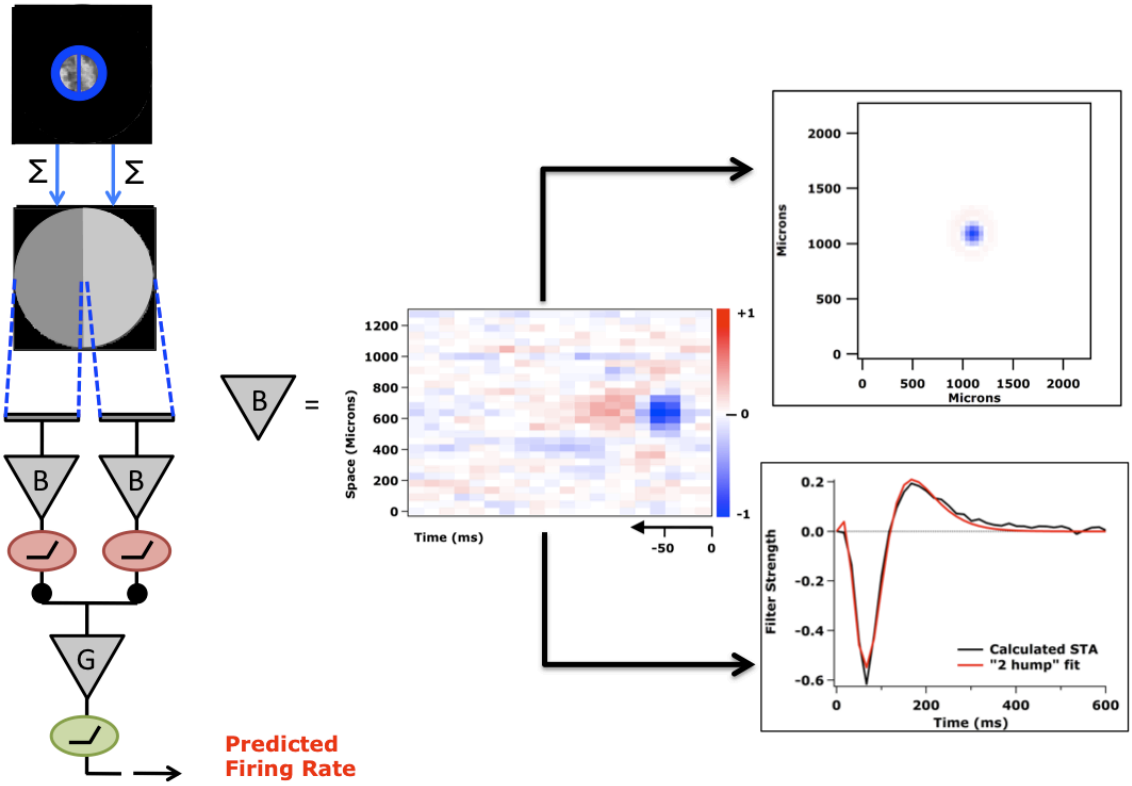

Figure 5.23: Diagrammed procedure of fitting the "split" 2-filter model to the natural movie responses. Each frame of the movie was split in half and the halves were independently summed to comprise the input to the model.

The performance of the "split" 2-filter model did not improve on the performance of the modified LN model. Additionally, the model was not affected by the method of averaging used to generate the model input. The predicted firing rates for the transient A-RGCs were still 13-20% less correlated, on average, than the data repetitions while the prediction errors for the sustained A-RGCs were within the neural noise.

After seeing no improvement in the predictive power of the "split" 2-filter center model to natural movie responses, we investigated whether this deviation from the white-noise stimuli was due to different spatial processing of the A-RGCs under the two stimulus conditions. As a preliminary test, we compared the 2D-nonlinearities of A-RGCs of the same type calculated from responses to both white-noise and the simulated mouse natural movie. We calculated the natural movie 2D-nonlinearities in a similar manner as above. Each half of the averaged movie was filtered by the temporal kernel for the receptive field center and plotted on the x- and y-axes respectively. The recorded firing rate was plotted on the z-axis. Comparing the natural movie and split spot white-noise 2D-nonlinearities, we found that the region of stimulus space explored during natural movie stimulation was smaller than during white-noise (Figure 5.24). Additionally, during the natural movie stimulus, the 2D-nonlinearity could be adequately approximated by a linear combination of the two averaged stimulus halves. This preliminary comparison indicated the A-RGCs performed equivalent processing of visual input under the two stimulus conditions, i.e. the 2D-nonlinearity was unchanged under white-noise and natural movie input, but that the region over which the nonlinearity was evaluated changed.

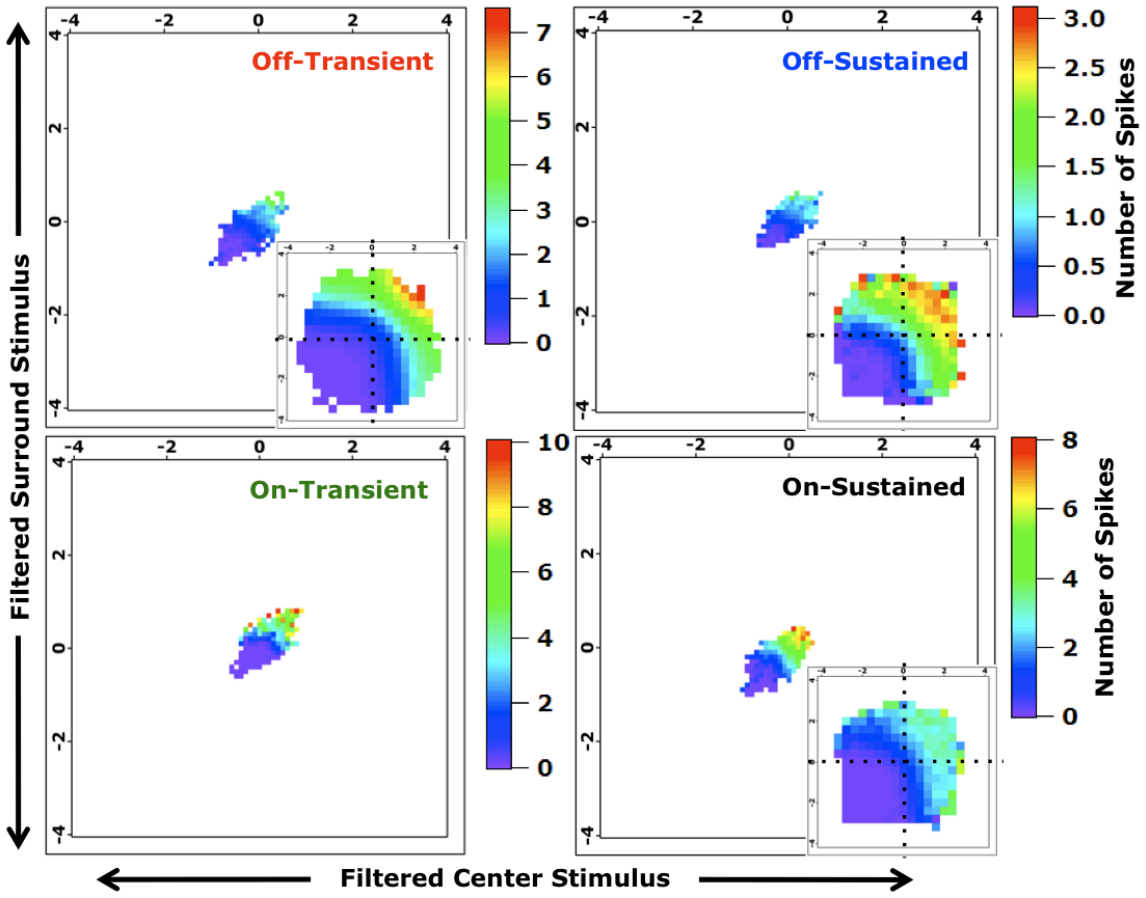

Figure 5.24: Comparison of the A-RGC 2D-nonlinearities calculated from responses to the simulated mouse movie and split center white-noise. The nonlinearities for the white-noise responses are reproduced from Figure 5.12 and placed in the lower right corner. The axes for all the 2D-nonlinearities range from -4 to +4.

So far we tested the predictive power of the LN and "split" 2-filter models on the A-RGC responses to natural movies. The LN model proved sufficient for modeling the sustained A-RGC responses to these movies, but both models failed to predict the transient cell responses within neural noise. To attempt to improve the prediction of the transient A-RGC responses, we decided to build a subunit model to locally sum and rectify the movie input. We chose this direction instead of applying the "center-surround" 2-filter model as used for the center-surround white-noise for two reasons. First, the 2D-nonlinearity of the Off-Transient cells indicated a minimal influence of the surround on the final firing rate output. Therefore, it would be unlikely for the "center-surround" 2-filter model to improve the Off-Transient prediction. Additionally, our earlier observation of responses to manipulated movies suggested local summation and rectification in the A-RGC surround rather than flat summation. To successfully implement a model with surround subunits would perhaps take many more additional parameters. Thus in an effort to find a model of minimal complexity to improve the prediction for both of the transient cells, we built the four-by-four subunit model.

5.6 Predicting responses to natural movies with the four-by-four subunit model

We established that the A-RGCs nonlinearly process visual input over their receptive field centers in two ways. For one, we found each stimulus channel in the 2D-nonlinearites under split spot white-noise to display a rectified shape and, second, we found all of the A-RGCs, except some of the Off-Sustained, to display responses similar to the frequency doubling indicative of nonlinear spatial summation (see Chapter 3, Figure 3.6)[10,34,38]. Models from other work explaining frequency doubled responses have

pooled over locally rectified regions of a large receptive field[10,38,39]. The crude, two-channel version of this model that we already tested, i.e. the "split" 2-filter model, failed to perform better than the LN model to predict natural movie responses despite having an additional parameter. We hypothesized that the equivalent performance of the two models was due to a model input that had been averaged over "too large" of an area. In this scenario, by averaging over half of the receptive field center, we had averaged out the important information to effectively drive local nonlinear subunits driving the response. Therefore, we created the last model in our beginning A-RGC modeling strategy by dividing the center stimulus into eight times the number of regions to build a nonlinear subunit model (Figure 5.2).

5.6.1 Description and fitting strategy of the four-by-four subunit model

Our model split the receptive field center into 16 subunits through a 4-by-4 grid (Figure 5.25). Each model subunit matched the same structure of the previous LN model extensions. Thus, the average stimulus across each subunit was filtered by a temporal kernel and passed through a sigmoidal nonlinearity. The temporal kernel and nonlinearity were identical for all subunits except that each subunit was allowed to have its own weight as implemented by a scaling of the nonlinearity. All the rectified outputs of the subunits were added together as they would be within the RGC. The sum of the subunit outputs was passed through a final sigmoidal nonlinearity representing the spike generation of the RGC. The final output of the model was interpreted as the time-dependent prediction of the A-RGC firing rate.

The number of parameters in the previous models had not exceeded 12, but the 4-by-4 subunit model more than doubled that number. The subunit model had 26 free parameters: 5 for the temporal kernel, 2 for the subunit nonlinearity, 16 for the weights of the subunits, and 3 for the RGC nonlinearity. We used the same starting parameters as before for the temporal kernel and the nonlinearities. All of the subunit weights were set to unity. To facilitate the algorithm with fitting the larger number of parameters, the fit iteratively went through subspaces of similar parameters until convergence (see section 5.2 on optimization).

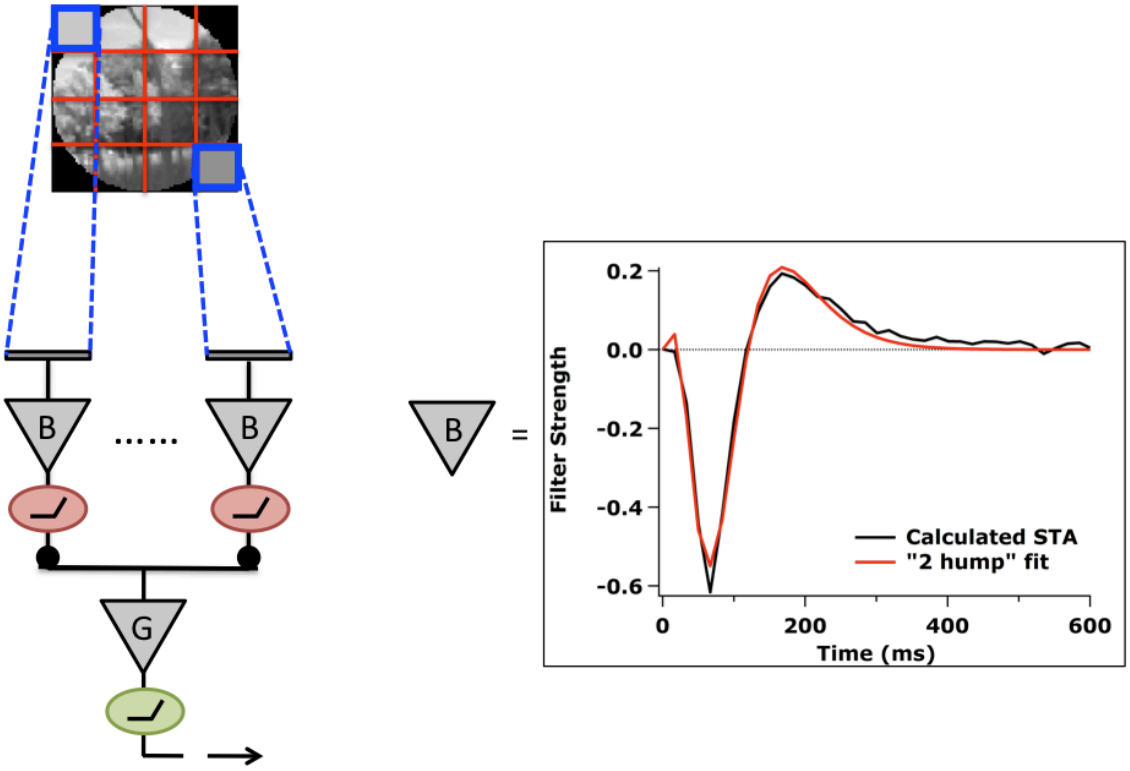

Figure 5.25: Schematic of the 4-by-4 subunit model. The natural movie, within a 1000 µm mask, was split into a 4-by-4 grid. The pixels within each of the 16 squares were linearly averaged and each served as an input to a bipolar subunit "B." The subunit outputs were rectified before summation within the retinal ganglion cell "G" and final transformation into the output firing rate. This model had 23 parameters, the most of all the models so far utilized.

5.6.2 Performance of the four-by-four subunit model

The performance of the 4-by-4 subunit model matched or exceeded that of the previous models for all of the A-RGCs. The predictions for the Off-Sustained and On-Transient responses both increased in correlation by 5% and the prediction for the Off-Transient A-RGCs increased by 7%. The prediction for the On-Sustained responses matched those of the previous models. Recall the modified LN model was already sufficient to explain the Off-Sustained responses within the error of neural noise. This additional 5% increase indicated the 4-by-4 subunit model could, on average, predict the responses of the Off-Sustained A-RGCs well within intrinsic neural noise. Example predictions and the calculated receptive field parameters are given for each A-RGC type (Figures 5.26-29). For each A-RGC type, the grey prediction closely follows the colored average response. Additionally, the temporal filters found by the model tend to differ somewhat from those calculated from the white-noise responses. The degree of rectification of the bipolar subunits varied depending on the cell, but we did not see a consistent relationship between rectification strength and A-RGC type. The lower right corners of Figures 5.26 -29 contain the weight matrices for the 16 bipolar subunit channels. Channels with larger weights, aka lighter colors, were often in the center of the receptive field as expected for Gaussian weighting. The range of nonlinearity shapes can be seen in the lower left corners with the magnitude of the weights represented by the peak subunit output values. Overall, the computations performed by the 4-by-4 subunit model and the final firing rate predictions were reasonable for each A-RGC type.

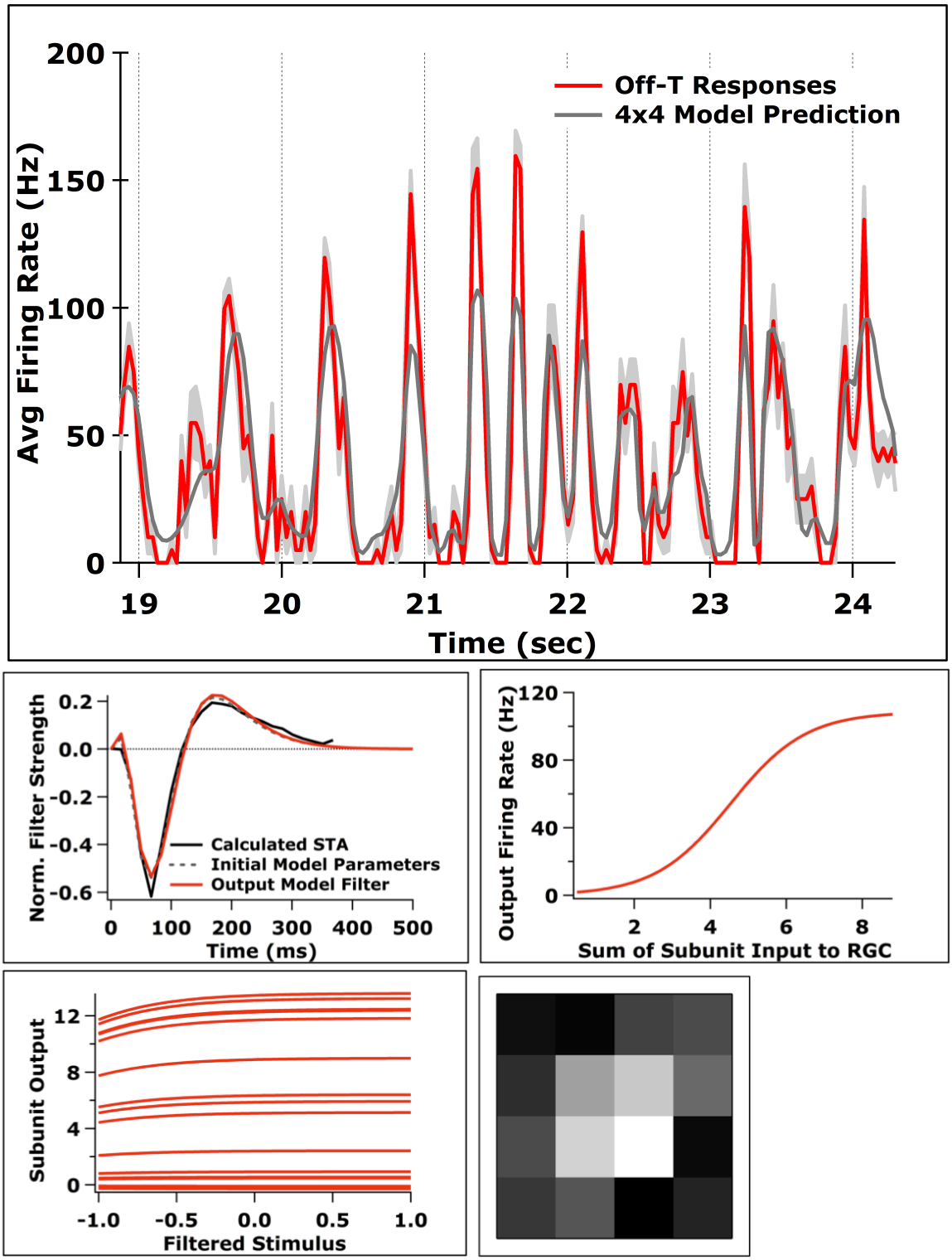

Figure 5.26: 4-by-4 model prediction and fit parameters for Off-Transient A-RGC. Correlation between data and fit: 80%. Lower right weight matrix shows location of lower left nonlinearities with lighter colors representing larger subunit outputs.

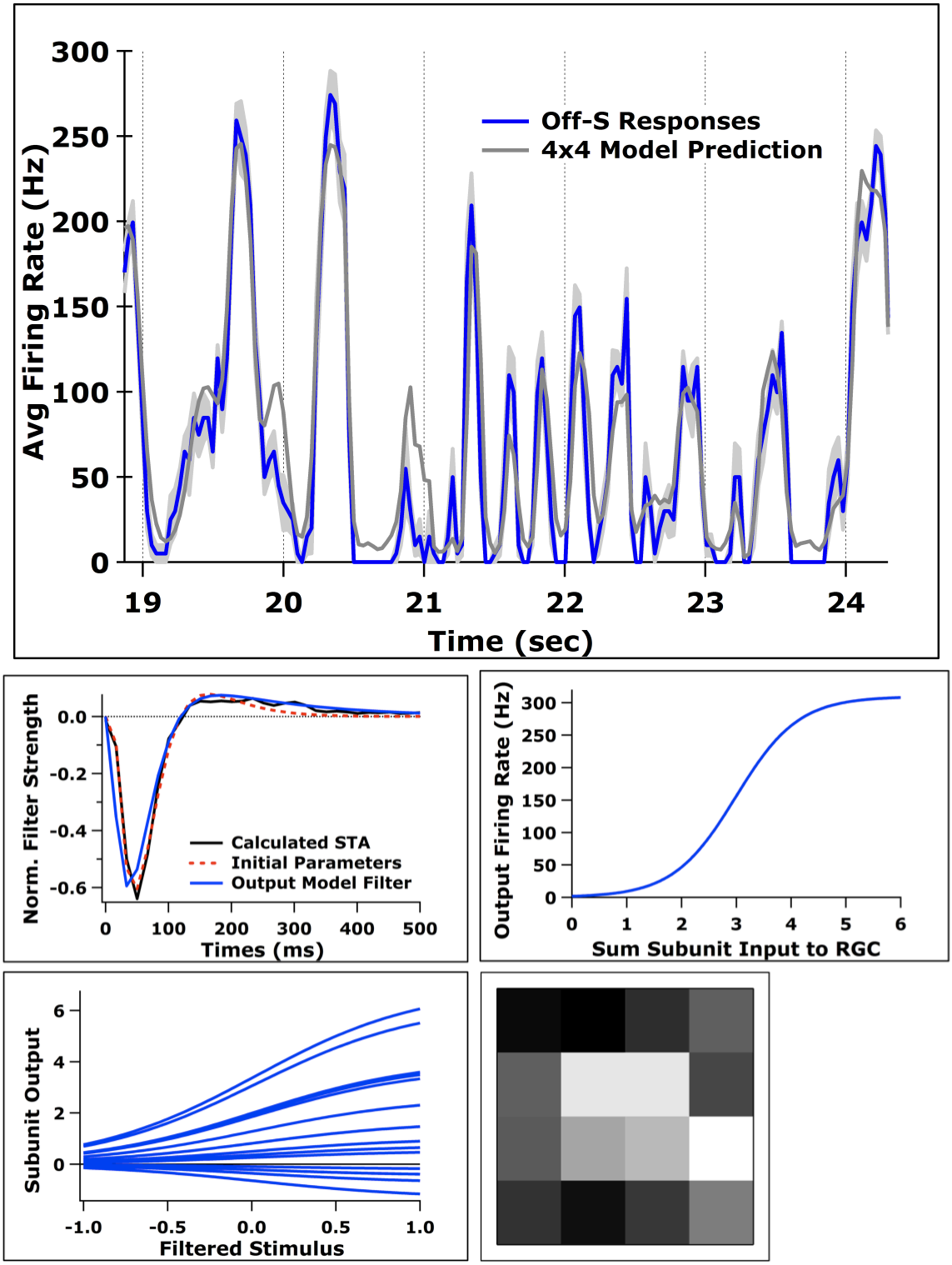

Figure 5.27: 4-by-4 model prediction and fit parameters for Off-Sustained A-RGC. Correlation between data and fit: 88%. Lower right weight matrix shows location of lower left nonlinearities with lighter colors representing larger subunit outputs.

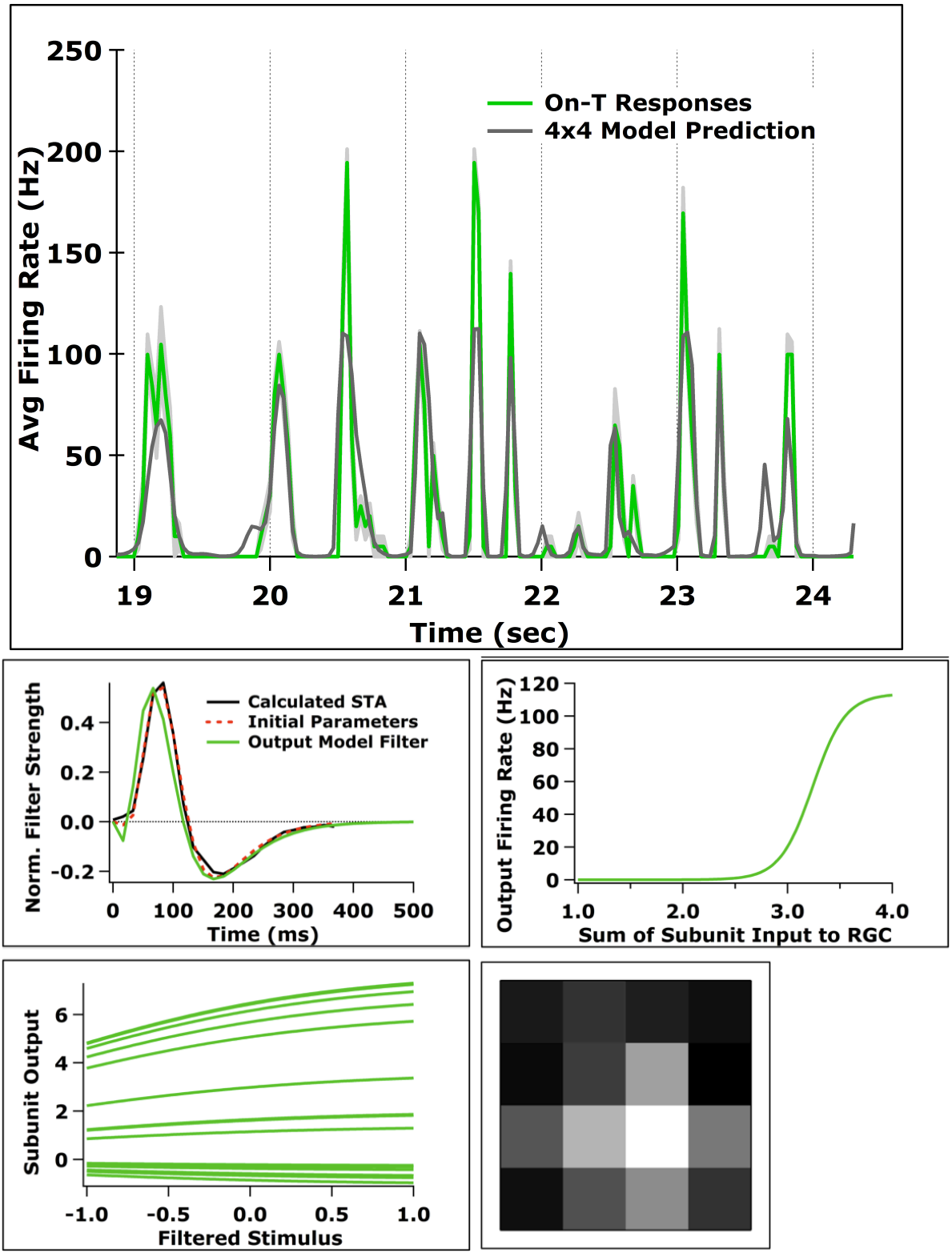

Figure 5.28: 4-by-4 model prediction and fit parameters for On-Transient A-RGC. Correlation between data and fit: 80%. Lower right weight matrix shows location of lower left nonlinearities with lighter colors representing larger subunit outputs.

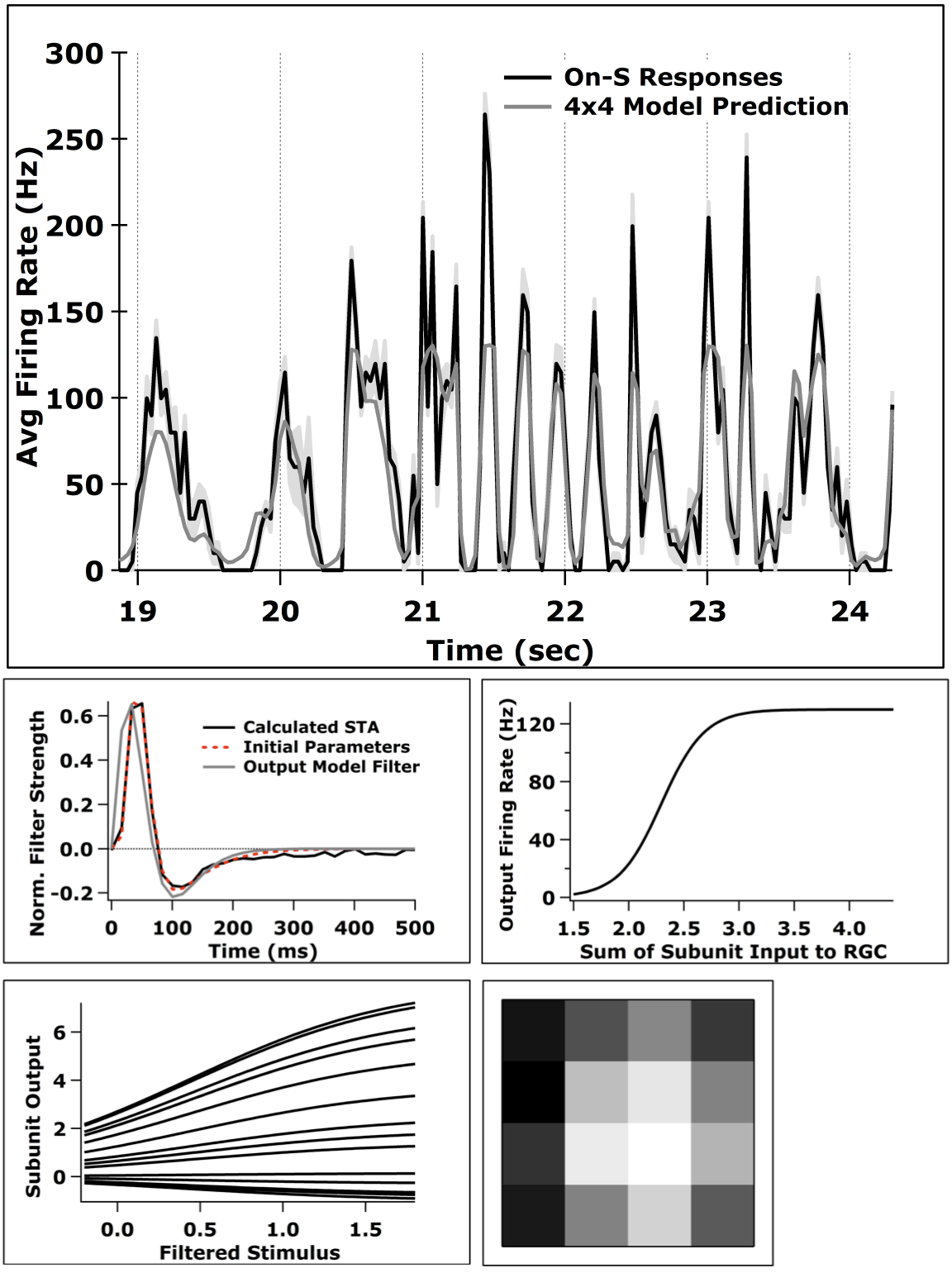

Figure 5.29: 4-by-4 model prediction and fit parameters for On-Sustained A-RGC. Correlation between data and fit: 88%. Lower right weight matrix shows location of lower left nonlinearities with lighter colors representing larger subunit outputs.

5.7 Testing the performance of simple LN models on non-alpha retinal ganglion cells

In addition to fitting the A-RGC responses to natural movies, we also fit our models to a few randomly selected RGCs. The responsiveness of the non-alpha RGCs to the natural movies varied. Some of the non-alpha RGCs only sporadically responded to the natural movie stimuli while others, such as the example in Figure 5.30, responded robustly. In all cases, fitting our LN models from Figure 2 elicited worse predictions than we obtained for the A-RGCs. The average correlation between the model prediction and the data was consistently below 30%. Our finding that a subset of non-alpha ganglion cells were poorly fit by simple models suggests our modeling results are unique to the A-RGCs.

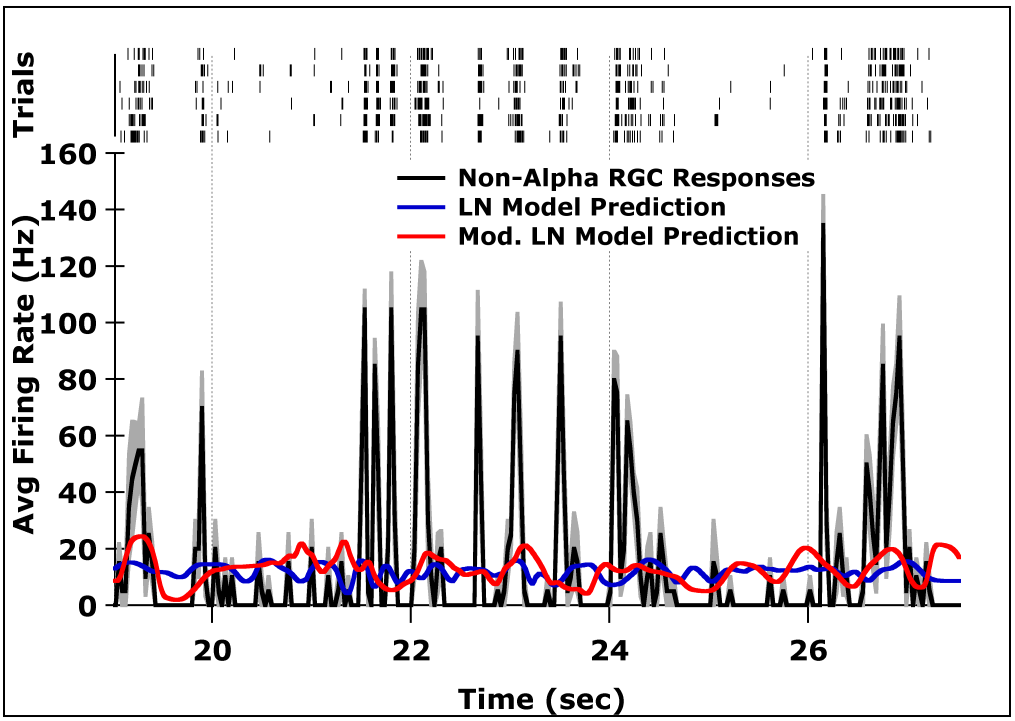

Figure 5.30: LN and modified LN model predictions for a non-alpha, On-Off RGC. The average correlations of the predictions to the data were 15% for the LN model and 20% for the modified LN model where the temporal kernel was fit by the model.

5.8 Summary of predicting alpha retinal ganglion cell responses to natural movies

We found the simple models successful in predicting white-noise responses, in some cases, equally successful at predicting responses to natural movies. We also found that allowing the model to fit the temporal kernel improved the model performance by 10-25%. In opposition to our results from predicting responses to white-noise, the "split" 2-filter model performance did not improve upon on the LN model. To improve the correlation between the model prediction and fit by the same degree (~5%), the model for the natural movies required 8 times the number of rectifications with the receptive field center. This result is consistent with more complex spatial structure of natural movies. As a final assessment of model performance, we compared the average model performance of predicting responses to natural movies with the intrinsic noise of each A-RGC (Figure 5.31). The models performed consistently better by at least 10% in predicting the output of the sustained A-RGCs versus the transient RGCs. This was especially true considering the slight bias of the transient cells toward more regular firing across stimulus repetitions (Figure 32, y-axis). In general all of the models performed well for predicting the output of the A-RGCs compared to non-alpha RGCs. The success of the LN and extended LN models suggested simple models with few processing stages were sufficient to capture the A-RGC computations on natural movie input.

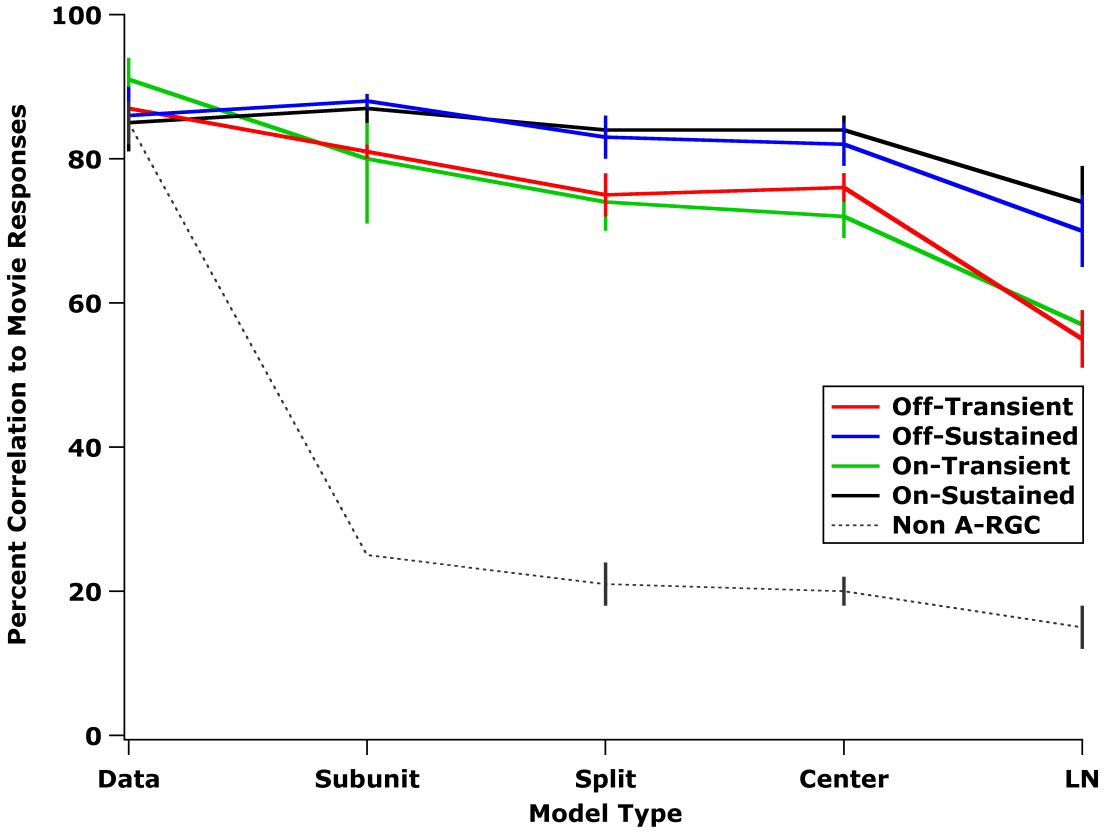

Figure 5.31: Comparison of model performance on predicting responses to natural movies with intrinsic neural noise. The y-intercept ("Data") represents the intrinsic error of each A-RGC calculated as the average response correlation across repeated trials of the same stimulus. The average correlation of the model prediction to these same trials is plotted for the 4-by-4 subunit ("Subunit"), split 2-filter ("Split"), modified LN to fit the temporal kernel ("Center"), and LN models.

5.9 Summary of predicting the alpha retinal ganglion cells with simple models

We found that across all stimuli the standard LN model, consisting of a fixed linear filter that was calculated from the white-noise data and a three parameter sigmoidal nonlinearity, succeeded in replicating over 50% of the trial to trial A-RGC responses (Figure 5.32). The predictions for the uniform, split spot, and center-surround white-noise stimuli were all within <10% of the intrinsic variation of the data, except for the Off-Transient center-surround prediction. Even for the natural movie responses, the LN model predictions were only 10-15% less correlated than the data for the sustained cells and 35% for the transient A-RGCs. Though models with additional nonlinearities improved upon the LN model in all attempted cases, the effectiveness of a single filter and nonlinearity at predicting the A-RGC responses suggests these cells perform simple computations on visual input.

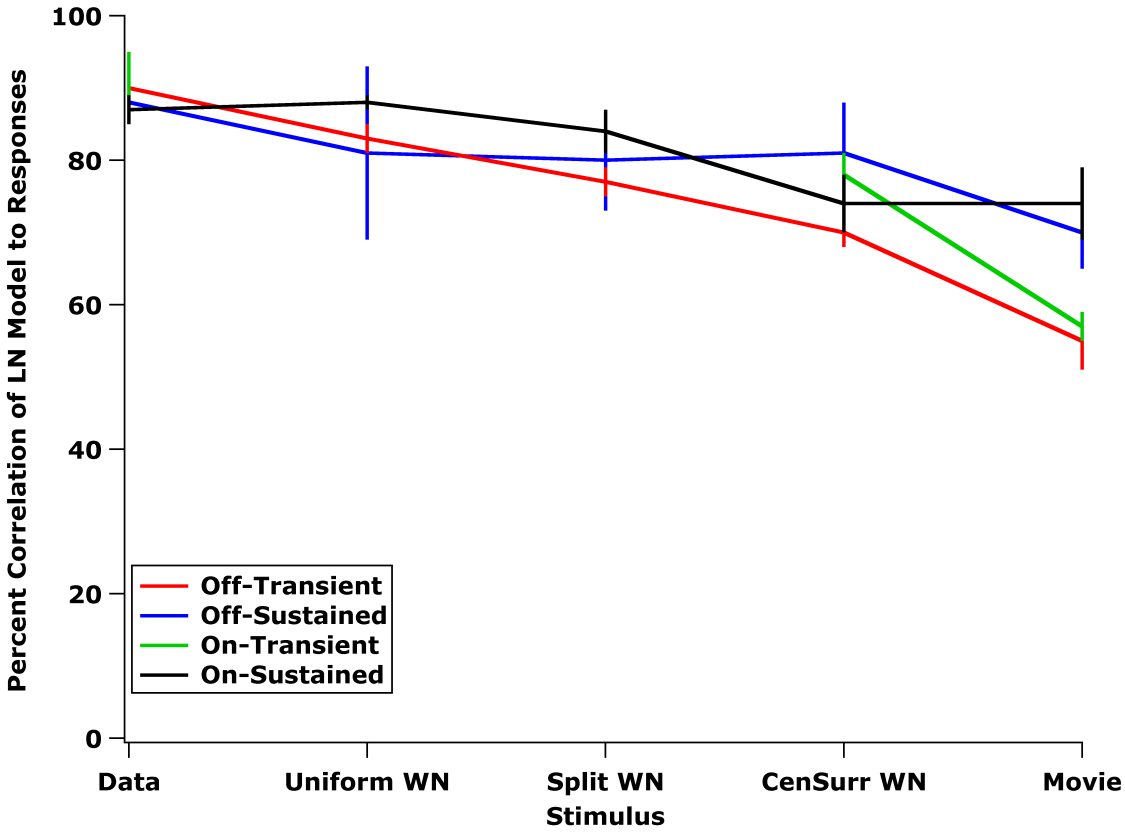

Figure 5.32: Comparison of the linear-nonlinear (LN) model across all forms of stimuli to the intrinsic neural error. The y-intercept ("Data") represents the error of each A-RGC calculated as the average response correlation across repeated trials of the same stimulus. On the x-axis, the stimulus variations and the performance of the LN model for that stimulus are plotted in increasing order of complexity.

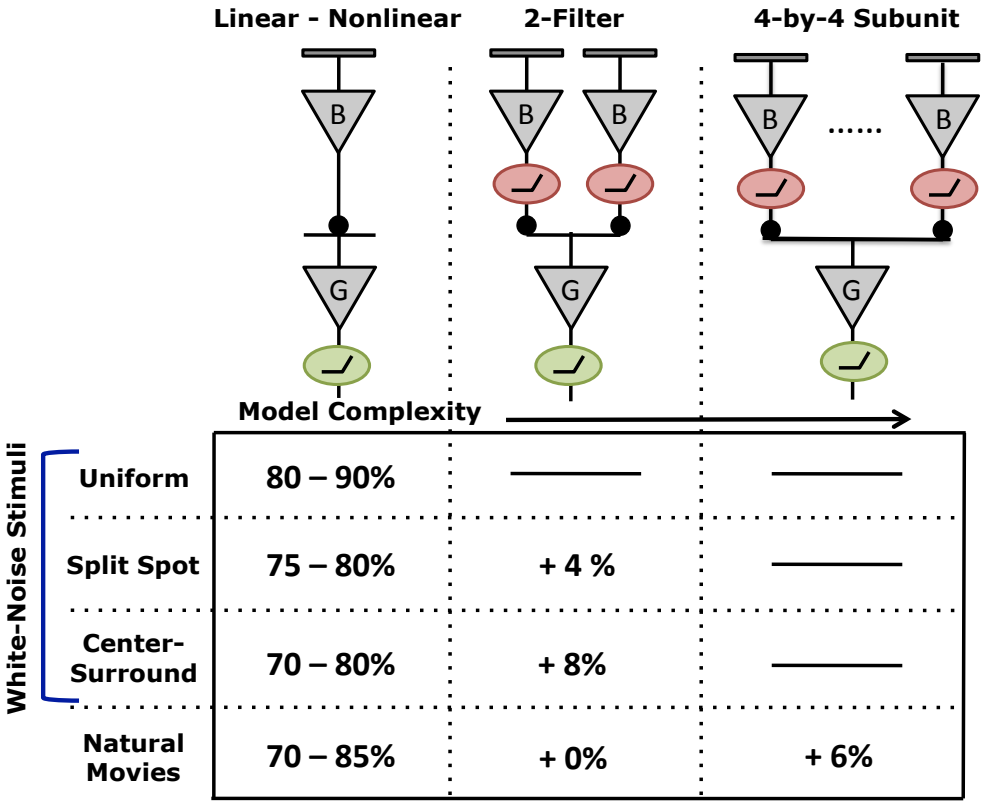

Figure 5.33: Summary of correlation values between data and model fit for responses of the A-RGCs to all tested stimuli. The range under the linear-nonlinear model indicates the span of correlation values for the standard LN model across all four A-RGC types. The percent improvements indicated under the 2-filter model and the 4-by-4 subunit model state the improvement in the two range values to fit the same data.

5.10 Discussion

We found the responses of the A-RGCs to white-noise stimuli and natural movies to be very amenable to prediction by simple models. All responses to visual stimuli were at least 50% correlated to the prediction by the standard LN model. The success of the standard LN model consisting of a temporal filter, calculated by reverse correlation, and three parameters for the nonlinearity suggested the computations performed by the A-RGCs on our visual stimuli were relatively simple. Our success modeling the mouse A-RGCs with the LN model was consistent with a past report on the potential A-RGC analogs in the guinea pig. Zaghoul *et al.* 2007 found the responses of the large RGCs to a spatially uniform Gaussian flickering spot were 80 ± 3% captured by the LN model[21]. We extended these results by verifying the RGC type through the use of the KCNG4-cre transgenic mouse line and by finding that the LN model performed reasonably well on more complex stimuli, including natural movies. Previous work predicting responses to natural movies from the feline lateral geniculate nucleus (LGN) used the LN model and found the predictions to be, on average, 48% correlated with the data[26]. It should be noted that in this study they calculated the correlation between the average neural response and the model prediction. Our model predictions were correlated with A-RGC responses to individual repetitions of the stimulus and our predictions with the LN model were 65% correlated on average. If Dan *et al.* 1996 had calculated the correlation using the noisier individual spike trains, as we have here, their average correlation value would have been lower than 48%. Our work builds upon previous successful applications of the LN model by predicting neural responses to natural movies more accurately than ever before.

By adding additional nonlinearities, we were able to improve upon the standard LN model predictions (Figure 5.21 and 5.31). The justification for adding further model complexity came from our finding via the 2D-nonlinearities that the A-RGC spatial processing of binary stimuli was nonlinear. This result was consistent with our earlier recordings of the neurons responding to inverting gratings in a manner similar to the frequency doubling reported in mouse A-RGC analogs (see Chapter 3, Figure 3.6). The extensions of the standard LN model successfully reproduced the computations of the A-RGCs as reflected in the predicted 2D-nonlinearities for the split-center and center-surround white-noise stimuli. The reproduction of those nonlinearities provided evidence that the increase in prediction quality over the LN model resulted from a better estimate of the A-RGC computation rather than the additional free parameters. It should be noted that there was no chance of overfitting because the model was optimized on one portion of the data and the prediction was calculated on another. Further subdividing the receptive field center improved the prediction for the natural movies. We found this result somewhat surprising considering the 16 stimuli inputs were highly correlated with each other (data not shown). The finding that separately rectifying highly correlated inputs improved the model performance supports the notion that A-RGCs possess spatially nonlinear receptive fields. It is important to remember that the contribution from these additional nonlinearities was significant, but below 10% and that the standard LN model with a single nonlinearity captured the majority of the A-RGC responses.

All stimuli we tested elicited robust responses from the A-RGCs. Qualitatively, the A-RGC responses to white-noise and natural movies were similar based on having roughly equal peaks in firing rate per second and similar jitter in response across stimulus

repeats. The frequent responses of the A-RGCs compared to those of other RGCs, that tended to be sparser, may partly explain our modeling success based on having larger quantities of data[2]. Under the current stimulus conditions, we were unable to predict A-RGC responses to movies using the LN model with the parameters found by fitting the white-noise responses. This was primarily due to differences in the nonlinearities resulting from the high contrast white-noise stimulus eliciting higher peak firing rates than the natural movies. Our preliminary results comparing the 2D-nonlinearities from white-noise and natural movies suggested those differences in the parameters were due to differences in the properties of the stimuli rather than a change in neural processing. For example, the "split" 2-filter model failed to improve the prediction for the natural movie responses as it had for the white-noise stimuli. This difference may have been due to the binary stimulus overall driving the retina harder than the natural movies to result in less exploration of the nonlinearities. Future experiments can use white-noise stimuli with a contrast range equal to that of the natural movies. In such a case, the parameters for the LN model prediction optimized to the white-noise stimulus should likely predict the responses to the natural movies. It should be noted that at times the temporal kernel found by the model for the natural movie prediction was shifted relative to the kernel calculated from the white-noise responses. In practice the receptive fields were measured at the end of the experiment and thus this shift could have resulted from the time delay between the recordings of the responses to the two stimuli.

Our key result from modeling the A-RGC responses was our success predicting the neural responses to natural movies. The responses of the Off- and On-Sustained A-RGCs were readily replicated by the standard LN model when fitting the temporal kernel.

The predictions were within the biological error measured from stimulus repetitions and thus the LN model was sufficient to explain the responses to the movies we tested. The model predictions for the Off- and On-Transient A-RGCs were never within the intrinsic biological error of those cells. Allowing optimization of the temporal filter in the standard LN model improved the fit by 15-20% and introducing local rectifying subunits in the center improved the fit by an additional 5-7%. Further modifications of the models by allowing for a different temporal kernel in the surround or even adding locally rectified surround subunits would perhaps completely reproduce the responses of the transient A-RGCs. Overall, our model results showed the computations performed by the A-RGCs to be mostly captured by the simple combination of a linear filter with a few nonlinear transformations.

5.11 References

1. Gollisch, T. & Meister, M. Eye smarter than scientists believed: neural computations in circuits of the retina. *Neuron* **65,** 150–164 (2010).

2. Zhang, Y., Kim, I.-J., Sanes, J. R. & Meister, M. The most numerous ganglion cell type of the mouse retina is a selective feature detector. *Proc. Natl. Acad. Sci. U. S. A.* **109,** E2391–8 (2012).

3. Münch, T. a *et al.* Approach sensitivity in the retina processed by a multifunctional neural circuit. *Nat. Neurosci.* **12,** 1308–1316 (2009).

4. Olveczky, B. P., Baccus, S. a & Meister, M. Segregation of object and background motion in the retina. *Nature* **423,** 401–408 (2003).

5. Shapley, R. & Enroth-Cugell, C. in *Prog. Retin. Res.* 264–346 (1984).

6. Baccus, S. a & Meister, M. Fast and slow contrast adaptation in retinal circuitry. *Neuron* **36,** 909–919 (2002).

7. Chichilnisky, E. J. A simple white noise analysis of neuronal light responses. *Network* **12,** 199–213 (2001).

8. Zaghloul, K. a, Boahen, K. & Demb, J. B. Contrast adaptation in subthreshold and spiking responses of mammalian Y-type retinal ganglion cells. *J. Neurosci.* **25,** 860–868 (2005).

9. Zaghloul, K. a, Boahen, K. & Demb, J. B. Different circuits for ON and OFF retinal ganglion cells cause different contrast sensitivities. *J. Neurosci.* **23,** 2645–2654 (2003).

10. Enroth-Cugell, C. & Freeman, A. The Receptive-field spatial structure of cat retinal Y cells. *J. Physiol.* 49–79 (1987).

11. Gollisch, T. & Meister, M. Rapid neural coding in the retina with relative spike latencies. *Science* **319,** 1108–1111 (2008).

12. Baccus, S. a, Olveczky, B. P., Manu, M. & Meister, M. A retinal circuit that computes object motion. *J. Neurosci.* **28,** 6807–6817 (2008).

13. Carandini, M. *et al.* Do we know what the early visual system does? *J. Neurosci.* **25,** 10577–10597 (2005).

14. Felsen, G. & Dan, Y. A natural approach to studying vision. *Nat. Neurosci.* **8,** 1643–1646 (2005).

15. Rieke, F. Temporal contrast adaptation in salamander bipolar cells. *J. Neurosci.* **21,** 9445–9454 (2001).

16. Geffen, M. N., de Vries, S. E. J. & Meister, M. Retinal ganglion cells can rapidly change polarity from Off to On. *PLoS Biol.* **5,** e65 (2007).

17. Pitkow, X. & Meister, M. Decorrelation and efficient coding by retinal ganglion cells. *Nat. Neurosci.* **15,** 628–635 (2012).

18. Keat, J., Reinagel, P., Reid, R. C. & Meister, M. Predicting every spike: a model for the responses of visual neurons. *Neuron* **30,** 803–817 (2001).

19. Van Hateren, J. H., Ruttiger, L., Sun, H. & Lee, B. B. Processing of Natural Temporal Stimuli by Macaque Retinal Ganglion Cells. *J Neurosci* **22,** 9945–9960 (2002).

20. Kim, K. J. & Rieke, F. Temporal contrast adaptation in the input and output signals of salamander retinal ganglion cells. *J. Neurosci.* **21,** 287–299 (2001).

21. Zaghloul, K. a, Manookin, M. B., Borghuis, B. G., Boahen, K. & Demb, J. B. Functional circuitry for peripheral suppression in Mammalian Y-type retinal ganglion cells. *J. Neurophysiol.* **97,** 4327–4340 (2007).

22. Pillow, J. W., Paninski, L., Uzzell, V. J., Simoncelli, E. P. & Chichilnisky, E. J. Prediction and Decoding of Retinal Ganglion Cell Responses with a Probabilistic Spiking Model. **25,** 11003–11013 (2005).

23. Garvert, M. M. & Gollisch, T. Local and global contrast adaptation in retinal ganglion cells. *Neuron* **77,** 915–28 (2013).

24. Berry, M., Brivanlou, I., Jordan, T. & Meister, M. Anticipation of moving stimuli by the retina. *Nature* **398,** 334–338 (1999).

25. Hosoya, T., Baccus, S. a & Meister, M. Dynamic predictive coding by the retina. *Nature* **436,** 71–77 (2005).

26. Dan, Y., Atick, J. & Reid, R. C. Efficient Coding of Natural Scenes in the Lateral Geniculate Nucleus : Experimental Test of a Computational Theory. *J Neurosci* **16,** 3351–3362 (1996).

27. Mante, V., Bonin, V. & Carandini, M. Functional mechanisms shaping lateral geniculate responses to artificial and natural stimuli. *Neuron* **58,** 625–38 (2008).

28. David, S. V. & Gallant, J. L. Predicting neuronal responses during natural vision. *Netw. Comput. Neural Syst.* **16,** 239–260 (2005).

29. Kuffler, S. Discharge patterns and functional origanization of mammalian retina. *J Neurophysiol* (1953).

30. Hubel, D. & Wiesel, T. Receptive fields of single neurones in the cat's striate cortex. *J. Physiol.* **148,** 574–591 (1959).

31. Meister, M., Pine, J. & Baylor, D. Multi-Neuronal signals from the retina: aquisition and analysis. *J. Neurosci. Methods* **51,** 95–106 (1994).

32. Pillow, J. W. & Simoncelli, E. P. Dimensionality reduction in neural models : An informatiOn-Theoretic generalization of spike-triggered average and covariance analysis. 414–428 (2006).

33. Rodieck, R. W. Quantitative analysis of Cat retinal ganglion cells to visual stimuli. *VR* **5,** 583–601 (1965).

34. Enroth-Cugell, C. & Robson, J. The Contrast Sensitivity of Retinal Ganglion Cells of the Cat. *J. Physiol.* **187,** 517–552 (1966).

35. Atick, J. J. & Redlich, A. N. Towards a Theory of Early Visual Processing. *Neural Comput.* **2,** 308–320 (1990).

36. Clark, D. a, Benichou, R., Meister, M. & Azeredo da Silveira, R. Dynamical adaptation in photoreceptors. *PLoS Comput. Biol.* **9,** e1003289 (2013).

37. Berry, M. J. & Meister, M. Refractoriness and neural precision. *J. Neurosci.* **18,** 2200–2211 (1998).

38. Hochstein, S. & Shapley, R. Linear and Nonlinear Subunits in Y Cat retinal ganglion cells. *J. Physiol.* **262,** 265–284 (1976).

39. Victor, J. D. & Shapley, R. M. The nonlinear pathway of Y ganglion cells in the cat retina. *J. Gen. Physiol.* **74,** 671–89 (1979).

Chapter 6: Conclusion

The work presented in this thesis has focused on the electrophysiological responses of the mouse alpha retinal ganglion cells (A-RGCs). The main conclusions from this work are as follows:

The mouse A-RGCs constitute a symmetric population of 2 transient and 2 sustained types with both Off- and On-center responses.

The cellular properties of the A-RGCs (active dendrites, thick axons) indicate they may be the fastest channel of information out of the retina.

As a population, the A-RGCs appear to continuously send information about natural visual scenes. In contrast, many other RGC types, such as the On-Off direction selective and W3 aka local edge detector, rarely respond to similar movies dominated by self-motion.

The responses of the four A-RGCs persisted under dramatic spatial movie manipulation suggesting their visual message is dominated by the average stimulus in the receptive field center.

Their responses are a simple filtered version of the input stimulus for both artificial and natural stimuli.

Our finding of the On-Transient A-RGC in Chapter 3 restores symmetry within the mouse alpha population. We are confident the On-Transient cells are indeed part of the alpha class based on staining positive for neurofilament, sharing many receptive field parameters with the other A-RGCs, and minimally processing the visual scene as assessed by movie manipulations and modeling. We found it especially surprising the On-Transient type had been previously missed considering in all other mammals tested, the A-RGCs only possessed transient light responses. We believe this cell type was initially overlooked because it constitutes a minority in the On population. Of all the On RGCs recorded in this study, $1/4^{th}$ were transient. Further work is required to illuminate whether the On-Transient and On-Sustained cell types are morphologically distinct. Previous publications indicate there may be slight differences in the densities of their

dendritic arbors. It will also be interesting to reveal whether the On-Transient and On-Sustained A-RGCs separately tile the retina or together form a full mosaic. For comparison, the Off and On alpha cells each evenly tile the retina in the cat. Recently, the On-Sustained alpha cells were shown to tile the retina in the mouse, but it is unclear whether the On-Transient A-RGCs were included in that population. My preliminary analysis on the population density of the Off mouse A-RGCs suggested the two types form separate mosaics. If the On and Off populations are truly symmetric, the On-Transient cells will tile the retina separate from the On-Sustained cells. If not, the mouse may be an evolutionary intermediate on the way to the full separation of cell types in the cat.

The mouse A-RGCs seem well positioned to deliver fast information to the brain. For one, their thick axons equate to the highest conduction velocity of all output cells from the retina. Additionally, we believe the unique spike shape of this class of cells with the prepotential may be due to dendritic spikes. If the dendrites of the A-RGCs are indeed active, this indicates a greater importance of local stimulation that may speed responses to potentially be used to trigger visual attention. Further work to block the somatic spike or initiate dendritic spikes will illuminate whether the dendrites are the cause of the prepotential. Regardless, the unique spike shape is shared across the A-RGC population suggesting similar biophysical mechanisms of spike generation.

Though the A-RGCs have served as a "model" RGC to test specifics of visual processing across mammals, their responses to natural movies had not been investigated or modeled until now. In Chapter 4 we showed that, as a population, the mouse A-RGCs were essentially continuously sending information about the visual scene under natural

stimulation. This was very different from other RGCs, such as the W3, that rarely responded to natural movies like the ones we used here. We also showed that the A-RGC responses to natural movies were primarily due to the average stimulus in the receptive field center. In Chapter 5, we demonstrated that with the same average stimulus information, we could predict the responses of the A-RGCs with a simple model including temporal filtering and a nonlinearity replicating spike generation machinery. In all cases, the responses of the A-RGCs were well predicted by simple models and sometimes even within intrinsic neural noise. Results from Chapters 4 and 5 suggest the computations the A-RGCs perform on visual input are fairly uncomplicated. This claim holds for both white-noise stimuli and natural movies. Therefore the A-RGCs may be sending a simple filtered version of the visual scene to higher brain areas that may then serve as a reference for other inputs. It will be interesting to know whether other mammalian alpha cells behave in a similar manner under natural stimulation. Based on our finding that the A-RGCs continually encode a simple filtered version of the natural world, combined with the knowledge that these retinal neurons are conserved across species, it is very likely that the A-RGCs play a fundamental role in natural vision.